Juel-4336

Jülich Center for Hadron Phyics (JCHP)
Institut für Kernphysik (IKP)
COSY

πN scattering lengths from pionic atoms

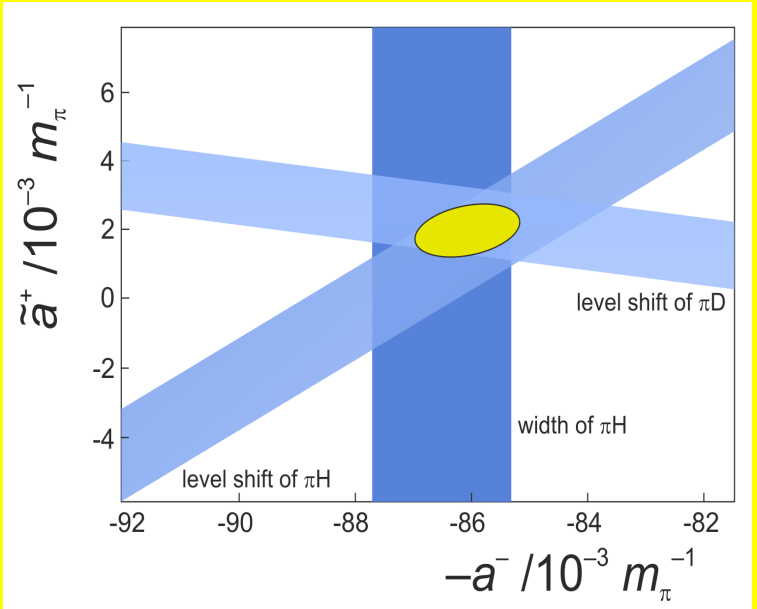

Annual Report 2010

JÜLICH
FORSCHUNGSZENTRUM

Annual Report 2010

Jülich Center for Hadron Physics / Institut für Kernphysik / COSY

Cover picture:

The most accurate method to measure the pion-nucleon scattering lengths, a^+ and a^-, is via measurements of the deviation of the spectra of pionic atoms from what is predicted for purely Coulombic bound states (see Sect. 3.1). The theoretical analysis, based on effective field theories, of each of the experiments for the energy shifts of pionic hydrogen and pionic deuterium as well as the width of pionic hydrogen gives a band in the $\tilde{a}^+$ (closely related to a^+), a^- plane — those bands including both theoretical as well as experimental uncertainties are shown in the figure (see Sect. 4). The ellipse shows the one-sigma area allowed for $(\tilde{a}^+, a^-)$. An update of the GMO sumrule with this improved input leads to a value of the πNN scattering length of $g_c^2/4\pi = 13.69 \pm 0.12 \pm 0.15 = 13.7 \pm 0.2$, thus excluding values above 14 with two sigma accuracy.

Preface

2010 marks the first year of the second period of Program oriented Funding (PoF) of the Helmholtz Association of German Research Centers. In October a further milestone for the FAIR project was accomplished by signatures of the international agreement on its construction and the subsequent foundation of the FAIR GmbH. The Institut für Kernphysik (IKP) of Forschungszentrum Jülich (FZJ) is heavily involved in FAIR as the consortium leader for the construction of the High Energy Storage Ring (HESR) and a major contributor to the PANDA detector. In addition IKP is working on a method to produce beams of polarized antiprotons by spin filtering for a possible future FAIR/HESR-upgrade.

In October, a Program Advisory Council, chaired by Stephan Paul (TU Munich), was held at IKP to advise IKP and FZJ management on the future plans and strategy of the institute. Besides the IKP program outlined for PoF-2 for COSY and FAIR, the committee strongly endorsed the PAX spin filtering project and the plans to investigate the possibilities of a search for an electric dipole moment (EDM) of proton and/or deuteron (^{3}He) at storage rings, which could lead to a future IKP facility. It also recommended to renew the position of the IKP-4 director (R. Maier) after his retirement in 2014 as early as possible.

The following experimental and theoretical highlights are worth mentioning:

- The decay of the eta into two charged pions and a photon has been measured by the WASA-at-COSY collaboration (see cover).
- Analyzing powers and cross sections for the reaction $\vec{p}n \to (pp)_S\pi^-$ have been obtained at ANKE for a beam energy $T_n = 353\,\mathrm{MeV}$. The results are in agreement with, but extend, existing data in literature. They allow to determine the low-energy-constant d in the $4N\pi$ constant interaction of Chiral Perturbation Theory in the most systematics-free way.
- The WASA collaboration has obtained new data on two-pion production in the proton-proton reaction at the invariant collision energy $\sqrt{s} = 2.46\,\mathrm{GeV}$. The data are compatible with a double Delta excitation.
- The COSY-TOF collaboration took data on the reaction $\vec{p}p \to pK\Lambda$ and extracted the Kaon analysing power, completing a first step in the determination of the spin triplet proton-Lambda scattering length.
- Theory has derived the pion-deuteron scattering length from a consistent treatment of both strong and electromagnetic few body effects. The systematic uncertainties of the pion nucleon coupling constant are now controlled, resulting in $g_c^2/4\pi = 13.7 \pm 0.2$.
- New insight into the nucleon electric dipole moment has been achieved by a chiral extrapolation of lattice results obtained for large pion masses. An upper limit of the vacuum angle $\Theta_0 < 2.5 \times 10^{-10}$ has been deduced.
- Chiral effective field theory of light nuclei has been solved in state-of-the-art nuclear lattice simulations at next-to-next-to-leading order. In ^{12}C, an excited 0^+state is found close to the astrophysically important Hoyle state.

The Ionization Profile Monitor designed for FAIR was installed in the COSY ring and successfully commissioned, reaching the design performance. The design and construction

of the 2 MeV electron cooler which boosts the luminosity in the presence of high-density internal targets is done in cooperation with the Budker Institute of Nuclear Physics(BINP) in Novosibirsk, Russia. The manufacturing of the cooler components at BINP is about 90% complete.

The modularized start version of FAIR required a modification of the HESR design, which now includes the anti-proton accumulation function in the HESR. A cost-efficient accumulation method that uses the already designed stochastic cooling system and the barrier bucket cavity has been chosen. Powerful stochastic cooling is not only essential for the accumulation of anti-protons in the HESR. It also indispensable for the preparation of the required beam quality in the internal target experiments. To enhance the performance of the stochastic cooling system the coupling structures of the (2 – 4) GHz system have been further optimized and successfully tested in COSY. First prototype structures operating in the (4 – 6) GHz range have been built to further improve the beam quality. They are currently under test.

SPIN2010, the 19th International Spin Physics Symposium, was held at Forschungszentrum Jülich in September/October 2010. Organized by IKP with Hans Ströher and Frank Rathmann as co-chairman, it attracted about 300 participants, who presented 38 plenary and 165 contributed talks. A public lecture was held at RWTH Aachen.

Hans Ströher received an Advanced Grant from the European Research Council (ERC) for the "Production of Polarized Antiprotons", which runs from 2010 to 2015.

Evgeny Epelbaum accepted the call as a Full Professor at the Ruhr-University Bochum.

It is a pleasure to thank all our collaboration partners, guests, and members of the institute for their dedication to our common work.

Jülich, March 2011 Rudolf Maier

Contents

Needs to be updated!!

1 Physics at COSY

1.1 Overview

The cooler synchrotron and storage ring COSY delivers unpolarized and polarized beams of protons and deuterons with momenta up to 3.7 GeV/c for three internal experiments — ANKE, PAX and WASA — and one experiment — TOF — at an external target position. All three detection systems are operated by large international collaborations.

- **ANKE** (Apparatus for Studies of Nucleon and Kaon Ejectiles) is a large acceptance forward magnetic spectrometer at an internal target station in the COSY ring. The central dipole is movable to adjust the momenta of the detected particles independent of the beam momentum. Using deuterium cluster targets, reactions on the neutron are tagged by detecting the low-energy recoil proton in silicon strip detectors in vacuum next to the target. In addition, a polarized internal target with a storage cell can be used.
- **PAX** (Polarized Antiproton EXperiment) is the test set-up to investigate spin filtering as a method to produce polarized beams. It uses an atomic beam source, an openable storage cell an a Breit-Rabi polarimeter in a low-β section of COSY.
- **TOF** (Time Of Flight) is a non-magnetic spectrometer combining excellent tracking capabilities with large acceptance and full azimuthal symmetry allowing to measure complete Dalitz plots. TOF is optimized for final states with strangeness. With the new straw tube tracking system (STT), TOF will have a significantly improved mass resolution and reconstruction efficiency.
- **WASA** (Wide Angle Shower Apparatus), an internal 4π spectrometer for neutral and charged particles, is operated at the internal COSY beam. WASA comprises an electro-magnetic calorimeter, a very thin superconducting solenoid, inner and forward trigger and tracking detectors, and a frozen-pellet target.

The unique COSY capabilities are also used by the Storage-Ring EDM (srEDM) collaboration to investigate spin-manipulations as preparation to build (a) dedicated storage ring(s) to search for electric dipole moments of light ions (p, d, ^{3}He).

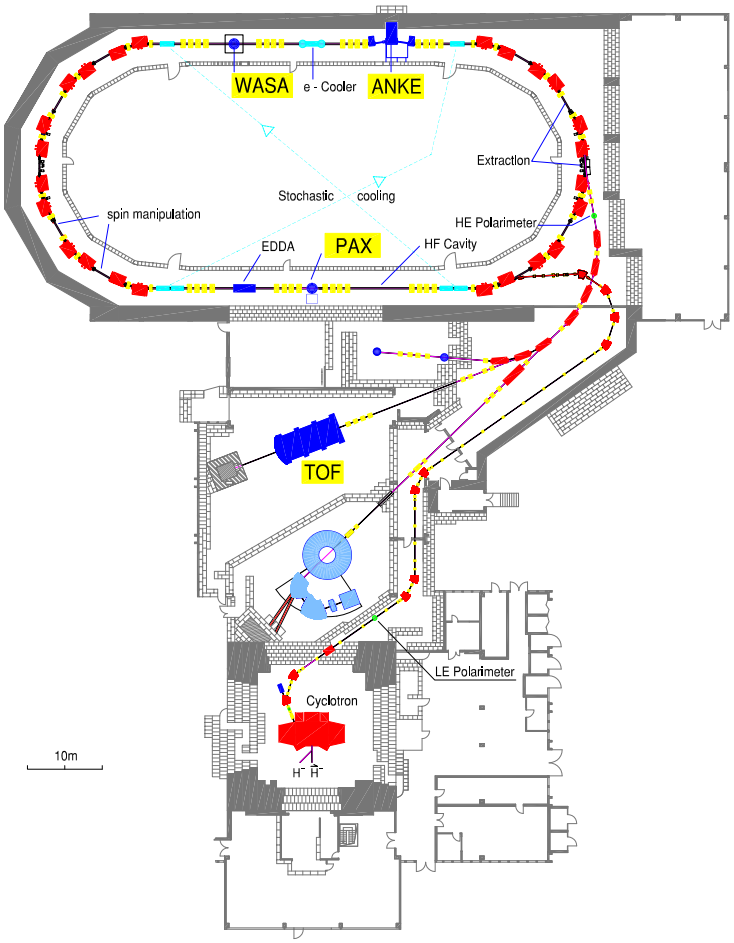

1.2 Major Physics Results at COSY

1.2.1 Rare meson decays

During the last years the WASA-at-COSY collaboration has studied η meson decays as a laboratory of the low energy regime of QCD: high precision measurements of differential distributions and decay rates are compared to calculations from Chiral Perturbation Theory and Standard Model predictions are tested to approach new physics.

At **WASA** light mesons are produced using two different methodss: the fusion reaction $pd \to {}^3\mathrm{He}\eta$ and the elementary reaction $pp \to pp\eta$. In both cases the mesons are tagged by a missing mass analysis using the nucleonic ejectiles in the forward detector. The first reaction allows a clean identification of the ^{3}He in the forward detector and guarantees low background from multi-pion production. Providing a yield of about 10 η mesons per second, this channel was used to study more probable decays and to start investigations of rare decays. In total, about $3 \cdot 10^7$ η decays (unbiased with respect to the decay system) have been recorded. The analyses of these data are currently being finalized and a number of PhD theses have been finished in 2010 or will be finished soon.

The decay $\eta \to \pi^+\pi^-\gamma$ was studied with the goal to test chiral QCD anomalies described by the Wess-Zumino-Witten (WZW) Lagrangian. The measured photon energy spectrum was found at variance with the simplest gauge invariant matrix element, but can be described by a Vector Meson Dominance ansatz. The pion angular distribution is consistent with a relative p-wave of the two-pion system. With 13740 ± 140 events these data represent the currently largest sample of an exclusive measurement. Further investigations include the symmetry-breaking decay $\eta \to \pi^0 e^+e^-$, tests of chiral perturbation theory ($\eta \to 3\pi$, $\eta \to \pi^0\gamma\gamma$), and single and double electromagnetic transition form factors in $\eta \to \gamma e^+e^-$, $\eta \to \pi^+\pi^- e^+e^-$ and $\eta \to e^+e^-e^+e^-$. For the latter, the pd data are used to establish the branching ratio. Corresponding publications are currently in preparation.

For the anticipated precision measurements on rare and very rare decays ($\eta \to \pi^+\pi^-e^+e^-$, $\eta \to e^+e^-e^+e^-$ and $\eta \to e^+e^-$) much higher statistics is needed. For this the elementary reaction has to be utilized, which provides a 20 times larger production cross section. Consequently, the experimental program now focusses on the reaction $pp \to pp\eta$ and a first long run (8 weeks) was carried out in 2010. In contrast to the production via $pd \to {}^3\mathrm{He}\eta$ the higher rates demand also trigger conditions on the decay system. Here, the focus was on charged decays (however, data on neutral decays have also been taken in parallel using a down scaled trigger).

Figure 1 shows the missing mass spectrum of two protons with an additional cut on two charged and two neutral particles in the central detector. In addition, an invariant mass analysis is used to test whether the two neutrals form a pion. Consequently, the spectrum should be dominated by $pp \to pp\pi^+\pi^-\pi^0$ events. Based on this analysis the total number of $\eta \to \pi^+\pi^-\pi^0$ decays on disk has been estimated at about $15 \cdot 10^6$. Thus, with the 8 weeks pp run the available statistics on η decays exceeds the $pd \to {}^3\mathrm{He}\eta$ data set already by one order of magnitude.

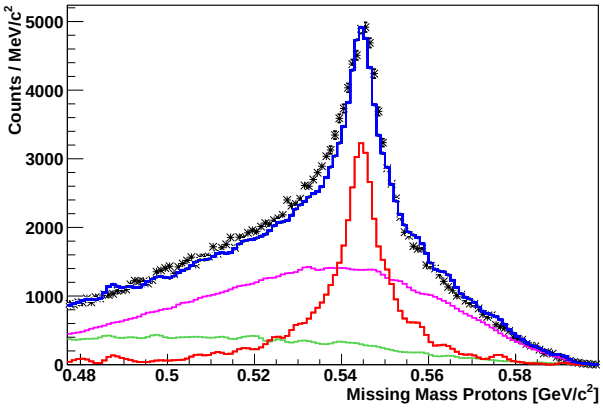

Fig. 1: Missing mass spectrum of two protons for $pp \to pp\pi^+\pi^-\pi^0$ requesting two protons in the forward detector and two charged particles and two photons in the central detector. A cut on the invariant mass of the two photons forming a pion has been applied. The data points show a small fraction of the available data, the blue curve represents the sum of Monte-Carlo simulations for signal (red) and direct multi-pion background (3π purple, 2π green) fitted to the data.

The long term goal of the experimental program of η decays is to approach Standard Model predictions of the decay $\eta \to e^+e^-$. In the Standard Model, the decay of pseudoscalar mesons into dileptons proceeds through the electromagnetic interaction and is suppressed relative to the two-photon decay by α^2 and $(m_e/m_{\pi^0,\eta})^2$ from helicity conservation. Currently, the best limit for $\eta \to \mathrm{e^+e^-}$ is $\mathrm{BR_{exp}} < 2.7 \cdot 10^{-5}$ at CL = 90% measured by CELSIUS/WASA. This number is four orders of magnitude larger then the value derived from Standard Model calculations $\mathrm{BR_{theo}} \approx 5 \cdot 10^{-9}$. Based on the available statistics, the WASA-at-COSY collaboration has already achieved a higher sensitivity than obtained in the CELSIUS run. The analysis is currently in progress. For future runs, a further increase of the effective luminosity is planned by introducing a sophisticated trigger which makes use of a fast feature extraction of the QDC modules.

Recently, the interest in the dilepton decay $\pi^0 \to e^+e^-$ was also revived due to an observed 3σ excess (KTeV) for the $\pi^0 \to \mathrm{e^+e^-}$ branching ratio compared to the Standard Model predictions. Taking into account only statistical considerations, the branching ratio of $(6.44 \pm 0.25 \pm 0.22) \cdot 10^{-8}$ is in range in a 8–10 weeks run. Thus, a two-week test run for $pp \to pp\pi^0$ at a kinetic energy of $T = 550$ MeV (i.e. below the two pion production threshold) has been carried out to check the feasibility of such a measurement with WASA-at-COSY.

1.2.2 Near threshold pion production in diproton reactions at ANKE

With the advent of chiral perturbation theory (χPT), the low-energy effective field theory of QCD, accurate calculations have become possible for hadronic reactions. The approach has been also extended to describe pion production in nucleon-nucleon collisions (T.D. Cohen *et al.*, Phys. Rev. C **53** (1996) 2661; C. Hanhart, Phys. Rept. **397** (2004) 155). This process is of special importance because of several reasons:

- being the first inelastic channel of NN interaction it contains informaltion about NN inelasticity that is needed to extend NN models above pion production threshold;
- it provides nontrivial tests of ChPT in the regime with large momentum transfer (V. Lensky *et al.*, Eur. Phys. J. A **27** (2006) 37);
- it allows one to quantify the pattern of charge symmetry breaking by studing the forward-backward assymetry of the differential cross section in $pn \to d\pi^0$ (Filin *et al.*, Phys. Lett. B **681** (2009) 423);
- the pion production mechanism in $NN \to NN\pi$ near threshold is closely connected to the physics behind the other low-energy hadronic reactions as demanded by chiral symmetry.

Let us focus on the last issue in more detail. The general idea of chiral effective field theory is based on clean separation of hadronic scales around chiral limit. According to the scheme, all long-ranged operators related to the small (dynamical) scale, such as one-pion exchange, pion loops etc., are explicitly included in the evaluation of the transition amplitude whereas all short-ranged mechanisms are parameterized by local contact operators. Specifically, the short range physics of p-wave pion production in $NN \to NN\pi$ (when pion is produced in p-wave with respect to the beam) is absorbed in the local $4N\pi$ contact term the strength of which — low energy constant (LEC) d — is unknown and may be extracted from the experimental data as will be discussed below. This LEC is very important in few body sector since it also contributes to the three-nucleon force, to electroweak processes such as $pp \to de^+\nu$, triton β decay and muon absorption on deuterium $\mu^- d \to nn\nu_\mu$ as well as to the reactions involving photons $\pi d \to \gamma NN$ and $\gamma d \to nn\pi^+$. Thus, it is of high importance to identify what is needed to allow for a reliable extraction of this LEC from $NN \to NN\pi$. Since the LEC accompanies the p-wave pion while the nucleons are still in S-waves the efforts should be focused on measuring the observables that would allow one to extract the corresponding p-wave amplitudes from data.

Of especial interest are thus the processes $pp \to \{pp\}_s\pi^0$ and $pn \to \{pp\}_s\pi^-$, with the formation of a $^1S_0$ proton pair (diproton) in the final state. The measurements of $d\sigma/d\Omega$, A_y and the spin-correlation coefficients $A_{x,x}$ and $A_{x,z}$ for both reactions will permit an amplitude analysis that is necessary to single out the relevant p-wave amplitudes from the rest.

The **ANKE** spectrometer is particularly well suited for the study of reactions with a final diproton. The excellent resolution in the excitation energy of the proton pair, $\sigma_{E_{pp}} < 0.5$ MeV, allows one to select the range of low $E_{pp} < 3$ MeV. This ensures the dominance of the $^1S_0$ state of the final proton pair. Single and double polarisation experiments can be conducted through the use of the polarised COSY beams and the ANKE polarised internal target.

As a first step in the programme, measurements with a polarised proton beam incident on unpolarised hydrogen and deuterium cluster targets were performed at ANKE in 2009 at a beam energy of $T_p = 353$ MeV.

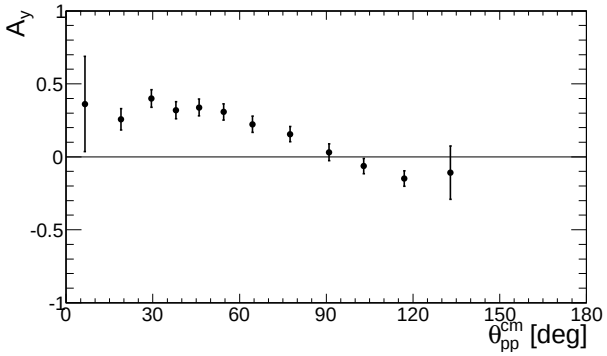

Fig. 2: Analysing power A_y of the $pp \to \{pp\}_s\pi^0$ reaction at $T_p = 353$ MeV.

Figure 2 shows the results obtained for the $\vec{p}p \to \{pp\}_s\pi^0$ reaction. Since A_y must be antisymmetric about 90°, the acceptance is effectively complete. If one considers only pion waves with $l \leq 2$, a non-zero value of the analysing power in this process must arise from the interference between the s and d waves. The strong signal observed here shows immediately importance of this interference.

The results for the $\vec{p}n \to \{pp\}_s\pi^-$ reaction are presented in Figs. 3 and 4. The ANKE data are shown together with the results from TRIUMF [H. Hahn *et al.*, Phys. Rev. Lett. **82** (1999) 2258] and compared to the prediction of the IKP theory group [V. Baru *et al.*, Phys. Rev. C **80** (2009) 044003]. The value of LEC $d = 3$ is favoured, though it must be stressed that the pion d-waves have not yet been included in the calculations.

The results were obtained with a 40 MeV wide range of effective beam energy in the free pn-scattering, *i.e.*, $T_{\rm free} = 353 \pm 20$ MeV. The $E_{pp} < 3$ MeV cut was imposed on the data but, to facilitate the comparison with previous results, the cross section has been recalculated for the $E_{pp} < 1.5$ MeV cut used at TRIUMF. This was done using the Migdal-Watson approximation for the final state interaction in the $^1S_0$ proton pair. The main advantage of the ANKE measurement is the extended angular range

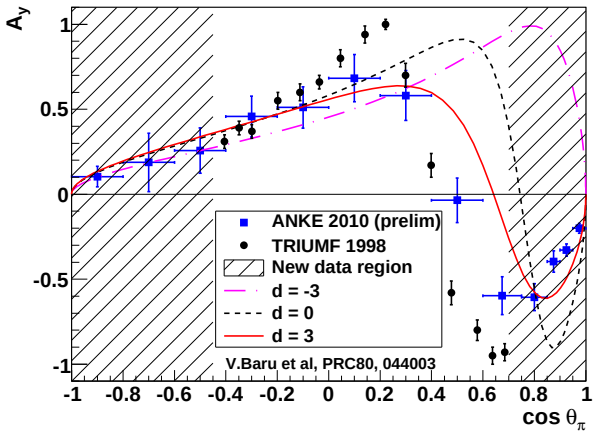

Fig. 3: A_y in the $\vec{p}n \to \{pp\}_s\pi^-$ reaction at T_n=353 MeV (blue squares). Also shown are the results of χPT calculation for $d = 3$ (red solid line), $d = 0$ (black dashed line), and $d = -3$ (magenta dash-dotted line). The data from TRIUMF are shown as black circles.

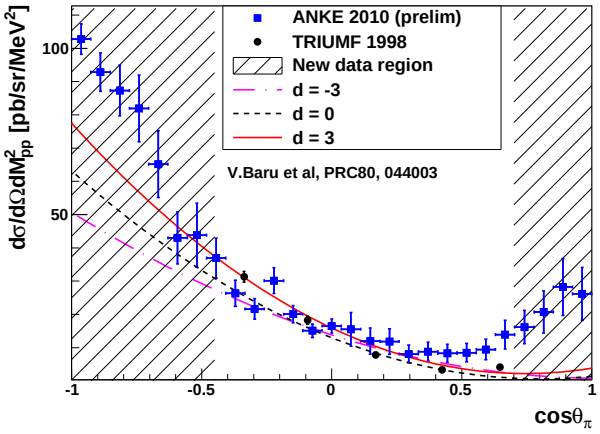

Fig. 4: ANKE Preliminary results for the cross section of the $\vec{p}n \to \{pp\}_s\pi^-$ reaction at T_n=353 MeV in the $E_{pp} < 1.5$ MeV range. The conventions are the same as those used in the caption to Fig. 3.

compared to the pre-existing data.

The transitions involving the $4N\pi$ contact interaction correspond to the p-wave pion production in the $np \to \{pp\}_s\pi^-$ reaction. The initial nucleons in this case appear in the partial waves that are coupled: ${}^3S_1 \to {}^1S_0 p$ and ${}^3D_1 \to {}^1S_0 p$. Due to the coupled channel effect the contact term contributes to both partial waves which may provide a more rich dependence of the observables on the LEC d. Note, that a linear combination of these p-wave amplitudes may be fixed by the only measurement of $\xi = (1 - A_{x,x}) \cdot \mathrm{d}\sigma/\mathrm{d}\Omega$ for $np \to \{pp\}_s\pi^-$ under the assumption that the interference of pion p- and d-waves is small. This linear combination could be compared directly to the ChPT calculation. Thus, the double polarisation experiment for the measurement of $A_{x,x}$ and $A_{y,y}$, scheduled for 2011, will greatly improve our knowledge of the LEC d.

The χPT predictions for $A_{x,x}$ and ξ are shown in Figs. 5 and 6 for several values of the LEC d. If one considers only s, p and d partial waves, then $\xi \propto sin^2\vartheta_\pi$. Thus, only the scale parameter proportional to the linear combination of the p-wave amplitudes, has to be extracted from the measurement of the angular dependence. The experiment will provide the most systematics-free way to fix the value of the LEC d.

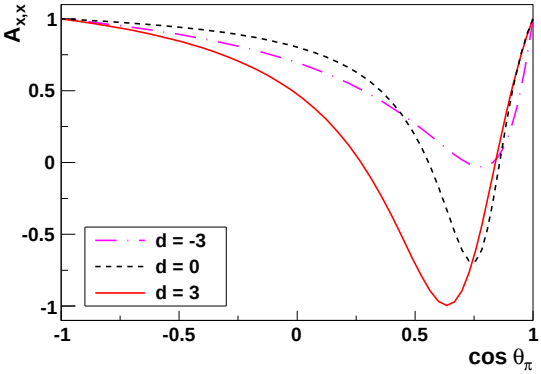

Fig. 5: Spin correlation coefficient $A_{x,x}$ of the $\vec{p}\vec{n} \to \{pp\}_s\pi^-$ reaction at $T_p = 353$ MeV. The curves present calculations for different values of LEC d.

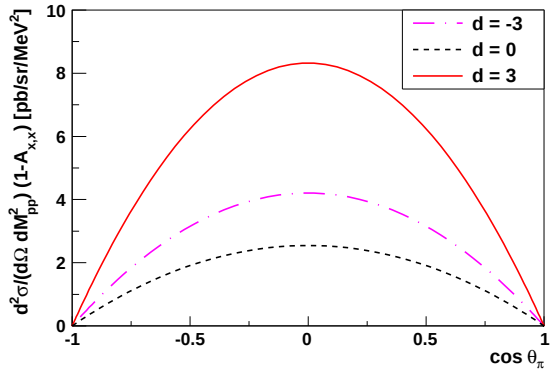

Fig. 6: Prediction for $(1 - A_{x,x}) \cdot \mathrm{d}\sigma/(\mathrm{d}\Omega \mathrm{d}M^2_{pp})$ of the $\vec{p}\vec{n} \to \{pp\}_s\pi^-$ reaction at $T_p = 353$ MeV. The curves present calculations for different values of LEC d.

At the same time, the magnitudes of the p-wave amplitudes individually and their relative phase should be deduced from a combined analysis of these results with our cross section and analysing power data for $pp \to \{pp\}_s\pi^0$ and $np \to \{pp\}_s\pi^-$, which have already been taken. Two determinations of the LEC d will therefore be possible.

1.2.3 Two-pion production, the $\Delta\Delta$ system and the ABC-effect

Two-pion production is a well-established tool for the study of hadron structure. Photo-, pion- and nucleon-induced two-pion production is successfully used for the investigation of the two-pion decay of mesons and baryons. Two-pion production in nucleon-nucleon collisions gives access to the study of the mutual excitation of two nucleons into their excited states and their subsequent decay. Of particular interest is the question, whether this intermediate baryon-baryon system exhibits features, which go beyond those of the individual baryons.

The pp-induced two-pion production has been extensively studied at CELSIUS by exclusive measurements from threshold up to T_p = 1.3 GeV. As a result it was shown that the production process is dominated by t-channel (π- and σ-exchange) nucleon excitation and decay. In the near-threshold region the excitation of the Roper resonance is the leading process. At energies $T_p >$ 1 GeV the Roper contributions are fading away and the reaction gets characterized by the mutual excitation of the nucleons into the Δ resonance. This situation provides the unique opportunity to study the intermediate $\Delta\Delta$ system in very detail by exclusive and kinematically complete measurements. Especially suited for such investigations is the $pp \to pp\pi^0\pi^0$ channel, where disturbing isovector $\pi\pi$ contributions are absent, and which can be measured reliably with the **WASA** detector now at COSY. Since the optimum condition for exciting the $\Delta\Delta$ system in pp collisions is at a center-of-mass energy of twice the Δ mass, we have measured the $pp \to pp\pi^0\pi^0$ reaction at $T_p = 1.4$ GeV corresponding to $\sqrt{s} = 2.48$ GeV.

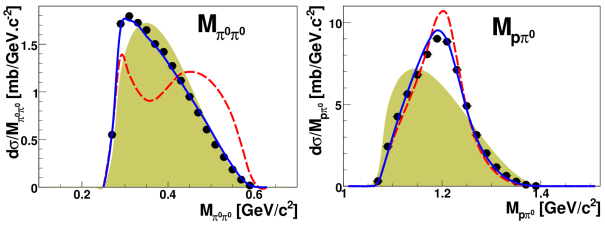

Fig. 7: Distributions of $M_{\pi^0\pi^0}$ (left)and $M_{p\pi^0}$ (right) of the $pp \to pp\pi^0\pi^0$ reaction at T_p = 1.4 GeV ($\sqrt{s}$ = 2.48 GeV). Dashed and full lines give original and modified Valencia calculations, respectively.

The total cross section of 324(61) μb obtained from the analysis of these data fits well to the CELSIUS data at lower energies as well as to previous low-statistics bubble-chamber results. As examples of differential cross sections the experimental distributions for the invariant masses $M_{\pi^0\pi^0}$ and $M_{p\pi^0}$ are shown in Fig. 7. The $M_{p\pi^0}$ distribution deviates markedly from phase space (shaded area) and exhibits clearly the $\Delta\Delta$ excitation. Note that a single Δ excitation in this four-body process would smear the Δ peak in this spectrum considerably. A calculation (solid lines) based on the model developed at Valencia and modified recently at Tübingen in order to account for the CELSIUS data at lower energies gives a quantitative description of the data. Publication of these results is in progress.

In contrast to the small low-mass enhancement observed in the $M_{p\pi^0}$ distributions, which is well accounted for by the t-channel $\Delta\Delta$ process of two-pion production in *isovector* NN collisions, we find a huge low-mass enhancement in the *isoscalar* $pn \to d\pi^0\pi^0$ reaction. This phenomenon is known as the so-called ABC effect, which shows up in fusion reactions associated with the production of an *isoscalar* pion pair. Since its discovery 50 years ago a convincing explanation has been pending. As reported previously we find this ABC effect to be correlated with a narrow resonance-like structure in the total cross section of the $pn \to d\pi^0\pi^0$ reaction peaking at an energy 80 MeV below the mass of two Δs with a width of only 70 MeV, *i.e.* three to four times smaller than the width expected for the t-channel $\Delta\Delta$ process. A publication of these results is in preparation.

In order to see, whether also other double-pionic fusion reactions exhibiting the ABC effect show such a resonance phenomenon in the total cross section, we have measured the $dd \to {}^4\mathrm{He}\pi^0\pi^0$ reaction exclusive and kinematically complete over the full energy region, where the ABC effect is present. The obtained differential cross sections are very similar in shape to those found for the double-pionic fusion to the deuteron — as already shown previously.

The total cross sections of both fusion reactions are compared in Fig. 8 in dependence of the excess energy, *i.e.* the energy above the $\pi\pi$-production threshold. We see that both cross sections peak at the same excess energy, *i.e.* at about 80 MeV below $2m_\Delta$. However, the structure is much broader in case of ^{4}He. This may be understood as being due to the increased smearing of the structure in the basic pn system by the Fermi motion of the nucleons both in the initial deuterons and particularly in ^{4}He — as well as by collision damping of this structure due to the surrounding nucleons. A corresponding calculation assuming a resonance in the basic pn system is shown by the solid line.

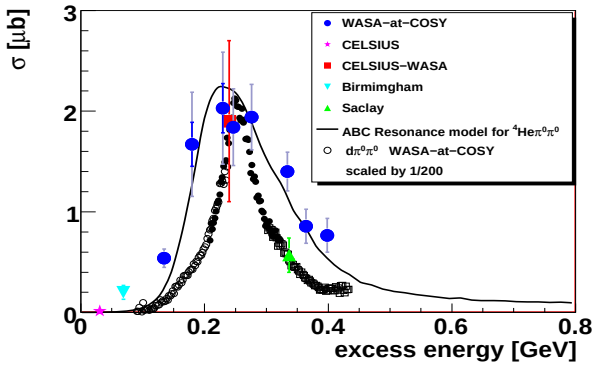

Fig. 8: Total cross section of the $dd \to {}^4\mathrm{He}\pi^0\pi^0$ reaction (colored symbols) in comparison to that of the $pn \to d\pi^0\pi^0$ reaction (black) as function of the excess energy. The solid line shows a calculation assuming a resonance in the basic pn system.

1.2.4 New results on polarization variables in the hyperon production

In the past the **COSY-TOF** experiment had proven by analyzing Dalitzplots of the hyperon production, that this reaction proceeds dominantly via nucleon resonance excitation and therefore by non strange meson exchange. The cross sections and angular distributions of different isospin channels had been determined.

Now the main goal of the COSY-TOF experiment is the examination of the hyperon production with polarized proton beam. The spin polarization of the hyperons and the analyzing power of all final state particles will be determined. Three areas of physical questions will be covered by the results from these data: a) Disentangling different nucleon resonances contributing to hyperon production by partial wave analysis. b) Determination of the spin transfer mechanism from the beam proton to the Λ particle. c) Extraction of the spin resolved Λp scattering length by analyzing the $p\Lambda$ invariant mass distribution.

In September 2010 COSY delivered a 2.95 GeV/c proton beam with a polarization of 60% . The beam polarization is determined by measuring the asymmetry of the elastic scattered protons and by adjusting the resulting analyzing power to literature values (Fig. 9).

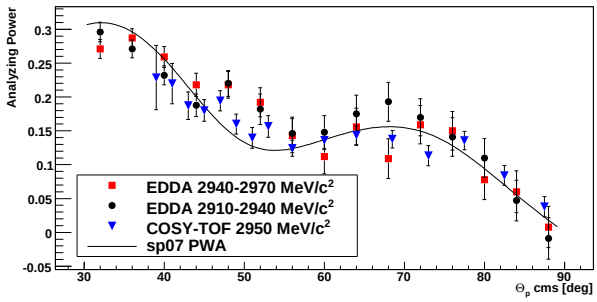

Fig. 9: Analyzing power distribution as as function of the proton center of mass scattering angle. The COSY-TOF data are extracted from the asymmetry measurement by assuming a beam polarization of $(61.0 \pm 1.7)\%$. This gives the best agreement with the result from the SAID partial wave analysis, shown by the solid line.

The reaction $\vec{p}p \rightarrow pK\Lambda$ is measured with nearly 100% acceptance and the Λ is identified by its decay into charged particles in the decay volume, which is between 3 cm and 25 cm in the COSY-TOF detector without any material which guarantees a clean identification of the Λ's without impurities due to straggling and secondary interactions. Figure 10 shows the measured decay length compared with the literature value of $c\tau$.

Due to the new Straw Tube Tracking system, consisting of 2704 tubes, the primary vertex of pK and the Λ decay vertex can be determined with a precision of better than 1 mm . The vertices and track directions allow for the reconstruction of the missing mass in the pK system, which shows a clear Λ signal over a background of 30%. The

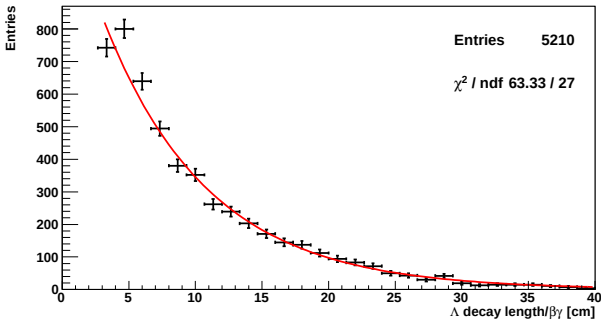

Fig. 10: The Λ decay length is determined using a kinematical fitted sub-sample of Λ events. The solid line represents the literature value of $c\tau(\Lambda) = 7.89$ cm fitted to the height of the measured distribution.

background arises from accidental tracks and from four primary track events as *e.g.* $pp\pi^+\pi^-$ which are misinterpreted to have a secondary vertex.

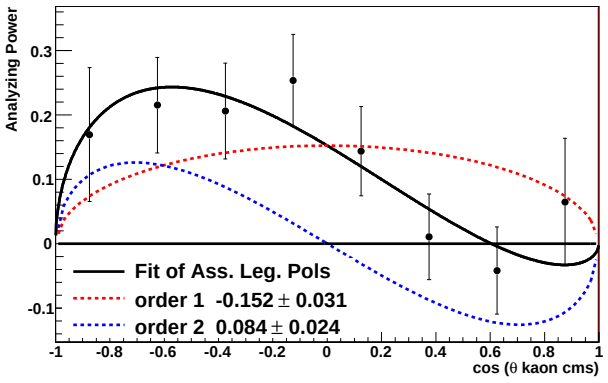

Fig. 11: Preliminary distribution of the kaon analyzing power in dependence on the cosine of the cm scattering angle of the kaon. Shown are the statistical errors of the signal and underlying background plus the systematic error of the beam polarisation.

Applying a signal background separation for each bin in the azimuthal and polar angle distributions and in the spin orientation, the analyzing power of the kaon is determined and shown in Fig. 11. This distribution is not yet given in literature; a pilot measurement of COSY-TOF showed similar properties.

The extraction of the analyzing power of the kaon is the first step towards a separation of the spin triplet scattering length in the $p\Lambda$ system. With the COSY-TOF data it will be possible for the first time to isolate the spin triplet component with known errors. In addition the analysis of the data will result in the determination of the spin transfer coefficients, the analyzing power of all final state particles, and will give further inputs for a partial wave analysis, which will identify the nucleon resonances that contribute to the hyperon production.

1.2.5 ϕ-Meson Production and the in-Medium ϕ-Width in Nuclear Matter

The properties of light vector mesons are expected to change in dense nuclear matter. The cleanest place where to test these ideas is in the case of the $\phi(1020)$ meson, where the narrow vacuum line-shape ($\Gamma = 4.3$ MeV/c^2) allows one to investigate small modifications of the in-medium width. Rather than studying the width directly, at **ANKE** the variation of the ϕ production cross section with atomic number A has been measured. The production rate depends on the attenuation of the ϕ flux in a nuclear target which, in turn, is governed by the ϕ width. In the low-density approximation, this can be related to an effective ϕN total cross section. The big advantage of this method is that one can identify the ϕ meson through its large K^+K^- branching ratio.

Protons of energy 2.83 GeV were incident on four nuclear targets, *viz.* C, Cu, Ag and Au. Positive kaons were first selected using a dedicated detection system that can identify a K^+ even if the π^+/p background is 10^5 more intense. The coincident K^- was subsequently isolated using the time-of-flight difference between the stop counters in the ANKE negative and positive detector systems. For all targets there was a clear ϕ peak sitting on a background of non-resonant K^+K^- production.

The relative luminosity for each target was obtained by measuring in parallel the production rate for positive pions. Since the acceptance corrections in ANKE are essentially target-independent, the ratio of luminosity-normalised counts corresponds to the ratio of the cross sections for ϕ production in the ANKE acceptance window. The resulting so-called transparency ratios, relative to carbon, are presented in Fig. 12 in the form

$$R = 12\,\sigma_{pA\to\phi X'} \big/ A\,\sigma_{p\mathrm{C}\to\phi X}\,.$$

The ratios shown correspond to ϕ production rates that follow the power law $\sigma(A) \propto A^\alpha$, with $\alpha = 0.56 \pm 0.03$. The interpretation of the obtained transparency ratios in terms of an in-medium ϕ width is model-dependent. The Paryev predictions for the transparency ratios shown in Fig. 12 indicate a value of 73^{+14}_{-10} MeV/c^2 for the in-medium width of a ϕ meson in its rest frame at nuclear density $\rho_0 = 0.16$ fm^{-3}. This corresponds to $\approx$ 50 MeV/c^2 in the nuclear rest frame for a ϕ with a momentum of 1.1 GeV/c, which is typical for the ANKE conditions.

The transparency ratios measured in the photoproduction of the ϕ on various nuclei up to copper at the SPring-8 facility have been interpreted in terms of a width of around 95 MeV/c^2 at a typical ϕ momentum of ≈ 1.8 GeV/c. The difference with the published ANKE value might be indicative of a momentum dependence of the width. To test this possibility, the ANKE data have been binned in intervals of ϕ momenta and preliminary values of the transparency ratios evaluated in each. The corresponding widths as a function of p_ϕ, extracted using two reaction models, are shown in Fig. 13.

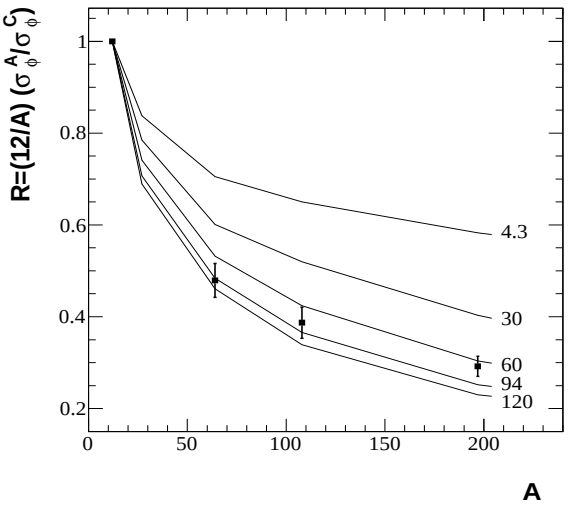

Fig. 12: Comparison of the measured transparency ratio R as a function of atomic number A with predictions of model calculations for different ϕ widths in the meson rest system at normal nuclear density. Both statistical and systematics uncertainties are shown.

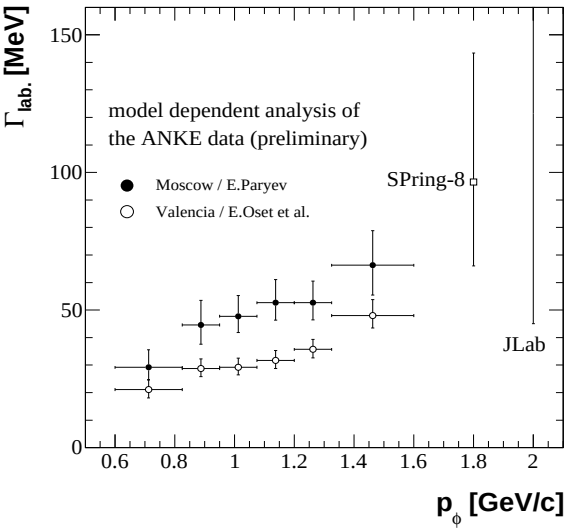

Fig. 13: Preliminary values of the width Γ of the ϕ meson in nuclear matter at normal density $\rho_0 = 0.16$ fm^{-3}, as extracted from the ANKE transparency ratios, using two different reaction models. The strong p_ϕ momentum dependence observed might help to explain the apparent difference from the SPring-8 result at higher p_ϕ. For completeness, results from a JLab experiment are also shown.

Although the width is model-dependent, the values obtained within the approaches of two different groups both show a strong growth with p_ϕ and this should explain much of the difference with the result of the SPring-8 group. In fact, the ANKE results would even have a slightly steeper p_ϕ dependence if nuclear targets only up to copper were considered, as in the SPring-8 work.

1.2.6 The total width of the η' meson

The excellent momentum resolution of the phase space cooled COSY beam in combination with the high measurement precision of the **COSY-11** detector system allowed a direct measurement of the width for the η' meson. The determination of partial widths of most η' decay channels requires the knowledge of the total η' width which is the limiting factor in various meson decay channels. The actual value for the η' width recommended by the PDG of $\Gamma_{\eta'} = 0.194 \pm 0.009$ MeV/c^2 results from a fit to a large amount of partial-width measurements where the $\eta' \to \gamma\gamma$ partial width derived from model dependent calculations is a dominant factor. The errors in the direct measurements are a factor of 7–15 larger which calls for an improved experimental determination of the η' width. With the COSY-11 internal magnetic spectrometer system (Fig. 14) the production of η' mesons in the $pp \to pp\eta'$ reaction has been studied very close to threshold.

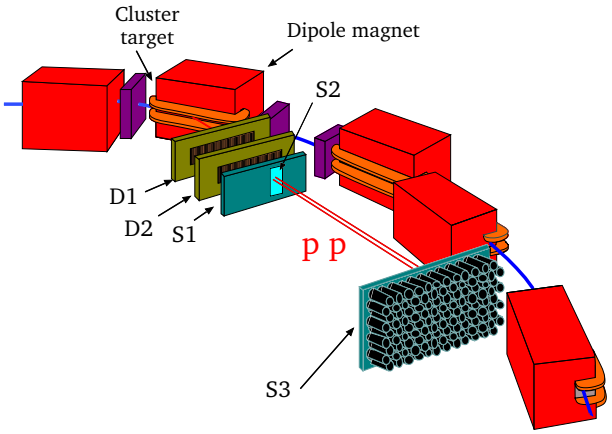

Fig. 14: The COSY-11 facility with a hydrogen cluster target in front of a COSY machine dipole. A system of drift chambers (D) and scintillor hodoscopes (S) allows a precise momentum reconstruction of charged ejectiles. The experiment was in operation till end of 2006.

The scattered protons were measured with drift chambers and scintillator hodoscopes and the η' meson was reconstructed via the missing mass technique. In order to increase the precision the width of the hydrogen cluster target beam was reduced by a factor of 10 compared to the typical operating conditions to 0.9 mm. Due to the dispersion at the COSY-11 target position the beam momentum spread is determined by the target-beam overlap and amounts to ± 0.06 MeV/c for the given COSY settings. The size and position of the target stream, being crucial for the analysis, was monitored by two independent methods. The first was based on the measurement of the momentum distribution of elastically scattered protons, while the second was a direct measurement of the target geometry by mechanically scanning the target stream position above and below the target area from time to time.

Measurements have been performed for 5 different beam momenta in an excess energy range $Q = 0.8 - 4.8$ MeV. Figure 15 shows as an example the missing mass distribution for Q=0.8 MeV. The nominal beam momentum was determined with an uncertainty of ± 0.2 MeV/c and the experimental resolution of the η' peak is 0.33 MeV/c^2 (FWHM).

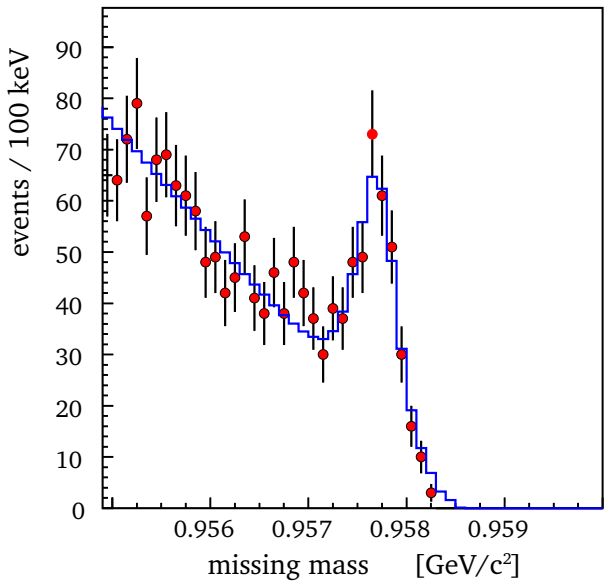

Fig. 15: Missing mass spectrum for the $pp \to pp\eta'$ reaction at an excess energy of 0.8 MeV.

In order to derive the η' width, simulated missing mass distributions were fitted to the measured spectra by adjusting the assumed η' width. The systematic errors due to detector geometry, beam-target overlap, magnetic field, or beam momentum were analyzed in detail. The extracted η' width amounts to $\Gamma_{\eta'} = 0.226 \pm 0.017\,(\text{stat.}) \pm 0.014\,(\text{sys.})$ MeV/c^2 which is consistent with the PDG value.
In Fig. 16 the result is compared to PDG and measured data for this number which demonstrates the big improvement. The precision achieved with the COSY-11 facility enabled for the first time to determine the mass spectrum of the η' meson with a resolution comparable to its total width.

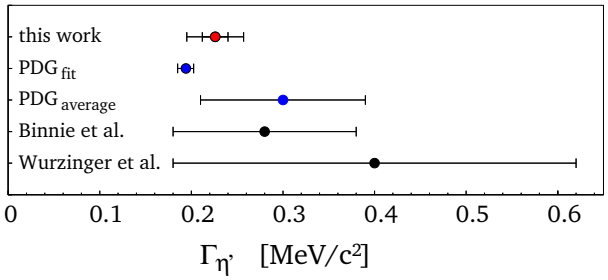

Fig. 16: Comparison of available values for $\Gamma_{\eta'}$. For the reported measurement the systematic and statistical errors are shown.

1.2.7 Energy dependence of hard bremsstrahlung production in proton-proton collisions in the $\Delta(1232)$ region

Study of the nucleon-nucleon bremsstrahlung $NN \to NN\gamma$ and the related photoabsorption reaction $\gamma\{NN\} \to NN$ is among the most direct ways for understanding the interaction of electromagnetic fields with hadronic systems. The primary task of such investigations is clarification of the dynamics of such fundamental processes. The shorter the distances are, the harder is the involved γ radiation.
The reaction

$$p + p \to \{pp\}_s + \gamma, \tag{1}$$

in which the two final protons are in the $^1S_0$ state, is favorable in this respect. At these kinematical conditions, most of the available energy is carried away by the bremsstrahlung. The process is therefore maximally far from the soft-photon limit and so is most sensitive for dynamics of the internal bremsstrahlung. An investigation of this reaction has been carried out by the **ANKE** collaboration at proton beam energies of 353, 500 and 550 MeV (V. Komarov *et al.*, Phys. Rev. Lett. **101** (2008) 102501). The next step consisted in measurements at 625, 700 and 800 MeV with the aim to obtain the energy dependence of the hard bremsstrahlung production in the $\Delta(1232)$ range. In Fig. 17 the differential cross section of the $pp \to \{pp\}_s\gamma$ reaction, averaged over the 0–20° angular range, is shown together with $pn \to d\gamma$ data deduced from the MAMI data. One can see a clear enhancement of the bremsstrahlung production in the region of the $\Delta(1232)$ excitation.

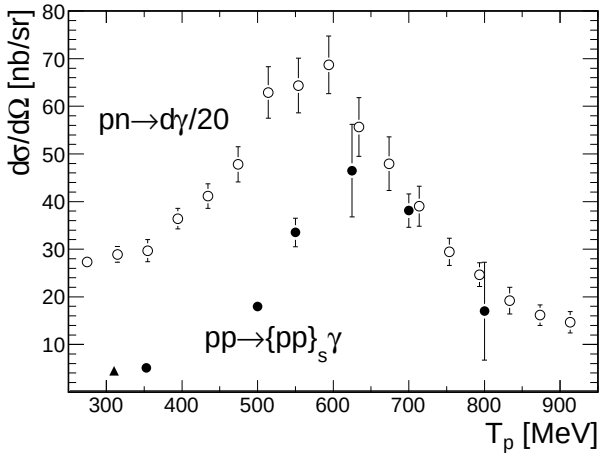

Fig. 17: Energy dependence of the $pp \to \{pp\}_s\gamma$ differential cross section in the 0–20° angular interval: full circles — ANKE, triangle — WASA-CELSIUS. Open circles — cross sections for $pn \to d\gamma$ deduced from MAMI data on the inverse reaction and scaled with a coefficient 1/20.

In the reaction with similar kinematics,

$$n + p \to d + \gamma, \tag{2}$$

the $M1$ multipole transition leads to strong enhancement of the cross section caused by excitation of the intermediate ΔN-baryon pair in an $^5S_1$ state. Such M-odd multipole transitions are forbidden in reaction 1 and hence there is no direct contribution from the S-wave ΔN states. Therefore, theoretical considerations advanced in the 90ths did not predict the enhancement of the reaction 1 cross section in the $\Delta(1232)$ range. This expectation has been supported by absence of the cross section bump in this energy region in the $^3\mathrm{He}(\gamma, pp)$ reaction data (TAGX, 1994), where the time-alternative of reaction 1, photodisintegration of the $^1S_0$ diprotons embedded in ^{3}He nuclei, was studied.
On the contrary, the ANKE measurement, free of any additional nucleon influence, reveals a strongly marked resonance behavior of the differential cross section for reaction 1 at small forward angles. The enhancement is even more evident than in reaction 2, as seen in Fig. 17. The shift of the peak position towards higher energies is apparently caused by the absence of the ΔN S-wave contribution in reaction 1. The other remarkable feature is a much lower reaction rate as compared to 2. This comparative behavior of reactions 1 and 2 is very similar to that observed in the Mainz experiments (1998) for the reactions $^{12}\mathrm{C}(\gamma, pp)$ and $^{12}\mathrm{C}(\gamma, np)$. This fact emphasizes importance of the elementary subprocesses of photon absorption by the nucleon pairs for correct determination of the short-range pp and np correlations in nuclei via the pair knockout by the electromagnetic probes, the old task revived last years.
There are strong reasons for further study of the hard bremsstrahlung process at COSY. Recently, a gauge-invariant formulation of the $NN \to NN\gamma$ processes, developed by H. Haberzett and K. Nakayama, resolved a long-term contradiction between the KVI data at 190 MeV and the attempts of their precise reproduction. This theory allows an extension from only nucleon currents consideration to the $N\Delta$ and $\Delta\Delta$ ones. In this respect, the recent ANKE results render a direct challenge for testing this perspective approach in the $\Delta(1232)$ region.
The ANKE experiments indicate COSY to be an effective tool to study the short-range interaction of the electromagnetic field with the pp pairs. Extension of experiments on hard bremsstrahlung to the highest COSY energies could allow investigation of this process in the region where the constituent counting rules were found to be valid for the $d(\gamma, np)$ reaction. The recent JEF LAB data on the $^3\mathrm{He}(\gamma, pp)$ reaction show that presence of the additional nucleon there seriously impedes analysis of the bound diproton photodisintegration just in this transition energy range. Reaction $pp \to \{pp\}_s\gamma$ is free of such complications.

1.2.8 Spin-dependent neutron-proton elastic amplitude studies

A good understanding of the Nucleon-Nucleon interaction still remains one of the most important goals of nuclear and hadronic physics. Apart from their intrinsic importance for the study of nuclear forces, *NN* data are necessary ingredients in the modelling of meson production and other nuclear reactions at intermediate energies. It goes without saying therefore that any facility that could make significant contributions to this important database should do so.

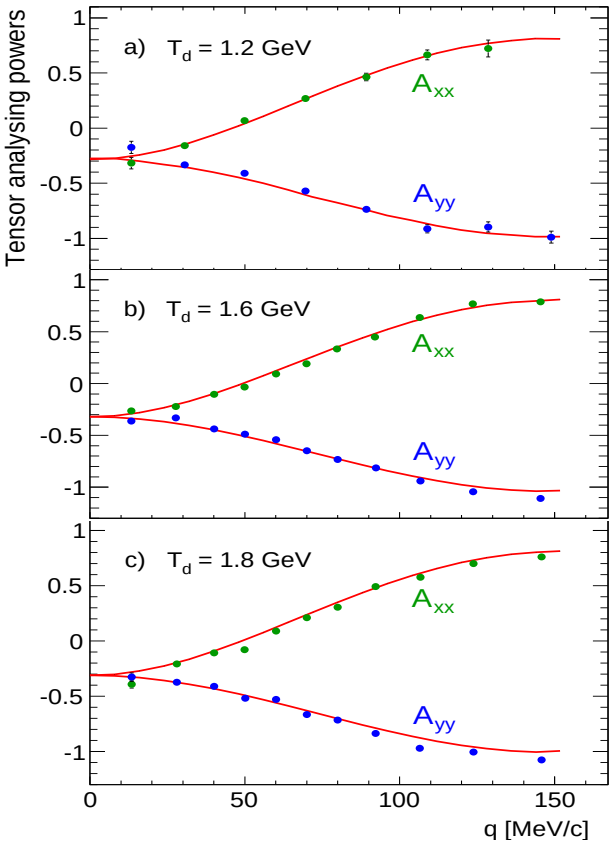

Fig. 18: Cartesian tensor analysing powers A_{xx} (green dots) and A_{yy} (blue dots) of the $dp \to \{pp\}_s n$ reaction at beam energies of $T_d = 1.2, 1.6$, and 1.8 GeV for low diproton excitation energy, $E_{pp} < 3$ MeV. The solid red curves are results of an impulse approximation calculation, where the input *np* amplitudes were taken from the SAID program at the appropriate energies.

The **ANKE** collaboration has embarked on a systematic program to measure differential cross sections, analysing powers, and spin correlation coefficients of the $\vec{d}\vec{p} \to \{pp\}_s n$ charge-exchange breakup reaction. The aim is to deduce the energy dependence of the spin-dependent *np* elastic amplitudes. By selecting two final protons with low excitation energy, typically $E_{pp} < 3$ MeV, the emerging diproton is dominantly in the $^1S_0$ state.
In impulse approximation the deuteron charge-exchange reaction can be considered as an $np \to pn$ scattering

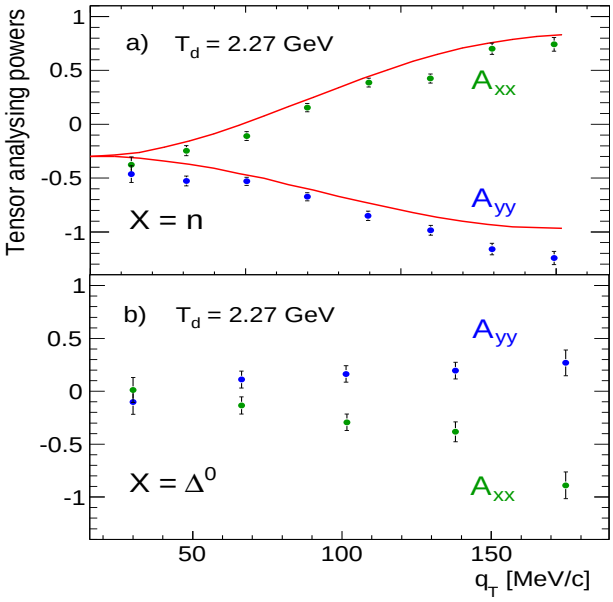

Fig. 19: Cartesian tensor analysing powers for the $dp \to \{pp\}_s X$ reaction at $T_d = 2.27$ GeV: with a neutron (a) or Δ^0 isobar (b) in the final state. In the Δ case the variable used is the transverse momentum transfer q_T. The red solid lines for the neutron are the results of an impulse approximation calculation.

with a spectator proton. The spin dependence of the *np* charge-exchange amplitude in the cm system can be displayed in terms of five scalar amplitudes as:

$$f_{np} = \alpha(q) + i\gamma(q)(\vec{\sigma}_1 + \vec{\sigma}_2)\cdot\vec{n} + \beta(q)(\vec{\sigma}_1\cdot\vec{n})(\vec{\sigma}_2\cdot\vec{n}) + \delta(q)(\vec{\sigma}_1\cdot\vec{m})(\vec{\sigma}_2\cdot\vec{m}) + \varepsilon(q)(\vec{\sigma}_1\cdot\vec{l})(\vec{\sigma}_2\cdot\vec{l}),$$

where α is the spin-independent amplitude between the initial neutron and final proton, γ is a spin-orbit contribution, and β, δ, and ε are spin-spin terms. In the $^1S_0$ limit of the impulse approximation, the $\vec{d}\vec{p} \to \{pp\}_s n$ observables are directly related to the *np* spin-dependent amplitudes through:

$$\begin{aligned}
\frac{d^4\sigma}{dt d^3k} &= \frac{1}{3} I \left\{ S^-(k, \tfrac{1}{2}q) \right\}^2, \\
I &= |\beta|^2 + |\gamma|^2 + |\varepsilon|^2 + |\delta|^2 R^2, \\
IA_y^d &= 0, \; IA_y^p = -2\mathrm{Im}(\beta^*\gamma), \\
IA_{xx} &= |\beta|^2 + |\gamma|^2 + |\varepsilon|^2 - 2|\delta|^2 R^2, \\
IA_{yy} &= |\delta|^2 R^2 + |\varepsilon|^2 - 2|\beta|^2 - 2|\gamma|^2, \\
IC_{y,y} &= -2\mathrm{Re}(\varepsilon^*\delta)R, \; IC_{x,x} = -2\mathrm{Re}(\varepsilon^*\beta),
\end{aligned}$$

where $R = \left\{ S^+(k, \frac{1}{2}q)/S^-(k, \frac{1}{2}q) \right\}^2$ and $S^\pm$ are form factors that can be evaluated using low energy *NN* information. Here $\vec{k}$ is the *pp* relative momentum in the diproton and $\vec{q}$ the momentum transfer between the deuteron and diproton.
Although corrections due to final *P*- and higher *pp* waves have to be taken into account in the detailed analysis, it is clear that in the low E_{pp} limit a measurement of the

differential cross section, A_{xx}, and A_{yy} would allow the extraction of $|\beta(q)|^2+|\gamma(q)|^2$, $|\delta(q)|^2$, and $|\varepsilon(q)|^2$ over a range of values of q.

For the above to be the realistic objectives, the methodology has to be checked in energy regions where the np amplitudes are reasonably well known. An extended paper (*D. Chiladze et al., Eur. Phys. J. A 40 (2009) 23*) has recently been published with this in mind. The new ANKE results for the deuteron Cartesian tensor analysing powers A_{xx} and A_{yy} at three beam energies are shown in Fig. 18 as functions of the momentum transfer. The agreement between the experimental data and the impulse approximation predictions obtained using the reliable SAID np amplitudes as input at $T_n = 600, 800, and 900$ MeV, is very encouraging. This success provides a motivation for repeating these measurements at higher energies where the np input is far less certain.

The maximum deuteron energy available at COSY is $T_d \approx 2.3$ GeV (1.15 GeV per nucleon) and the ANKE results for A_{xx} and A_{yy} near this energy are shown in Fig. 19a. The neutron-proton amplitudes are here not as well known and the deviations of the data from the predicted curves strongly suggest that there are deficiencies in the SAID values of the np amplitudes in this region.

The deficiencies of the SAID input np amplitudes at 1.135 GeV can be shown more explicitly by forming the following combinations of the observables:

$$\begin{aligned}(1-A_{yy})/(1+A_{xx}+A_{yy}) &\approx (|\beta|^2+|\gamma|^2)/|\varepsilon|^2,\\ (1-A_{xx})/(1+A_{xx}+A_{yy}) &\approx |\delta|^2/|\varepsilon|^2,\\ (1-A_{xx})/(1-A_{yy}) &\approx |\delta|^2/(|\beta|^2+|\gamma|^2).\end{aligned}$$

The variation of these quantities with q are presented in Fig. 20 for the 1.2 and 2.27 GeV data. Whereas at the lower energy all the ratios are well described by the model, at the higher it is seen that it is only $|\delta|^2/(|\beta|^2+|\gamma|^2$ which is well understood. It seems that the SAID program currently overestimates the values of $|\varepsilon|$ at small q. This will become clearer when absolute values of the cross sections are extracted at 2.27 GeV.

The final goal is to go to even higher energies by using a proton beam (available up to 3 GeV at COSY) incident on a polarised deuterium target, $pd \to \{pp\}_s n$. This could be very fruitful because so little is known about the spin dependence of the np charge exchange reaction much above 1 GeV.

In order to determine the relative phases of the spin-spin amplitudes $(\beta, \delta, \varepsilon)$ it is necessary to determine the spin correlation parameters $C_{x,x}$ and $C_{y,y}$. A large amount of data was successfully obtained from the first double-polarised neutron-proton scattering experiment at ANKE (*cf.* Annual Report 2009). The *preliminary* results for the vector-vector spin correlation coefficients in the $\vec{d}\vec{p} \to \{pp\}_s n$ reaction at T_d = 1.2 GeV are shown in Fig. 21, where they are seen to be in satisfactory agreement with impulse approximation predictions. The analysis of the higher energy data is in progress.

It was shown at Saclay that at $T_d = 2$ GeV the $\Delta(1232)$ isobar can be excited in the $\vec{d}p \to \{pp\}_s \Delta^0$ reaction and

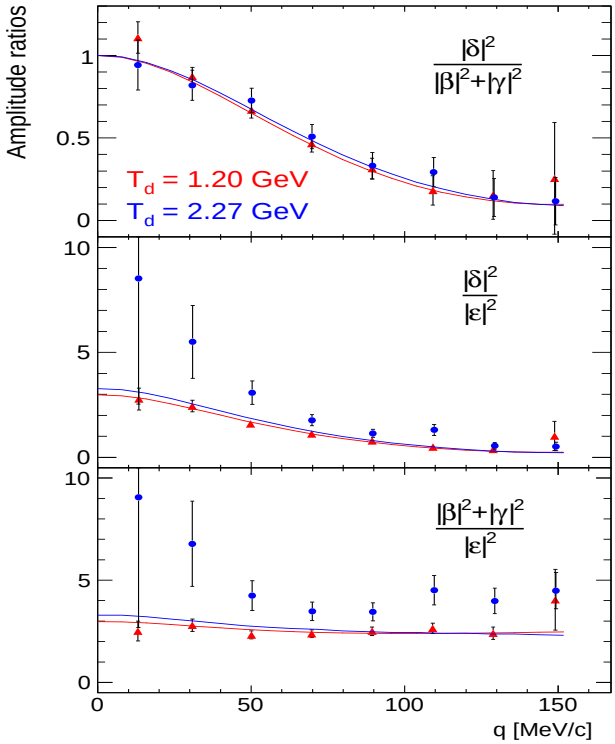

Fig. 20: Measured observable ratios as functions of q for two different beam energies. Solid lines are impulse approximation predictions.

substantial tensor analysing powers were measured. In impulse approximation, these are also sensitive to a spin-transfer from the neutron to the proton in $np \to p\Delta^0$. The Δ^0 is seen clearly also in the ANKE charge-exchange breakup data at 1.6, 1.8, and 2.27 GeV. The values of A_{xx} and A_{yy} deduced at 2.27 GeV and shown in Fig. 19b are very different to those measured for the 'normal' neutron breakup with even changes of the signs. ANKE will therefore also provide useful information on the spin structure of Δ excitation in neutron-proton collisions.

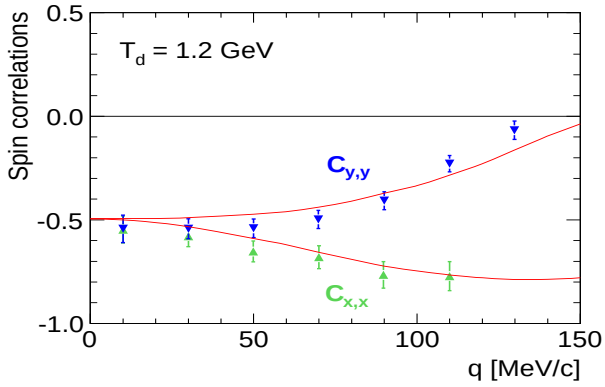

Fig. 21: Vector spin-correlation coefficients in $\vec{d}\vec{p} \to \{pp\}_s n$ reaction at $T_d = 1.2$ GeV. The red curves are the predictions of the impulse approximation calculation.

1.3 Developments for the Experimental Facilities

1.3.1 Status of the PAX Experiment

The activity of the PAX Collaboration during 2010 was focused on the preparation and the commissioning of the experimental apparatus for the spin-filtering studies in COSY. These studies were requested by the CERN-SPS Committee as an entrance card for the proposed measurements with antiprotons at AD. After installation in summer 2009, the four new quadrupoles, necessary for the implementation of the low beta section, have been successfully operated at COSY in January 2010. In summer 2010 the polarized Atomic Beam Source and the Breit-Rabi polarimeter, after assembling and commissioning in the LKW-Schleuse, have been moved and installed, together with the target chamber, at the PAX interaction point in COSY (Fig. 22).

Fig. 22: The PAX installation at COSY showing the newly installed quadrupoles (blue color and the support structure for the polarized source, the polarimeter and the target chamber.

An important achievement of the commissioning phase is the demonstration of the complete functionality of the openable storage cell concept (Fig. 23). Actually, the usage of such a cell opens new perspectives for increasing the luminosity of storage ring experiments.
The October 2010 beam time was dedicated to the commissioning of the complete experimental setup for the spin-filtering measurements at COSY. The first part of the beam-time was devoted to the optimization of the lifetime in the ring. The study has been stopped when a beam-lifetime higher than 6000 s was reached for the PAX optics. The minimal lifetime we aimed for the spin-filtering feasibility study at COSY was 5000 s. A movable frame system has then been installed at the PAX interaction point. The machine acceptance has been carefully measured, together with beam position and size. On the movable frame a round tube of 400 m length and 10 mm diameter, was also installed. With the tube in position, the injection efficiency in the ring was about 70%. With a start-

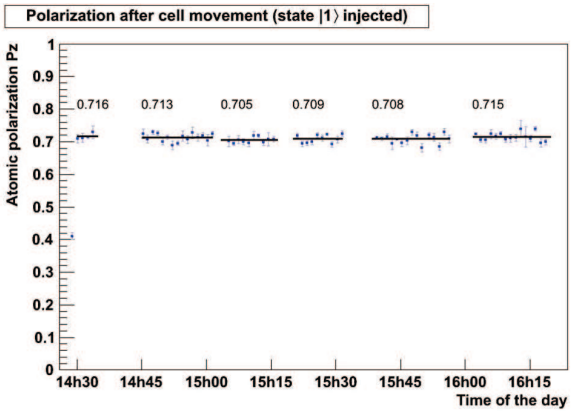

Fig. 23: Behaviour of the target polarization after various opening and closing procedures of the target cell: no change was evidenced.

ing value of $1.5 \cdot 10^{10}$ protons, more the $1 \cdot 10^{10}$ protons could be stored in the ring, which was the value aimed for the spin-filtering studies. The openable storage cell has then been installed and gas from the polarized atomic beam source has been injected. The measured lifetime in the ring was then measured to be 2000 s, below the mentioned necessary condition for the spin-filtering. The lifetime was dominated by the limited total pumping speed in the PAX chamber amounting to less than 2000 l/s. To properly pump the hydrogen gas in the target chamber we are designing and constructing a 15000 l/s NEG pump. The installation of this pump below the target chamber together with the activation of the NEG coating of the (already installed) beam tubes in the nearby section (which was not accomplished this time), should bring the necessary conditions to perform the spin-filtering studies.
The spin-filtering tests are planned for Fall 2011. Besides the mentioned polarized target setup at the PAX interaction point necessary for the spin-filtering, a beam polarimeter will be also implemented. For this purpose, two silicon telescopes will be installed at the cluster target of ANKE to exploit the analyzing power in proton-deuteron elastic scattering. Given the unfavourable experimental conditions presented by the COSY environment, a build-up rate of 0.0018 h is expected and the measurement will constitute by itself a severe challenge and a crucial test of the control of all the systematics involved.

2 COSY Operation and Developments

2.1 Beam Time at COSY

For 2010 in total 6888 hours of operation were scheduled. 4648 hours were scheduled for user beam time, 1296 hours were scheduled for dedicated beam dynamic studies and equipment tests for HESR, 944 hours were used for COSY machine development and experimental set-up, see Fig. 24. 404 hours were lost due to different technical breakdowns, mainly caused by faults in the RF-system of the cyclotron. For user beam times this results in an overall reliability of 94%. The distribution of user hours is listed in Table 1.

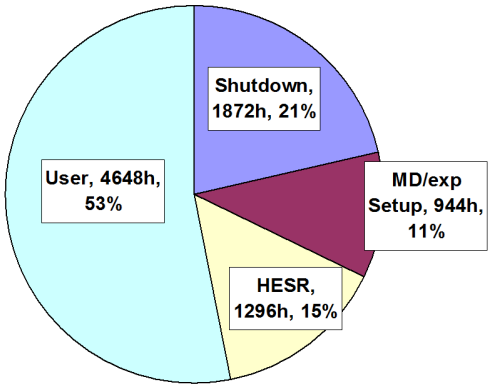

Fig. 24: COSY beam-time statistics. The scheduled beam time sums up to 6720 hours with a reliability of 98%.

Table 1: Overview over COSY user beam time in 2010.

Date	Experiment	Duration	Reaction, experiment #
15.01.10.–31.01.10	PAX	2 weeks	commissioning of mini-β-section, 199
12.02.–07.03.	WASA	3 weeks	$pp \to pp\eta$, 182.1
19.03.–04.04.	WASA	2 weeks	$pp \to pp\pi^0$, 196.1
23.04.–30.05.	WASA	5 weeks	$pp \to pp\eta$, 182.1
11.06.–20.06.	ANKE	1 week	pp elastic, 200
30.07.–29.08.	TOF	4 weeks	Strangeness Physics at COSY-TOF, 193.1
10.09.–26.09.	PAX	2 weeks	Lifetime optimization PAX, 199.1
15.10.–24.10.	PAX	1 week	Lifetime optimization PAX, 199.1
05.11.–14.11.	WASA	1 week	η-production, 185.1
26.11.–12.12.	WASA	2 weeks	Heη-bound state, 186.2
Total '10		23 weeks	

2.2 Performance of the Ionization Profile Monitor

The installation and successful commissioning of the Ionization Profile Monitor (IPM) at COSY is a result of collaborative effort of beam instrumentation groups at IKP and GSI. The IPM is meant to be a standard tool for future FAIR machines and thus has to satisfy a broad range of requirements. The conceptual design, developed at GSI, foresees two modes of operation: high resolution mode and turn-by-turn mode. Both rely on a detector consisting of an MCP stack and a luminescent screen. The high resolution mode based on detection of residual gas ions is implemented both at SIS18 and COSY. The turn-by-turn mode based on electron detection and fast photomultiplier readout is under development at GSI. The magnet system is being developed in collaboration between iThemba LABS, IKP and GSI.

The IPM is installed in COSY in the arc following the cooler telescope between dipoles 14 and 15. In its current configuration it is equipped with two GigE CCD cameras each capturing an 80 mm wide region inside the vacuum chamber resulting in the camera related spatial resolution of 0.125 mm. At full resolution of 640×480 pixels the cameras deliver frame rates up to 200 fps. Setting a smaller region of interest allows even higher rates. However, the DAQ rates are practically limited by camera exposure time which in turn depends on vacuum conditions, beam density and MCP gain. Generally, longer exposure times produce better signal to noise ratios at lower MCP gains that prolongs the MCP lifetime. Aging leads to inhomogeneous sensitivity distribution across the MCP surface. This problem is coped with by homogeneously irradiating the MCP surface with hard UV light and deriving correction functions. These are automatically taken into account for each time profile measurement. UV calibration is a 10 min procedure performed regularly. Camera aging is taken into account by recording the data without the beam and subtracting it from the beam profile data. The new device reliably delivers transverse beam profile data in real-time. Besides the profiles, the DAQ software, written in LabVIEW, directly displays the time evolution of the most important parameters like beam size and position in both transverse planes.

Figure 25 shows time evolution of the horizontal and vertical beam widths. The proton beam is injected at $t = 0$ s. The initial cooling with 170 mA of electron current is shown in the first region. This process is accompanied by initial losses, so the reduction of beam width is a result of cooling and beam loss. After the beam has reached equilibrium at $t \approx 30$ s, electron current was turned off allowing the beam size to grow (region 2). After another 30 s, electron current is turned on again, leading to fast decrease of beam size (region 3). In the fourth region emittance blow-up without electron cooling is shown again. No beam losses are observed after 10 s, corresponding to regions 2–4. An fit $y = y_0 + \exp(-(t-t_0)/\tau)$ was performed in region 3 corresponding to beam cooling. In region 4 exponential and linear fits were applied.

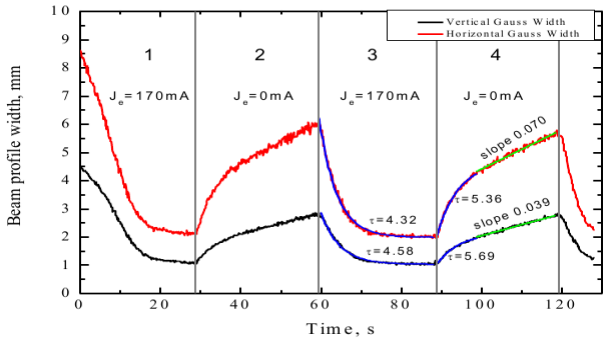

Fig. 25: Horizontal and vertical beam width (Gaussian standard deviation) plotted *vs.* time with electron cooling on and off. Beam intensity after initial losses amounted to about 5×10^9 protons, average vacuum in COSY was about 10^{-9} mbar. Profile snapshots are shown in Fig. 26.

The IPM was the main workhorse of the electron cooling beam studies carried out in April 2010 which were joined by the Novosibirsk and Dubna groups. The monitor delivered valuable data allowing detailed studies of the longitudinal and transverse cooling forces. The presence of horizontal dispersion at the IPM location was shown to be helpful for fine tuning of the electron cooler. Dedicated studies were also carried out on emittance evolution as a result of beam target interaction as well as transverse excitation of the beam. Up to now profiles were measured successfully in the beam intensity range of $1 \cdot 10^8 - 5 \cdot 10^{10}$ particles in the ring.

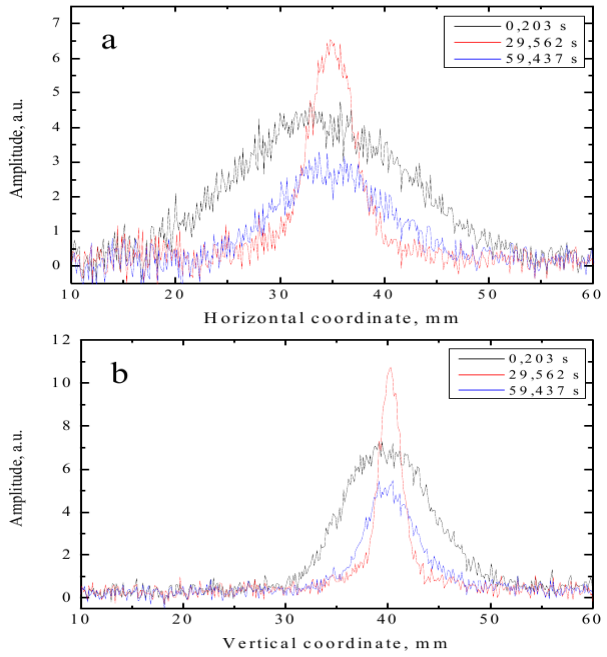

Fig. 26: Horizontal (a) and vertical (b) beam profiles after injection (0.2 s), at equilibrium after cooling (29.5 s) and after 30 s without cooling (59.4 s). Continuous evolution of beam width is shown in Fig. 25.

3 Further Experimental Activities

3.1 Level Shift in Pionic Deuterium

Pion-nucleon scattering lengths are accessible via X-ray spectroscopy of pionic hydrogen (πH) and deuterium (πD) where the strong s-wave interaction manifests in a level shift ε and broadening Γ of the atomic ground state 1s. In principle, a measurement of πH is sufficient, because of

$$\begin{aligned} \varepsilon_{1s}^{\pi H} &\propto a_{\pi^- p\to\pi^- p} = a^+ + a^- + \ldots \\ \Gamma_{1s}^{\pi H} &\propto (a_{\pi^- p\to\pi^0 n})^2 \propto (a^-)^2 + \ldots \end{aligned}$$

both quantities of interest — the isoscalar and isovector *pi*N scattering lengths a^+ and a^- — are extractable hereof by using Deser-type formulae. Ellipses stand for higher order corrections owing to the nature of the Coulomb bound state as well as strong and electromagnetic isospin- and non-isospin breaking terms, which may be calculated, *e.g.*, in the framework of chiral perturbation theory.

In pionic deuterium (πD) the leading order contribution for the hadronic shift is proportional to a^+.

$$\varepsilon_{1s}^{\pi D} \propto \Re a_{\pi D} + Coul.\,bound\,state\,corrections\,,$$

where

$$\begin{aligned} \Re a_{\pi D} &\propto a_{\pi^- p\to\pi^- p} + a_{\pi^- n\to\pi^- n} + \ldots \\ &= 2a^+ + \ldots . \end{aligned}$$

Ellipses stand here, in addition, for multiple scattering, absorptive, and few-body contributions which are assumed to be sufficiently well under control. Hence, $\varepsilon_{1s}^{\pi D}$ provides an effective constraint on a^+ and a^- when combining the triple $\varepsilon_{1s}^{\pi H}$, $\Gamma_{1s}^{\pi H}$, and $\varepsilon_{1s}^{\pi D}$, *cf.* Sect. 4.

X-rays from the πD$(3p-1s)$ transition (3075 eV) were measured at the high-intensity low-energy pion beam πE5 of the Paul Scherrer Institut using a Bragg spectrometer equipped with a spherically bent silicon crystal and an array of charge-coupled devices as position-sensitive X-raydetector. The energy calibration was performed using the Ga Kα_2 line (9224.484 ± 0.027 eV), which has in third order reflection the same Bragg angle as the πD line in first order (Fig. 27).

The πD$(3p-1s)$ transition was measured at three different densities adjusted by means of a cryogenic target cell in order to study possible radiative de-excitation after formation of molecules like $[(dd\pi)d]ee$ formed in πD + D_2 collisions. Such a de-excitation would manifest in a density dependence of the X-ray energy. The level shift is obtained from the difference of the measured and the calculated purely electromagnetic line energy.

Figure 28 shows the new results for $\varepsilon_{1s}^{\pi D}$ together with the values obtained in the two previous precision measurements. The values around 3 bar are about one standard deviation below suggesting an energy dependence on density. However, shifts are expected to be of opposite direction if caused by de-excitation of molecules and

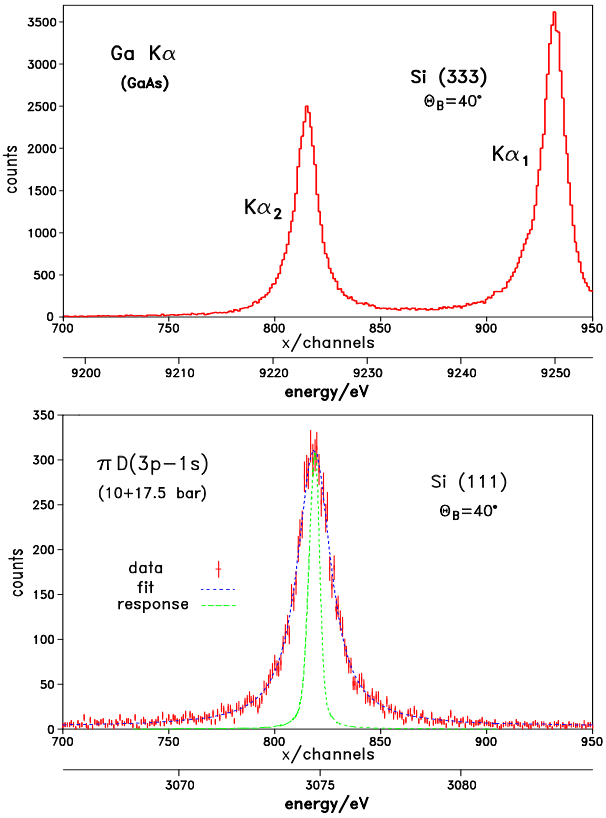

Fig. 27: Top – Ga Kα_2 calibration line. Bottom – πD$(3p-1s)$ transition (sum spectrum of the measurements at densities equivalent to 10 and 17.5 bar (STP). The narrow structure represents the response of the crystal spectrometer.

we assume this difference to be a statistical fluctuation. Weighted average of the measurements at 3.3, 10. and 17.5 bar equivalent density is

$$\varepsilon_{1s} = -(2356 \pm 31)\,\text{meV}. \qquad (3)$$

The negative sign indicates a repulsive interaction, *i.e.*, the strong interaction reduces the atomic 1s level binding energy. The error is dominated by the uncertainty of the Ga Kα_2 energy.

The real part of the πD scattering length is found to be

$$\Re a_{\pi D} = (-24.99 \pm 0.33)] \times 10^{-3}\, m_\pi^{-1}.$$

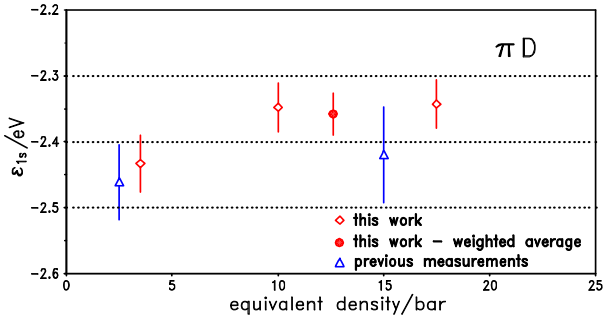

Fig. 28: Experimental results for the hadronic shift $\varepsilon_{1s}^{\pi D}$ in pionic deuterium.

3.2 Studies of Laser-Accellerated Protons

In recent years, the physics of laser-induced particle acceleration has undergone a vast development. Figure 29 reveals an increase of about 10 orders of magnitude in the achievable laser focus intensity over the last few decades and the corresponding characteristic energy of the plasma electrons. This development even dwarfs the remarkable growth of the achievable beam energies in hadron and e^+e^- colliders.

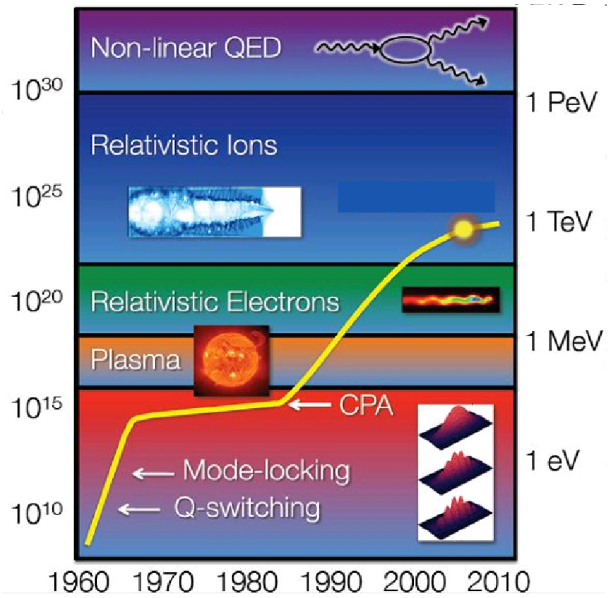

Fig. 29: Development of laser intensities and the corresponding characteristic electron energy during the last decades.

Conventional accelerator technology is about to reach fundamental and technological limits of the achievable particle energies. These limitations do not apply to laser-driven particle acceleration and hence the possible electron energies have increased rapidly into the GeV regime since the invention of the so-called chirped pulse amplification (CPA) in the mid-eighties.

Ti:sapphire laser systems, like the ARCturus Laser at Heinrich Heine University Düsseldorf (HHUD), operate at a pulse energy of a few J, compressed to a pulse length of values around 30 fs, reaching a pulse power of 100 TW and a focus intensity of approx. 10^{20} W/cm^2. To give a vivid impression of such intensities one may imagine the average intensity of sunlight illuminating the full surface of the earth, given by the solar constant of 1367 W/cm^2, focused on the tip of a pencil (0.1 mm^2). By directing such a high-intense laser pulse on a foil or a gas jet it is possible to ignite a plasma in the focus point. Plasma electrons are then driven from the target directly by the electromagnetic fields of the laser. The quasi-static electric fields produced by this charge separation can consecutively accelerate protons that are present in impurities of hydrocarbons on the surface of foil targets. For protons the maximum energy up-to-date is 58 MeV, produced at the NOVA PW laser system at Lawrence Livermore National Laboratory. Typical values of the maximum particle energies reached at the ARCturus facility are about 100 MeV for electrons and 10 MeV for protons.

However, fundamental and technological challenges still have to be overcome for the realization of reliable and continuously operating "table-top" accelerators. The particle beams typically are poly-energetic with a broad angular distribution. The repetition rate of high intense lasers is limited to about 10 Hz which also sets limits to the luminosity of these accelerators.

While the development of laser-induced particle accelerators is rigorously driven forward, it is yet a completely untouched issue whether the laser-generated beams are or can be spin-polarized. Since many high-energy and nuclear-physics experiments require polarized beams it is vital to investigate this possibility. This is a major goal of a joint working group of the IKP, the Jülich Supercomputing Centre and the Institut for Laser and Plasma Physics of HHUD.

During the acceleration of particles in laser-generated plasmas high magnetic fields are formed in and around the target, for example by the current of escaping hot electrons. These fields typically have values in the order of 10^4 T at the center of the laser focus and decrease over 10 or 20 μm radially away from the beam axis of the laser pulse, producing very high field gradients in the order of 10^{10} T/m. This is illustrated in Fig. 30, which shows the quasi-static magnetic field distributions simulated with a Particle-in-Cell code.

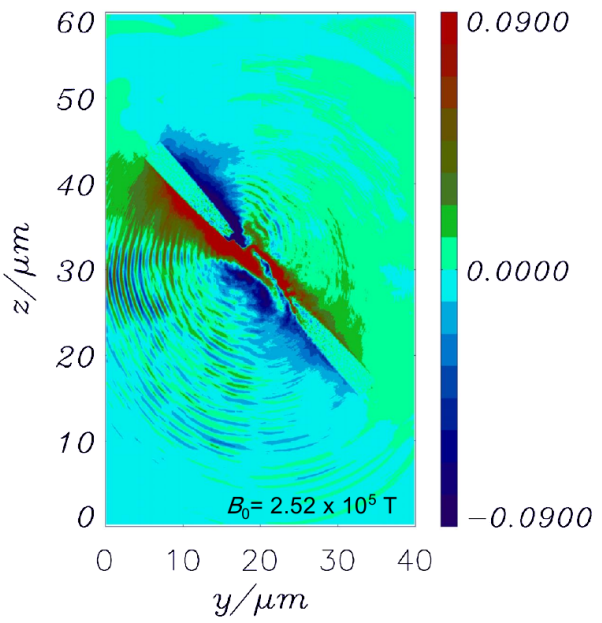

Fig. 30: Simulated magnetic field distribution for laser parameters resembling those of our measurements at the ARCturus laser ficilty. The target is gold foil of 3 μm thickness. The incident angle of the laser pulse is 45° to the target normal. The simulation has been performed on the JuRoPA parallel processor at the Jülich Supercomputing Centre.

Similar to the effect in a Stern-Gerlach apparatus one might expect the particles to encounter forces, that are quantized according to their spin orientation. However, a fundamental concern is the "thesis of Bohr", who stated that, due to the uncertainty principle, spin states of electrons, or any other charged particle, cannot be spatially separated by a magnetic force on the electron dipole moment. Bohrs argument stands true for protons as well, since it is based on the variation of the Lorentz force over the non-vanishing particle-beam size. On the other hand, in 2002 Garraway and Stenholm showed, that it is in principle possible to achieve spin-separation for charged particles under certain conditions, like a small beam diameter in the field region and a sufficiently long propagation time in an interaction-free region afterwards — conditions that may be fulfilled in laser-plasma experiments.

In case that the magnetic fields of the plasma do not effect the particle spins, this clears the way for a second scenario which is to use polarized targets. One may then expect that the produced beams carry a polarization in the order of magnitude of the initial target polarization.

Up to the present, neither with simulations nor experimentally, it has been investigated, whether the conditions during laser-induced acceleration meet the requirements leading to an observable spin-separation. To reverse this argument, an observation of polarized beams from laser-induced plasmas could settle the long-standing discussion whether the Stern-Gerlach effect is measurable also for charged particles.

For our measurements of the degree of polarization of the laser-accelerated protons, the spin dependence of elastic proton scattering off silicon nuclei is utilized. A setup has been developed and optimized for a proton energy range around 3 MeV, comprising a beam monitor, a set of aluminium and lead collimators, the secondary scattering target and CR-39 detectors. The complete setup is depicted in Fig. 31.

As rate monitor a stack of RadioChromic Films (RCF) is used that is located 2.5 cm away from the production target. These are self-developing films changing colour and optical density when irradiated by ionizing radiation. The RCF detectors are calibrated, so that a calculation of the deposited energy and, thus, of the particle flux from the colour depth is possible. Through a central hole with 0.5 cm diameter a part of the beam passes the RCF detectors and arrives at a first set of collimators. An aluminium collimator with an aperture of 1 mm a part of the beam is selected, thus defining the emission angle of the protons that are used for the polarization measurement. One centimeter behind this, the next collimator of aluminium with a thickness of 0.5 cm and an aperture of about 2 mm blocks secondary particles that are produced at the edges of the first collimator. For the scattering of the protons a silicon target of 24 μm thickness has been used. Differential cross sections and analyzing powers of the Si(p, p')Si reaction are provided by measurements at the Tandem accelerator at the University of Cologne in 1994.

The beam to be analyzed has an angular divergence of approx. 1° and hits the Si target in an area of 2 mm diameter. Behind the scattering target solid state nuclear track detectors of CR-39 are placed, which cover a scattering angle ϑ of up to 68° and the complete azimuthal range ϕ from 0° to 360°. These detectors have been chosen due to their insensitivity to the γ and X-ray background radiation from the plasma target. The setup was optimized during a first measurement in Spring 2010. Data with higher statistics, that should allow us to draw unambiguous conclusions about the degree of polarization of protons accelerated in foil targets, have been taken in Nov. 2010. These data is currently being analysed.

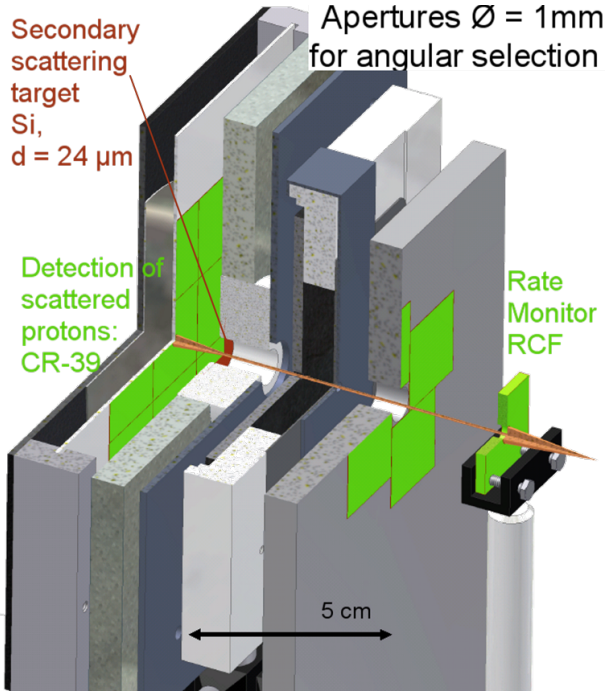

Fig. 31: Technical drawing of the setup for proton-polarization measurements.

In the long term, the study of ions accelerated in gas-jet targets is planned, since there is the possibility to use pre-polarized ^{3}He as target material. Acceleration of α particles from ^{4}He targets has already been observed, which is expected to work just as well for ^{3}He. During a usual ionization process the electrons are removed consecutively from the atom. The single ionized ^{3}He has a very short spin-polarization relaxation time, which is the reason why currently no polarized sources for ^{3}He ions are available. The strong electric fields of a high intense laser, however, might be able to remove the two electrons within a ps or less, sustaining the nuclear spin during the acceleration process.

3.3 Jülich EDM Search with Storage Rings

Although extremely successful in many aspects, the Standard Model of Particle Physics is not capable to explain the apparent matter-antimatter asymmetry of our universe, and thus fails to explain the basis for our existence, for it has way too little *CP*-violation. There are two strategies to hunt for physics beyond the Standard Model: one option is to explore highest energies, as presently done, *e.g.*, at the LHC. The other alternative is to perform experiments of ultimate precision that employ novel methods. Permanent electric dipole moments (EDMs) violate both time reversal and parity invariance, and are therefore *CP*-violating. Searches for permanent electric dipole moments of protons, deuterons and heavier nuclei provide highest sensitivity for the exploration of physics beyond the SM, thus possess an enormous physics potential. The reach in energy scale for finding new physics beyond the Standard Model is estimated to range up to 3000 TeV, way beyond that of the LHC. In turn, these searches require a long-term engagement (> 10 yr).

We are planning to search for EDM of the proton and other charged particles in a storage ring with a statistical sensitivity of $\approx 2.5 \times 10^{-29}$ e·cm per year, pushing the limits even further and with the potential of an actual particle-EDM discovery. It is, however, essential to perform EDM measurements on different targets with similar sensitivity in order to unfold the underlying physics, and in this way widen the window to new physics. While neutron EDM experiments are pursued at many different locations worldwide (wherever neutrons are available), no such measurements are conducted yet for proton and other light nuclei.

EDM searches of charged hadrons have hitherto been impossible, because of the absence of the required new class of storage rings. The new method proposed for these searches is based on the spin precession of magnetic and electric dipole moments in external electric and magnetic fields. Freezing the horizontal spin motion, *i.e.*, forcing the particles' spin to always point along the direction of motion, cancels the $(g-2)$ precession. For protons, this so-called magic momentum can be achieved using a storage ring that contains only electric fields (no magnetic elements, see Table 2); it corresponds to a Lorentz $\gamma = \sqrt{\frac{1}{G_p}+1}$, where $G_p = 1.792847$ is the proton G-factor, resulting in a proton beam momentum of 700.740 MeV/c (232.792 MeV). For d and ^{3}He the frozen spin concept requires additional magnetic fields (see Table 2). The spins of vertically polarized ions injected into an EDM ring can be rotated into the horizontal plane by turning on a solenoidal magnetic field in a straight section of the EDM ring and turning it off at the appropriate time. During a typical spin coherence time (SCT) of about 1000 s, the build-up of a vertical polarization component in the beam indicates the signal for a finite EDM of the orbiting particles.

COSY has a history of highly successful operation of cooled polarized beams and targets — in fact, COSY is a unique facility for spin physics with hadronic probes on a world-wide scale. Many foreign groups have exploited its capabilities, *e.g.*, the Spin-at-COSY and the dEDM collaboration. Over the years, the accelerator group and the two experimental institutes have acquired in-depth experience in polarized beam/target manipulation and polarimetry. The IKP-COSY environment, including the theoretical group is thus ideally suited for a major (medium-sized) project involving spin and storage rings as it will be required for the search for permanent electric dipole moments (EDM) of charged fundamental particles (*e.g.*, protons, deuterons, and other light nuclei). The proposed new machine employs radial electric and magnetic fields to steer the particle beam, magnetic or electric quadrupole magnets to form a strong focusing lattice (*e.g.*, FODO), and internal polarimeters to probe the particle spin state as a function of storage time. An RF-cavity and sextupole magnets will be used to prolong the SCT of the beam. For protons, for example, a storage ring with highly uniform radial E-field with strength of ≈ 17 MV/m between stainless steel plates 2 cm apart must be designed. The bending radius of such a machine will be ≈ 25 m, and including the straight sections, it will have a physical radius of ≈ 30 m.

Table 2: Parameters for the transverse electric and magnetic fields required for an EDM storage rings of radius $r = 30$ m.

Particle	p (GeV/c)	E (MV/m)	B (T)
Proton	0.701	16.798	0.000
Deuteron	1.000	−3.983	0.160
^{3}He	1.285	17.158	−0.051

In Table 3, we give current and anticipated EDM bounds and sensitivities for nucleons, atoms, and the deuteron. The last column provides a rough measure of their probing power relative to the neutron (d_n). It should be noted that the proposed proton and deuteron EDM measurements will be an order of magnitude more sensitive than the currently planned neutron EDM experiments at SNS (Oak Ridge), ILL (Grenoble-France), and PSI (Villigen, Switzerland).

A measurement of the EDM of the proton using a purely electrostatic storage ring has been proposed by the Storage Ring EDM (srEDM) Collaboration and was recently approved by the program advisory committee of Brookhaven National Laboratory (BNL). Physicists of the IKP in Jülich, together with the SREDM Collaboration and the neighboring universities (RWTH Aachen, University Bonn, and others), are currently working on the development of a different concept for a dedicated storage ring that allows for the study of EDMs of proton, deuteron, and ^{3}He in one and the same machine.

Table 3: Current EDM limits in units of [e·cm], and long-term goals for the neutron, ^{199}Hg, ^{129}Xe, proton, and deuteron are given here. Neutron equivalent values indicate the EDM value for the neutron to provide the same physics reach as the indicated system.

Particle	Current Limit	Goal	d_n equiv.
Neutron	$< 1.6 \times 10^{-26}$	$\approx 10^{-28}$	10^{-28}
^{199}Hg	$< 3.1 \times 10^{-29}$	10^{-29}	10^{-26}
^{129}Xe	$< 6.0 \times 10^{-27}$	$\approx 10^{-30} - 10^{-33}$	$\approx 10^{-26} - 10^{-29}$
Proton	$< 7.9 \times 10^{-25}$	$\approx 10^{-29}$	10^{-29}
Deuteron		$\approx 10^{-29}$	$3 \times 10^{-29} - 5 \times 10^{-31}$

4 Theoretical Investigations

Introduction

The IKP theory group studies the strong interactions in their various settings — spanning topics in hadron structure and dynamics, the nuclear many-body problem and high-energy Quantum Chromodynamics (QCD). The main focus is on the formulation and application of effective field theories for precision hadron and nuclear physics based on the symmetries of QCD. A shift of focus with more emphasis on high performance computing is presently taking place, spear-headed by the work on nuclear lattice simulations. Within the virtual institute on "Spin and strong QCD" work focuses on applications for physics at COSY and FAIR. Some of the high-lights of these activities are discussed in the following.

4.1 The πd scattering length and its implications for the pion-nucleon coupling

Pion-nucleon scattering offers some of the best tests of the QCD chiral dynamics. For that, it is mandatory to extract the scattering lengths with high precision from data, being able to cleanly separate strong and electromagnetic contributions. An important ingredient to this problem is πd scattering, which has been studied theoretically already for many decades using phenomenological approaches. Nowadays, however, the high accuracy of modern experiments calls for improved tools for the analysis. Especially, a consistent treatment of strong and electromagnetic few-body effects is essential for a controlled extraction of the quite small isoscalar pion-nucleon scattering length a^+. The values for the hadronic scattering lengths are best deduced from high accuracy measurements of pionic atoms together with properly improved Deser-type formulae, that relate the atomic energy shift and width to combinations of the scattering lengths in a well-defined and precise manner. We have performed a calculation of the $\pi^- d$ scattering length with an accuracy of a few percent using chiral perturbation theory including virtual photons. At the end it turns out that most of the additional contributions from soft photons as well as nucleon recoils cancel pairwise. The cancellation pattern can be largely understood as a result of the Pauli principle at work for the intermediate two-nucleon states. Thus, already the leading diagram, pion double scattering, largely exhausts the value of the πd scattering length. The numerically most important corrections are provided by an isospin violating piece to the πN scattering length and the triple scattering diagram. In addition, from pionic atoms it is not possible to extract a^+ directly, but only the combination

$$\tilde{a}^+ \equiv a^+ + \frac{1}{1+M_\pi/m_N}\left\{\frac{M_\pi^2 - M_{\pi^0}^2}{\pi F_\pi^2} c_1 - 2\alpha f_1\right\},$$

with F_π for the pion decay constant, $M_\pi (m_N)$ the charged pion (nucleon) mass and c_1 and f_1 are dimension two strong and electromagnetic low-energy constants, in order. The combined analysis for pionic hydrogen and pionic deuterium data (cf. Sect. 3.1) yields from the 1σ error ellipse (cf. Fig. 32) in units of $10^{-3} M_\pi^{-1}$

$$\tilde{a}^+ = (1.9 \pm 0.8)\ , \quad a^- = (86.1 \pm 0.9)$$

with a correlation coefficient $\rho_{a^-\tilde{a}^+} = -0.21$. An important ingredient to arrive at this result is the fact that the inclusion of the πD energy shift reduces the uncertainty of $\tilde{a}^+$ by more than a factor of 2. Note that in the case of the πH level shift the width of the band is dominated by the theoretical uncertainty in $\Delta\tilde{a}_{\pi^- p}$, whereas for the πH width the experimental error is about 50 % larger than the theoretical one. The final result for $a^+ = 7.6 \pm 3.1$ is only a little larger than several of the contributions considered in our analysis. Still, this is the first determination of a^+ with a definite sign with 2.5σ certainty. This emphasizes the importance of a systematic ordering scheme, and a careful treatment of isospin violation and three-body dynamics. A reduction of the theoretical uncertainty beyond that of the present analysis will be hard to achieve without additional QCD input that helps pin down the unknown contact-term contributions in both the πN and πNN sectors.

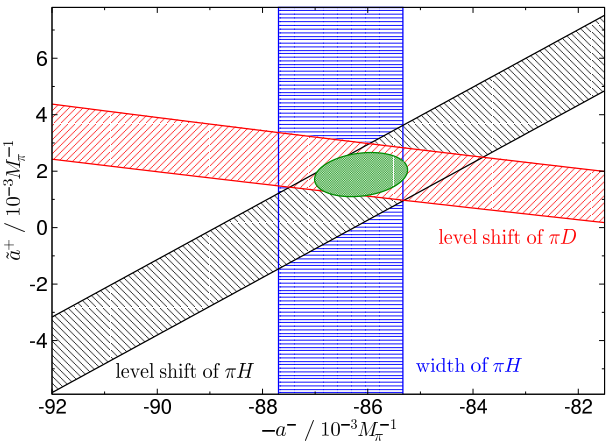

Fig. 32: Combined constraints in the $\tilde{a}^+$–a^- plane from data on the width and energy shift of πH, as well as the πD energy shift.

The pion-nucleon scattering lengths further provide an important link between pion-nucleon and nucleon-nucleon scattering and in this sense a non-trivial consistency check for our current understanding of these fundamental reactions. There has been some controversy of the precise value of the pion-nucleon coupling constant g_c in the past. The most recent extraction of g_c from πN data from the GWU group is $g_c^2/4\pi = 13.76 \pm 0.03$. The Nijmegen group has extracted its value from NN scattering, $g_c^2/4\pi = 13.54 \pm 0.05$. In both these determinations the error is largely statistical and does not include all possible systematic uncertainties. The present work does give a significant contribution to this question utilizing the time-honored Goldberger-Miyazawa-Oehme (GMO)

sum rule. The GMO sum rule was used before to pin down the value of g_c, however, different analyses came to different answers. There were no further developments in the last three years. The basic improvements provided by the analysis discussed are that for the first time isospin violating corrections were included completely and consistently and, as the result of using a systematic effective field theory, it became possible to properly control the uncertainties of the πN scattering lengths. With the in this way improved input we find

$$g_c^2/4\pi = 13.69 \pm 0.12 \pm 0.15 = 13.7 \pm 0.2 \,,$$

where the first error gives the uncertainty in the scattering lengths and the second in the integral. From our analysis we therefore conclude that a value for $g_c^2/4\pi$ above 14 is largely excluded.

4.2 New insight into the nucleon electric dipole form factors

The neutron electric dipole moment (nEDM) is a sensitive probe of CP violation in the Standard Model and beyond. The current experimental limit $d_n \leq 2.9 \cdot 10^{-26}\, e\,\text{cm}$ is still orders of magnitude larger than the Standard Model prediction due to weak interactions. However, in QCD the breaking of the $U(1)_A$ anomaly allows for strong CP violation, which is parameterized through the vacuum angle θ_0. Therefore, an upper bound on d_n allows to constrain the magnitude of θ_0. New and on-going experiments with ultracold neutrons strive to improve these bounds even further. On the theoretical side, first full lattice QCD calculations of the neutron and the proton electric dipole moment are becoming available. These require a careful study of the quark mass dependence of the nEDM to connect to the physical light quark masses. In addition, there is a BNL proposal to measure the proton and the deuteron EDM in a storage ring and there are also plans to build such type of machine in Jülich. It is thus of paramount interest to improve the existing calculations of these fundamental quantities in the framework of chiral perturbation theory, This was recently done. The calculation is based on $U(3)_L \times U(3)_R$ covariant baryon chiral perturbation and includes *all* diagrams contributing at one loop order. Besides the standard expansion in small momenta and quark masses, an additional expansion in $1/N_C$, with N_C the number of colors, is utilized. The nucleon matrix element of the electromagnetic current in the presence of strong CP-violation is given by

$$\langle p'|J^\nu_{em}|p\rangle = \bar{u}(p')\Big[\gamma^\nu F_1(q^2) - \frac{i}{2m}\sigma^{\mu\nu}q_\mu F_2(q^2) - \frac{1}{2m_N}\sigma^{\mu\nu}q_\mu\gamma_5 F_3(q^2) + \ldots\Big]u(p)$$

with $q_\mu = (p'-p)_\mu$. Here, F_1 and F_2 denote the P-, CP-conserving Dirac and Pauli form factors, m_N is the mass of the nucleon, and F_3 the P- and CP-violating electric dipole form factor. The ellipsis denotes the anapole form factor that we do not consider here. The electric dipole moment of the neutron/proton and the corresponding electric dipole radii follow as:

$$d_{n,p} = \frac{F_{3,n,p}(0)}{2m}\,, \quad \langle r^2_{ed}\rangle = 6\frac{dF_3(q^2)}{dq^2}\bigg|_{q^2=0}\,.$$

The most interesting results of our study are: 1) a bound for the vacuum angle could be given, $|\theta_0| \lesssim 2.5 \times 10^{-10}$. 2) the chiral expansion of the electric dipole radii takes the form (where δ denotes a genuine small parameter)

$$\begin{aligned}\langle r^2_{ed}\rangle_n &= -20.4\,\big[1 - 0.67 + O(\delta^2)\big]\;\theta_0\, e\,\text{fm}^2\,,\\ \langle r^2_{ed}\rangle_p &= +20.9\,\big[1 - 0.70 + O(\delta^2)\big]\;\theta_0\, e\,\text{fm}^2\,, \quad (4)\end{aligned}$$

where the large contribution of the NLO correction can be traced back to an enhancement of the pion loop effect due to an extra factor of π, similar to what was observed in the analysis of the isospin-violating nucleon form factors. 3) to compare results from (two-flavor) lattice QCD at unphysical quark masses with predictions from chiral perturbation theory, it is necessary to perform an extrapolation of the analytic results in the pion mass. In Fig. 33 we show the resulting pion (quark) mass dependence of the loop contribution to the neutron electric dipole moment in comparison to the available data points from two-flavor lattice QCD. It is interesting to see that the complete one-loop calculation (solid line) reproduces the trend of the lattice data (the order of magnitude and the global sign) even without the unknown tree contribution, quite in contrast to the leading one-loop contributions (dot-dashed line). However, only below pion masses of the order of about 400 MeV the corrections are sufficiently small for a stable chiral extrapolation as indicated by the theoretical uncertainties also shown in Fig. 33.

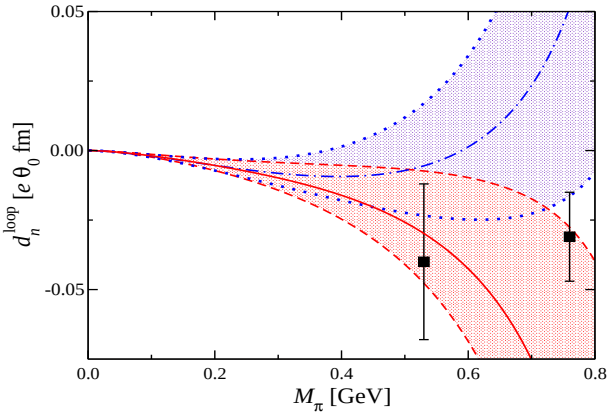

Fig. 33: Chiral extrapolation of the loop contribution to d_n. Dot-dashed line (with dotted borderlines): leading one-loop result, solid line (with dashed borderlines): full one-loop result. For comparison, some lattice data are large pion masses are shown.

4.3 Lattice simulations for light nuclei

Since a few years, we have started a systematic study of light nuclei and neutron matter combining methods from chiral effective field theory (EFT) and Monte Carlo simulations to solve the nuclear few- and many-body problem. The state-of-the-art nuclear lattice simulations are performed at next-to-next-to-leading order (NNLO) in the chiral expansion including strong and electromagnetic isospin violation (the Coulomb force between protons). At this order, one has 9 isospin symmetric four-nucleon low-energy constants (LECs) that can be determined from a fit to the *np* S- and P-wave phase shifts. Two further isospin-violating 4*N* LECs are fixed from the *nn* and *pp* S-wave scattering lengths. In addition, at this order one has the leading contributions to the three-nucleon forces. These contain two LECs that are fixed from the triton binding energy and the *nd* doublet scattering length. A first prediction is then the momentum dependence of the proton-proton $^1S_0$ phase shift, which is rather well reproduced. A parameter-free prediction for the energy difference between the triton and ^{3}He can also be given, $E(^3\mathrm{H}) - E(^3\mathrm{He}) = 0.78(5)$ MeV, in good agreement with the empirical value of 0.76 MeV. In the calculation of nuclei with four or more nucleons, the largest theoretical error at NNLO is generated from the configuration when four nucleons are located on the same lattice site, leading to a clustering instability when no smearing of the nucleon fields is applied. This can be simulated by adding an effective for-nucleon operator to the effective potential and fixing its strength from the binding energy of ^{4}He. With that, we are able to predict the ground-state energy of ^{6}Li and ^{12}C. making use of JUGENE at the JSC. The ground-state energies of ^{6}Li and ^{12}C are calculated as

$$\begin{aligned} E(^6\mathrm{Li}) &= -32.9(9)\ \mathrm{MeV}\ , \\ E(^{12}\mathrm{C}) &= -99(2)\ \mathrm{MeV}\ , \end{aligned}$$

not far from the empirical values of -32.0 and -92.2 MeV, respectively, cf. also Fig. 34. These numbers are obtained at finite volumes of $V = (9.9\ \mathrm{fm})^3$ and $V = (13.8\ \mathrm{fm})^3$, respectively, so that one expects a further reduction of the magnitude of the binding energies in the infinite volume limit. This issue is presently under investigation. The accuracy obtained is comparable to other so-called ab initio calculations (like the no-core-shell-model or Greens function Monte Carlo), that often are based on a less consistent formulation of the underlying nuclear forces. We are presently working on improving the lattice action and extracting signals of excited states, in particular the Hoyle state in ^{12}C.

4.4 The light quark mass ratio from bottomonia transitions

Although fundamental parameters of the Standard Model, the masses of light quarks have not been well determined. The is due to the fact that the light quark

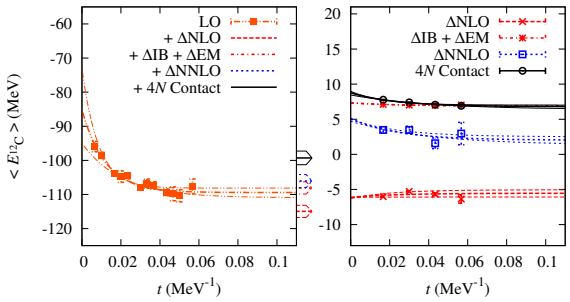

Fig. 34: Left panel: Ground-state energy of ^{12}C as a function of Euclidean time. Right panel: Various contributions to the ground-state energy.

masses are a significantly lighter than the typical hadronic scale and as such their impact on most of the hadron masses is very small. As a consequence of the spontaneous chiral symmetry breaking, the low-energy region of QCD can be described by chiral perturbation theory (CHPT). The most direct way is to relate the light quark masses to the masses of the lowest-lying pseudoscalar mesons, which are the Goldstone bosons of the spontaneous chiral symmetry breaking of QCD. To leading order (LO) in the chiral expansion, one may express the ratio of the masses of the *u* and *d* quarks as

$$\frac{m_u}{m_d} = \frac{M_{K^+}^2 - M_{K^0}^2 + 2M_{\pi^0}^2 - M_{\pi^+}^2}{M_{K^0}^2 - M_{K^+}^2 + M_{\pi^+}^2} = 0.56\ . \qquad (5)$$

In the above equation, the electromagnetic effects have been taken into account according to Dashen's theorem. There might be sizable higher order corrections to this LO result. The isospin breaking decays of the eta into three pions may also be used to extract the quark mass ratio, however, it is known to be subject to huge rescattering corrections. The up-to-date knowledge of the light quark mass ratio from various sources including recent lattice calculations was summarized by Leutwyler as

$$m_u/m_d = 0.47 \pm 0.08\ .$$

In a completely independent approach it was proposed to use the decays ψ' into $J/\psi\pi^0$ and $J/\psi\eta$, which break isospin and SU(3) symmetry, respectively. It was assumed that these decays are dominated by the emission of soft gluons, and the gluons then hadronize into a pion or an eta. Using the QCD multipole expansion (QCDME), one obtains

$$\frac{\Gamma(\psi' \to J/\psi\pi^0)}{\Gamma(\psi' \to J/\psi\eta)} = 3\left(\frac{m_d - m_u}{m_d + m_u}\right)^2 \frac{F_\pi^2}{F_\eta^2}\frac{M_\pi^4}{M_\eta^4}\left|\frac{\vec{q}_\pi}{\vec{q}_\eta}\right|^3\ , \qquad (6)$$

where $F_{\pi(\eta)}$ and $M_{\pi(\eta)}$ are the decay constant and mass of the pion (eta), respectively, and $\vec{q}_{\pi(\eta)}$ are their momenta in the ψ' rest frame. These two decays were then widely used in determining the quark mass ratio. Using the most recent measurement of the decay widths from the CLEO

Collaboration, one gets $m_u/m_d = 0.40 \pm 0.01$, which is much smaller than the one resulting from the meson masses in Eq. (5). If using the measurement by the BES Collaboration, the resulting value $m_u/m_d = 0.35 \pm 0.02$ is even smaller. Recently we found that these inconsistencies in the value for m_u/m_d from different sources is due to an incomplete treatment of the charmonium decays within the QCDME. It was demonstrated that, relative to the tree level contributions considered so far, there are in addition long-ranged heavy meson loop contributions and, for the mentioned transitions, those are even enhanced. Thus, Eq. (6) is afflicted by large corrections and the corresponding amplitudes are more sensitive to heavy meson mass differences rather than the quark masses directly. It can also be shown that the importance of these heavy meson loops is closely connected to the quantum numbers of the charmonia involved in the transitions. Especially, in cases where the angular momentum of the charmonium gets changed, the loops are typically suppressed. Unfortunately, within the limited energy range, where the effective field theory used applies, there is no such transition between charmonia that at the same time allows for a transition into a π^0 and into an η.

The situation is markedly different in the bottomium sector: we proposed as a new method to extract the light quark mass ratio to use the transitions between bottomonia, *i.e.*, $\Upsilon(4S) \to h_b \pi^0(\eta)$. This formula is similar to the one for charmonia decays discussed above but is not afflicted by large corrections from heavy meson loops. This is largely due to the extremely small B-meson mass splitting, $M_{B^0} - M_{B^+} = (0.33 \pm 0.06)$ MeV, which is due to an destructive interference effect between strong and electromagnetic contributions. The estimated uncertainty of this determination of the quark mass ratio $(m_d - m_u)(m_s + \hat{m})/(m_d + m_u)/(m_s - \hat{m}) \simeq (m_d - m_u)/(m_d + m_u)$, with $\hat{m}$ the average light quark mass, is about 23%. As a side result our work identified the decay branch $\Upsilon(4S) \to h_b \eta$ as a promising discovery channel for the h_b. To confirm the scheme described it is important to test the predictions from the effective field theory used also for other transitions. Especially, we predicted a large number of branching ratios for charmonium transitions. Those measurements could be performed at Belle, BES-III or PANDA.

4.5 Kaon-Sigma production in pion-nucleon scattering

The reaction $\pi^+ p \to K^+ \Sigma^+$ provides access to a pure isospin $I = 3/2$ two-body reaction channel in meson-nucleon dynamics. Moreover, the weak decay $\Sigma^+ \to p\pi^0$ allows to determine the polarization of the produced Σ^+. In the 1980's, Candlin et al. measured differential cross sections and polarizations at the Rutherford Appleton Laboratory, performed a partial wave analysis, and extracted resonance parameters which show significant differences from the ones obtained from pion-nucleon reactions. The spin-rotation parameters which correlate the spin of the target proton and the spin of the produced Σ^+ were measured at CERN-SPS by Candlin et al. in 1988, and were found to be in disagreement with the predictions based on the partial wave analysis. We have performed a first combined analysis of the reactions $\pi N \to \pi N$ and $\pi^+ p \to K^+ \Sigma^+$ within the Jülich coupled reaction channels approach, which respects analyticity and two-body unitarity and uses SU(3) flavor symmetry in the effective Lagrangians which determine the coupling strengths of the interacting hadrons. The different partial waves are related via the t- and u-channel hadron exchanges which provide a theory of the non-resonant background and thus impose strong restrictions on the free parameters.

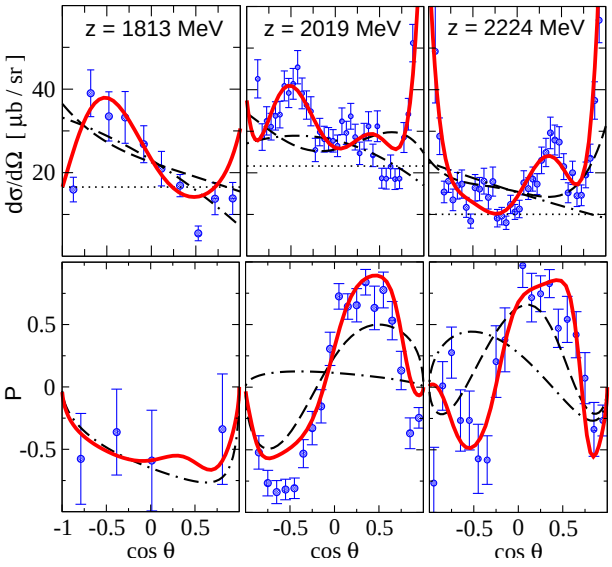

Fig. 35: Differential cross sections and polarizations of the reaction $\pi^+ p \to K^+ \Sigma^+$ for three energies (solid red line). Contributions from S-, S+P-, and S+P+D-waves are shown by the dotted, dash-dotted, and dashed lines, respectively.

In Fig. 35, the differential cross sections and polarization data are compared with the results of the Jülich model. Near threshold (at a cms energy of $z = 1813$ MeV), the interference between S- and P-waves suffices to reproduce the polarization data, but fails to describe the cross section at backward angles. At higher energies, S-, P-, and D-waves by themselves are unable to reproduce the data, contributions from higher partial waves are clearly required. The spin-rotation parameters are compatible with the present approach, see Fig. 36. Note that the spin-rotation parameter is cyclic with a period of 2π, which leads to an ambiguity in its determination as displayed by the filled and empty circles.

Resonance masses and widths are obtained by analytic continuation of the amplitudes into the relevant Riemann sheets and subsequent pole searches. The partial wave analysis of pion-nucleon data performed by the George Washington University group does not find evidence for a $\Delta(1920)P_{33}$ resonance. In contrast, the present analysis finds a mass of 1884 MeV and a width of 229 MeV, thus

pointing out the importance of a coupled channel analysis in the energy region above the first resonance. Indeed, the $\Delta(1920)P_{33}$ resonance nicely illustrates Isgur's concept of *the missing resonances*, as it is weakly coupled to elastic the pion-nucleon channel. The present approach finds no evidence for the $\Delta(1900)S_{31}$ and $\Delta(1940)D_{33}$ which are listed as resonance candidates by the Particle Data Group.

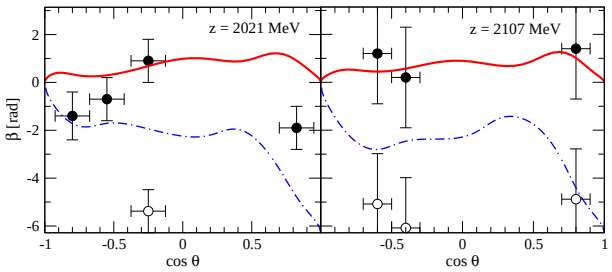

Fig. 36: Spin rotation parameter for $\pi^+ p \to K^+ \Sigma^+$. Solid line: present model; dash-dotted line: Candlin et al.

5 Anti-Proton Accumulation in the HESR

Detailed theoretical studies of stochastic cooling have been performed in order to fulfil the requirements for the $\overline{\text{P}}$ANDA internal target experiment at the High-Energy Storage Ring (HESR) of the future International Facility for Antiproton and Ion Research (FAIR) at the GSI in Darmstadt. A Fokker-Planck model and a particle tracking code for the Filter and time-of-flight momentum cooling method including a model for the signal transfer from pickup to kicker have been developed and applied to predict the momentum cooling performance of the 2 to 4 GHz cooling system. A barrier bucket cavity has been included in the model to compensate the mean energy loss due to the beam-target interaction. In a series of experiments the Fokker-Planck code including the beam-target interaction has been experimentally verified at the cooler synchrotron COSY.

In view of the budget limitation the construction of the RESR is postponed in the modularized start version of FAIR and instead it is proposed to include the anti-proton accumulation function in the HESR downstream of the Collector Ring (CR), the pre-cooling ring of the anti-proton beam. The accumulation of anti-protons can be accomplished with the stochastic stacking method developed and well established at CERN and FNAL (*cf.* F. Caspers and D. Möhl, Stacking with Stochastic Cooling, CERN-AB-2004-028 RF). This method requires pickups positioned in a region with large dispersion where the orbits of the injected and already stacked beam can be separated. A large horizontal acceptance is thus required. A sophisticated stochastic cooling system with a cooling force decaying radially with an exponential gain profile from the injection position to the stack top is necessary. Applying this accumulation scheme would result in a completely new and additional cooling system in the HESR. Instead a different way of beam accumulation has been selected that uses the already designed stochastic cooling system and the barrier bucket (BB) cavity of the HESR. The BB cavity is used to separate the circumference of the HESR ring into two regions, one reserved for the injected beam and the other one for the accumulated beam. Beam cooling is used to move the beam from the injection area into the accumulation area.

The accumulation process assisted by stochastic cooling was studied in detail with a particle tracking code (*cf.* T. Katayama and H. Stockhorst, Internal Rep. Dec. 2010, FZJ). It includes the synchrotron motion of anti-protons in the RF field induced by the barrier cavity, the stochastic cooling force, diffusion forces such as Schottky diffusion, thermal diffusion and Intra-Beam-Scattering effects. In this report the two cases fixed barrier and the moving barrier bucket will be presented. In the first method two half waves of barrier voltages are produced within one revolution period to create an unstable and stable area. The beam delivered from the CR every 10 s with 10^8 anti-protons and a rms relative momentum spread of $5 \cdot 10^{-4}$ is injected into the unstable area. Due to synchrotron motion the particles move outside around the stable area in phase space (τ, ΔE) as shown after 1 s in Fig. 37. Stochastic cooling which is permanently switched on cools these particles into the stable area. As is seen in the figure almost all particles are confined and significantly cooled in the stable area after 9 s.

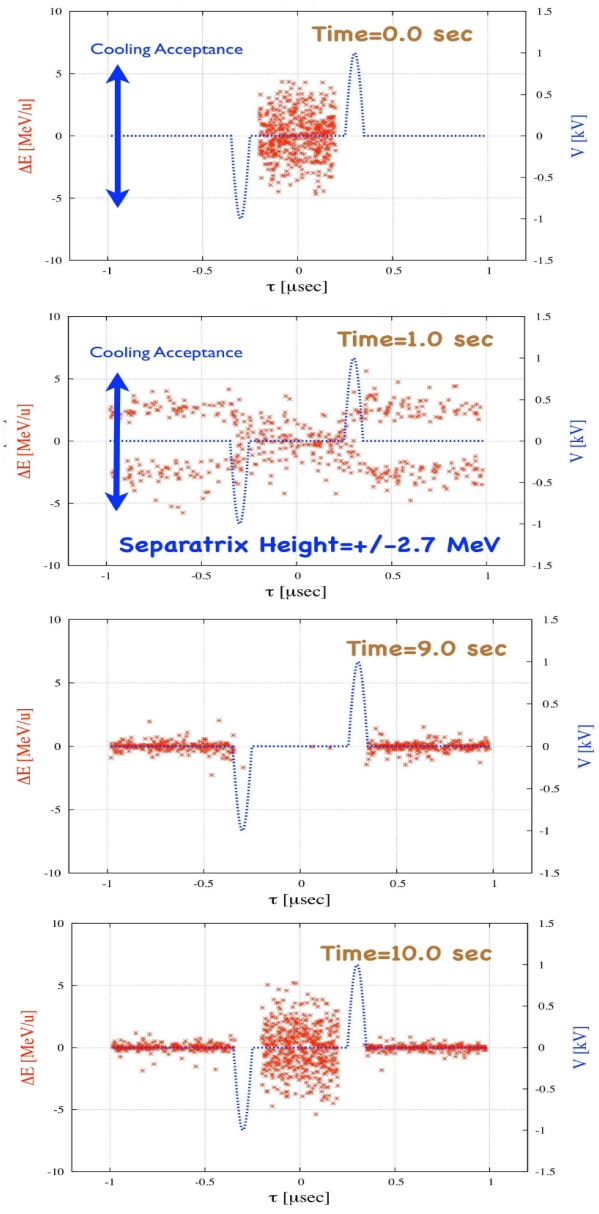

Fig. 37: Accumulation with a fixed barrier voltage (blue) with 1 kV amplitude and barrier frequency 5 MHz, corresponding to an half wave length of 100 ns. The gap length is 500 ns and the revolution period is 2 μs. The anti-protons (red) are injected with the injection kicker at time $t = 0$ s and are tracked in phase space (time τ, energy deviation ΔE) over 10 s including stochastic cooling. At time $t = 9$ s almost all particles are cooled into the accumulation area. The next batch of 10^8 anti-protons is injected at $t = 10$ s.

The unstable area is now again nearly empty and ready for the next injection of the CR batch at $t = 10$ s. The injected beam bunch is 500 ns long and the kicker pulse length is assumed to be 600 ns.
Figure 38 shows the number of accumulated anti-protons and the accumulation efficiency versus time for the fixed barrier case. The accumulation efficiency is defined as the ratio of the number of accumulated particles to the number of particles totally injected. It can be seen that the accumulation efficiency continuously drops during accumulation. This is due to the fact that particles which initially move outside the separatrix will stay outside if the voltage is too high. In this case the energy deviation of particles is too large and can not be cooled down effectively before the next injection cycle occurs. On the other hand if the BB voltage is too small the cooling is fast as the deviation of energy is small. But the separatrix height is too small to keep the accumulated particles inside the separatrix area when the momentum spread becomes larger after the accumulation of many particles.

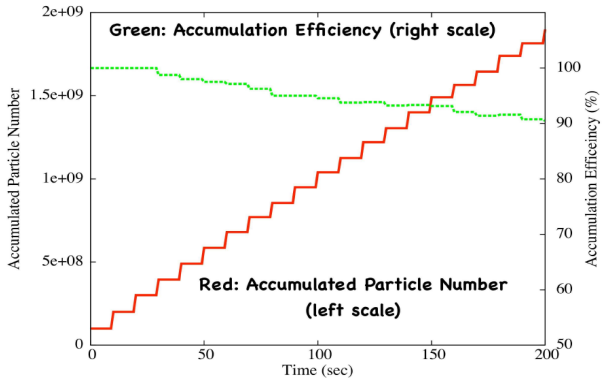

Fig. 38: Number of anti-protons during accumulation (red) and accumulation efficiency (green). The accumulation process has been stopped after 200 s when the accumulation efficiency has dropped down to 90%.

Considerably better results of anti-proton beam accumulation are achieved when the moving barrier method is applied. This is best illustrated in Fig. 39.
Two one wave-length pulses with 2 kV peak voltage are prepared within one revolution period (2 μs) and the beam is injected between the two pulses (Fig. 39, $t = 0$ s). Subsequently after 0.5 s, the two pulses are adiabatically switched off and the beam becomes a coasting beam (Fig. 39, $t = 1.0$ s). It is efficiently cooled down and the barrier pulses are re-excited at the same phase place adiabatically at $t = 9.5$ s. The adiabatic compression of the cooled coasting to the bunched beam (the bunching factor is around 1/2) is performed with the moving barrier voltage within 500 ms to prepare the gap for the next injection at $t = 10$ s. The figure clearly shows that the injected particles are completely moved into the accumulation area so that no particles losses occur at the second injection at $t = 10$ s. The number of accumulated anti-protons for the moving barrier scheme is depicted in Fig. 40.

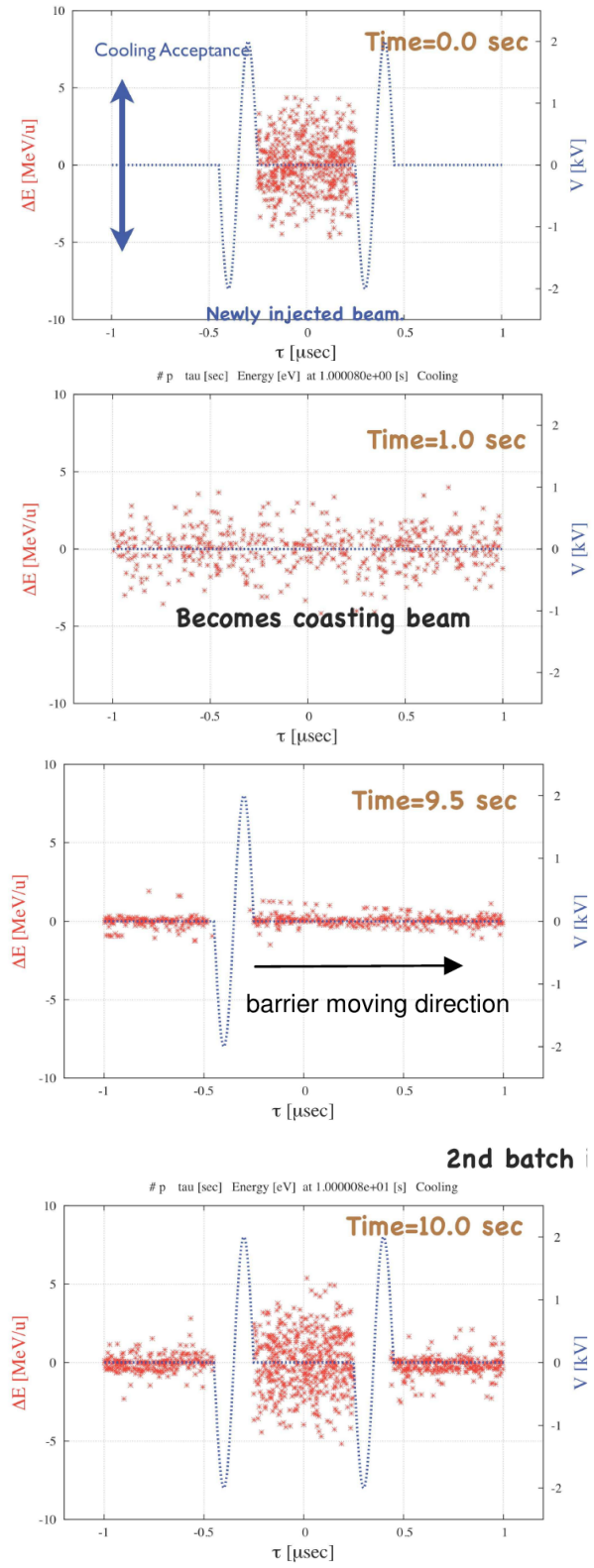

Fig. 39: First cycle of anti-proton accumulation with a moving barrier. At $t = 9.5$ s the initially overlapping two barrier pulses are shown at half height of the final voltage. One barrier is then moved in the direction indicated by the arrow. The second batch is injected at $t = 10$ s.

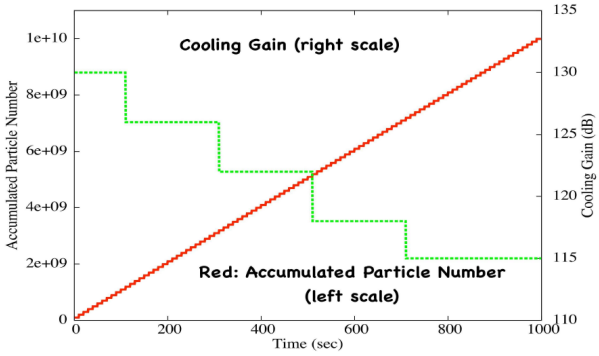

Fig. 40: Number of anti-protons during accumulation (red) and cooling voltage gain (green) for the moving barrier scheme. The accumulation process reaches an accumulation efficiency of 100%. After 1000 s (100 cycles) 10^{10} anti-protons are stored in the HESR. The relative momentum spread is reduced to $5 \cdot 10^{-5}$ due to stochastic cooling. For an efficient accumulation the electronic voltage gain of the cooling system must be reduced as shown.

To ensure an efficient accumulation it is essential to reduce the electronic gain of the cooling system during accumulation. This is due to the fact that Schottky noise heating being proportional to the amplifier gain squared increases with an increasing anti-proton density in the HESR.

From the detailed simulation studies of the moving barrier scheme with application of the envisaged (2–4) GHz momentum cooling system it can be concluded that an efficient accumulation of 10^{10} anti-protons in the HESR within 1000 s should be possible at 3 GeV. Albeit not very practicable for regular operation, a collection of up to 10^{11} anti-protons is possible in the simulation within 10000 s. The great advantage of the proposed accumulation scheme is that a significant cost increase can be avoided.

To gain confidence in the accumulation simulation results and to prove the reliability of the method a proof-of-principle experiment is indispensable. The best choice to carry out such an experiment was found in the Experimental Storage Ring (ESR) at the GSI in Darmstadt. There, the concept of beam accumulation with barrier bucket system and beam cooling was already tried in 2007 with an heavy ion beam $^{40}Ar^{18+}$ with 60 MeV/u that was injected into the ESR from SIS 18 (*cf.* C. Dimopoulou *et al.*, Proceedings of COOL07, Bad Kreuznach, Germany (2007) 21). Electron cooling was used to support the accumulation process. The experiment successfully demonstrated the possibility of beam stacking with a BB system assisted by electron cooling. The electron cooling is quite effective for the low energy and high charge state ions while in the present concept a 3 GeV anti-proton beam has to be accumulated in the HESR ring. In this case the simulation studies revealed stochastic cooling as the more favorable cooling tool.

An international collaboration consisting of members from GSI, Japan, Russia, CERN and FZJ Jülich carried out the beam experiments (*cf.* C. Dimopoulou *et al.*, Ann. Rep. 2010, GSI, Darmstadt). Various waveforms for the BB, such as fixed and moving barriers have been prepared. As the ESR is not equipped with a dedicated BB system a modified ESR cavity was applied with a rf peak voltage up to 120 V. In addition a sinusoidal rf wave form at harmonic number one with an injection onto the unstable fixed point has been considered. The option of electron cooling and stochastic cooling was available and has been utilized extensively. Again an Argon $^{40}Ar^{18+}$ beam with a kinetic energy 400 MeV/u has been used. The main beam and ESR-ring parameters are summarized in Table 4.

Table 4: Basic ESR machine and beam parameters.

Ion type	$^{40}Ar^{18+}$, 0.4 GeV/u
β	0.713
γ	1.43
$\eta = 1/\gamma^2 - 1/\gamma_{tr}^2$	0.31
ESR Circumference	108.4 m
Revolution period	500 ns
Initial $\Delta p/p$	$5 \cdot 10^{-4}$
Equilibrium $\Delta p/p$ after 10 s stochastic cooling	$\sim 3 \cdot 10^{-4}$
Injected bunch length	150 ns
BB peak voltage	120 V
BB frequency	5 MHz
Bucket half height $\Delta p/p$	$3 \cdot 10^{-4}$

Figure 41 shows the experimental outcome of Argon ion accumulation of over 1000 s for the moving barrier bucket case. About $2 \cdot 10^6$ ions were injected every 20 s. Initially the stored beam intensity increases linearly. After about 400 s the curve tends to attain a saturation at 1000 s with a beam current of 320 μA ($6 \cdot 10^7$ ions). Due to the small revolution period in the ESR, the timing between the incoming bunch and the ESR rf system which bunches the accumulated stored particles and the injection kicker is a very sophisticated procedure. Also kicker ringing longer than the injected bunch length introduced losses. Nevertheless the beam intensity is increased by a factor of 30. Simultaneously stochastic cooling and electron cooling was applied.

The experiments emphasized that strong cooling was unavoidable to attain a significant accumulation. First test experiments and simulation results showed that stochastic cooling alone was not able to reduce the beam momentum spread enough for the moving barrier bucket with a 120 V peak voltage. No clearly visible accumulation effect was received. The reason is that during 20 s of stochastic cooling a reduction of the relative momentum spread by only a factor of 2 is achieved. In the subsequent beam compression phase by the moving barrier a significant fraction of particles remains in the injection area when the barrier voltage is 120 V. These particles are kicked out at the next injection.

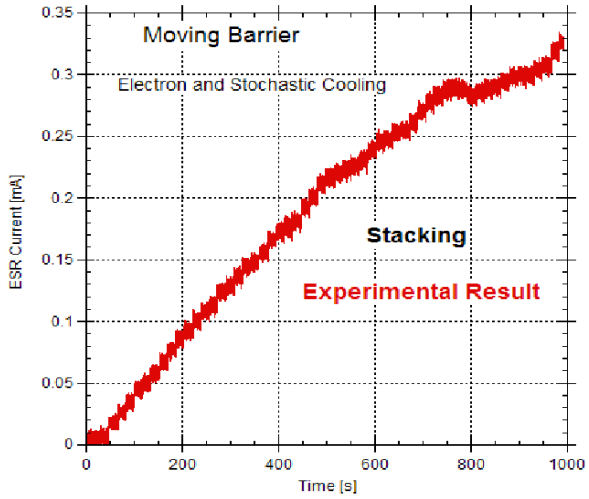

Fig. 41: Argon accumulation in the ESR over 1000 s. Electron and stochastic cooling was simultaneously applied.

The experimental results are described remarkably well by the simulation shown in Fig. 42. A constant number of $5 \cdot 10^6$ ions is assumed to be injected every 20 s. After 1000 s the beam intensity is increased by a factor of 30 as observed experimentally.

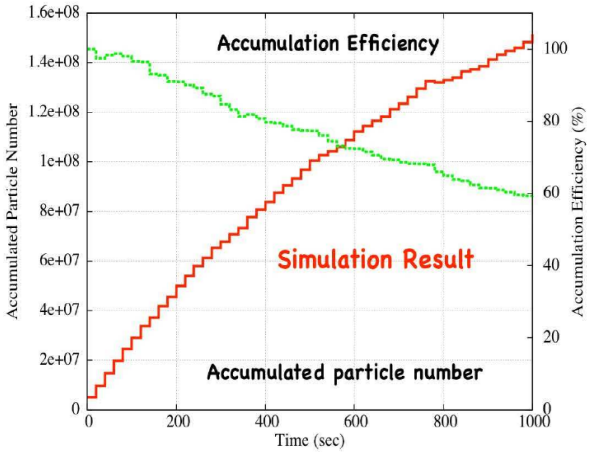

Fig. 42: Simulation of Argon accumulation (red) and efficiency (green) in the ESR over 1000 s. Electron and stochastic cooling is applied.

It is also observed that the shape of the accumulation curve is predicted in very good agreement with the experimental one. The accumulation efficiency is about 60%. This can be boosted by improving the kicker performance and higher BB voltages. The data analysis and comparison with simulation results is still continued. But already now it can be concluded from experiment and theory that the moving barrier bucket method with stochastic cooling will be a reliable and cost- efficient accumulation method for the HESR as long as the number of anti-protons is restricted to 10^{10}.

6 The PANDA Experiment at FAIR

6.1 Introduction

The new Facility for Antiproton and Ion Research (FAIR) will be one of the largest accelerator facilities in the world giving access to a large variety of different experiments to gain new insights into the structure of matter and the evolution of the universe. A big step towards the realisation of the project was the foundation of the FAIR GmbH on October 4, 2010. Now the build up of the facility can start and first construction work is ongoing.

The $\overline{\text{P}}$ANDA experiment is one essential part of FAIR. Its goal is to improve the understanding of Quantum Chromo Dynamics (QCD) in the charmonium energy regime. In this regime many new and unexpected hidden and open charm states were found in the last years. Two of these states, the $D_s(2317)$ and the $X(3872)$, are hot candidates to be exotic objects consisting of four quarks. To distinguish the various theories about the origin of theses states a precise knowledge of the width is important. With existing experiments only an upper limit of a few MeV has been given. Here $\overline{\text{P}}$ANDA would be able to improve the width measurement by more than an order of a magnitude down to about 100 keV which is shown in the following simulation studies.

Important for the measurement of these two states is a powerful background suppression which requires the identification of secondary vertices from D-meson decays separated by several $100\,\mu$m from the production point. This can only be done by a modern tracking system for charged particles with a Micro Vertex Detector (MVD) in combination with a large volume gaseous detector like a Straw Tube Track (STT). Both systems are under development in Jülich together with other groups inside the $\overline{\text{P}}$ANDA collaboration.

To determine the absolute cross section of states and the relative normalization of a resonance scan, a precise knowledge of the integrated luminosity is essential. Therefore a luminosity monitor is under development which measures the Coulomb elastic scattering in the strong interference region.

To speed up the process of building and setting up the detector the $\overline{\text{P}}$ANDA collaboration has decided to do a pre-assembly of major parts of the detector at the FZ-Jülich. This has the big advantage that a mechanical and electrical integration of the components can be tested in advance and the time consuming field mapping of the solenoid magnet is possible before the setup at FAIR. With this approach $\overline{\text{P}}$ANDA is able to start doing physics measurements as early as possible once an antiproton beam is available at FAIR.

6.2 Physics Analysis Simulation

6.2.1 Estimation of the resolution of the $D^*_{s0}(2317)$ width

The $D^*_{s0}(2317)$ meson was first discovered by BaBar in 2003 and later confirmed by Belle. It has a surprisingly low width and a mass close to the DK threshold. Several theoretical models try to explain the nature of its properties and a precise knowledge of mass and width of the $D^*_{s0}(2317)$ is a good criterion to evaluate these models by comparing their predictions with the measured data. Up to now, only an upper limit of 3.8 MeV$/c^2$ is known for the width, while the mass has been measured with an accuracy of 0.6 MeV$/c^2$.

A direct width measurement by simply measuring the invariant mass distribution of the decay products only works where the experimental resolution is similar or better than the width to be measured. As this is usually not the case for very narrow particles, a resonance or threshold scan can be carried out instead.

For this, the cross section is measured as a function of the center of mass energy. The shape of this excitation function depends on the particle width, thus the measurement of the shape can be used to deduce the particle width. In the experiment, the production rate of the $D^*_{s0}(2317)$ can be measured for different beam momenta, *i.e.*, center of mass energies. The experimental data then yield the mass and width of the $D^*_{s0}(2317)$ by fitting the excitation function to the scan points.

The potential of this measurement to be done with the $\overline{\text{P}}$ANDA detector has been estimated with extensive simulations in the PandaRoot framework.

The procedure works as follows: Excitation functions with different width hypotheses as input are used to generate sample data as it would be produced by a threshold scan. The measurable excitation function is the result of a convolution of the physical excitation function and the finite beam momentum distribution (compare Fig. 43).

For the simulation, this measurable excitation function is taken as a basis to determine the total number of signal events which can be detected for each scan point. The signal is then added to a background modelled after the Argus function with the total number of background events based on the signal to noise ratio. In the reconstruction step, mass and width are taken as free parameters of the excitation function and their values obtained by the best fit to the scan points (compare Fig. 44).

The results on the resolution for a total measurement time of 60 days with a signal cross section of 1 nb and a signal to background ratio of 1 are summarized in Fig. 45.

The following beam parameters are used throughout the simulations: The uncertainty in the determination of the nominal beam momentum has been assumed to be $\delta p_0/p_0 = 10^{-4}$ with a relative momentum spread of $\delta p/p = 10^{-4}$ around the nominal beam momentum. For the precision of changing a fixed beam momentum by Δp_0, an uncertainty of $\delta\Delta p_0/\Delta p_0 = 10^{-5}$ has been assumed.

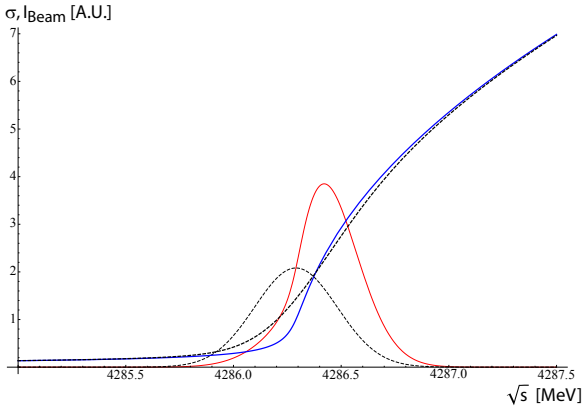

Fig. 43: Expected behavior of the measurable signal cross section for an assumed 100 keV wide $D^*_{s0}(2317)$. Blue thick: Physical excitation function describing the cross section as a function of the center of mass energy. Black dashed: Example center of mass energy distribution due to the finite beam momentum resolution for a nominal beam momentum at threshold. Red: Resulting signal distribution due to the center of mass energy distribution (beam momentum spread) and cross section distribution (excitation function). Black thick dashed: Measurable cross sections as a result of the convolution of the center of mass energy distribution with the excitation function.

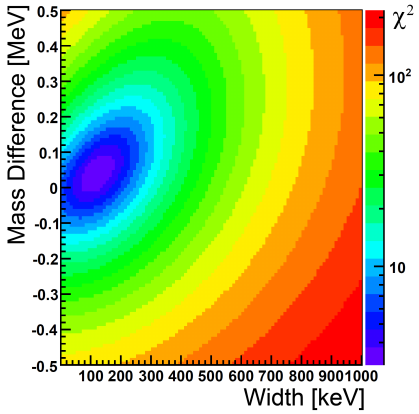

Fig. 44: χ^2 distribution of a simulated excitation function to expectations with varying mass and width hypotheses. The underlying scan points are generated for 100 keV wide $D^*_{s0}(2317)$ with a signal cross section of 1 nb, a signal to background ratio of 1 and a total measurement time of 60 days.

While the total measurement time has been kept constant, the distribution of the scan points has been changed. Generally, a smaller energy range around the threshold seems favorable. Including a yet to be eliminated systematic shift which has been observed throughout the simulation, a width resolution in the order of 100 keV seems feasible for the shown set of parameters.
In the future, detailed studies of the background shape

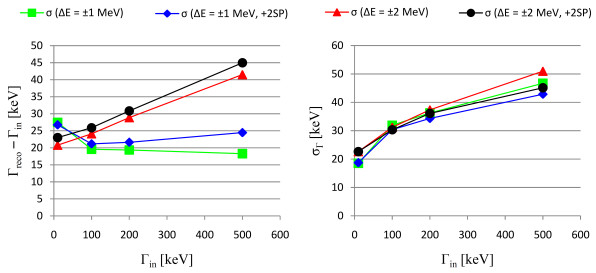

Fig. 45: Achievable width resolution for a signal cross section of 1 nb, a signal to background ratio of 1 and a total measurement time of 60 days. The resolutions for a total of 15 scan points distributed 1 MeV and 2 MeV around the threshold are shown as a function of the input width. In addition, both scan point distributions are extended by two additional scan points 4 MeV above the threshold. However, the additional points have little impact on the resolution. Left: Systematic offset of the reconstructed width from the input width. Right: Standard deviation of the reconstructed width

and suppression are needed in order to get a more accurate estimate on the achievable mass and width resolution and in order to optimize the extraction of the signal from the background.

6.2.2 Mass and width reconstruction of the $X(3872)$ meson with the $\overline{\text{P}}$ANDA experiment.

The $X(3872)$ meson has been observed by the Belle collaboration on 2003 through its decay to $J/\psi\pi^+\pi^-$. Since then a few models were proposed to explain its properties. An important feature of the $X(3872)$ meson is the closeness of its mass to the $D^0\bar{D}^{*0}$ threshold, as show the equation (7), that it may be interpreted as a $D^0\bar{D}^{*0}$ loosely bound molecule. Furthermore, relation (8) is consistent with an interpretation of this meson being a virtual state of charm mesons. Nevertheless, other theoretical interpretations are not rejected due to different observed decay channels.

$$M_{J/\psi\pi^+\pi^-} - (M_{D^0} + M_{\bar{D}^{*0}}) = -0.6 \pm 0.6\, MeV \quad (7)$$
$$M_{D^0\bar{D}^0\pi} - (M_{D^0} + M_{\bar{D}^{*0}}) = +4.1 \pm 0.7\, MeV \quad (8)$$

The PDG value of the $X(3872)$ mass is $M_X = 3871.56 \pm 0.22\, MeV$ and only an upper bound of its width is known, $\Gamma_X < 2.3\, MeV$. Two assignments of its quantum numbers $J^{PC} = 1^{++}$, 2^{-+} are compatible with the existing data.
Due to its good energy resolution, the $\overline{\text{P}}$ANDA experiment will provide additional knowledge on the properties of the $X(3872)$ meson by measuring its width more accurately. A scan simulation has been performed in order to study how precise the mass and the width of the resonance will be measured.

The study was focused on the $X(3872)$ decay to $J/\psi\pi^+\pi^-$. The calculated $J/\psi\pi^+\pi^-$ final state cross sections from $\bar{p}p$ annihilation in which the $X(3872)$ meson was interpreted as $\chi_{c1}(2P)$ meson. For three width values, the corresponding cross section and expected daily rate are shown in Table 5. These values of the cross section correspond not only to $X(3872)$ production but also to all $J/\psi\pi^+\pi^-$ final states, which means that a physical background is included. Therefore, to generate the $X(3872)$ mass distribution, a non-relativistic Breit-Wigner distribution and a constant polynomial of $1.2nb$ have been used for the resonance and the physical background, respectively. Besides that an instrumental background, modeled by an Argus distribution, was folded with the signal.
The $\overline{\text{P}}$ANDA high resolution mode was considered : $\delta_p/p = 3\cdot10^{-5}$, $\int Ldt = 864\ nb^{-1}/day$. The value of $M_X = 3872\ MeV$ was taken for the mass at which the $J/\psi\pi^+\pi^-$ reconstruction efficiency for the $\overline{\text{P}}$ANDA detector is expected to be equal to 0.3. The leptonic decays of J/ψ have been only considered where $Br(J/\psi \to e^+e^-,\ \mu^+\mu^-) = 12\%$. The expected rate per day is given by Table 5 depending on the input width.

Table 5: Input parameters value for the scan simulation

Γ (MeV)	0.136	0.5	1
σ at peak (nb)	238	20	6
Rate (events/day)	7402	622	186

10 scan points were chosen within $\pm\Delta E = 2$MeV centered around M_X for a 40 days run, 4 days per scan point.

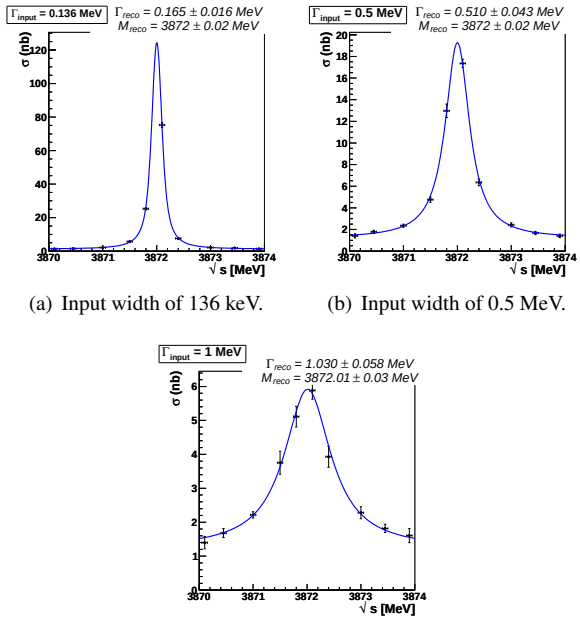

(a) Input width of 136 keV. (b) Input width of 0.5 MeV.

(c) Input width of 1 MeV.

Fig. 46: Reconstructed cross-section as a function of center-of-mass energy.

The plots in Fig. 46 show the reconstructed cross section for different center-of-mass energies around the input mass resonance for three different input width. The blue line is a Breit-Wigner convoluted with a Gaussian resolution function fit to the distribution. For all three input widths the resolution is better than 60 keV, showing the excellent mass and width resolution achievable with the $\overline{\text{P}}$ANDA experiment.

6.3 MVD

The purpose of the Micro Vertex Detector (MVD) of $\overline{\text{P}}$ANDA is the precise measurement of the track of charged particles close to the interaction point. With this data it is possible to identify short living particles which decay after a short flight path before they can be measured in a detector system and to determine the momentum of these particles with a very high resolution together with the central tracker. The MVD has four barrel layers with a radial distance from 4 up to 14 cm from the interaction point and six disk layers in the forward direction. Two different detector systems are used inside the MVD. The inner layers are equipped with silicon hybrid pixel detectors, which are able to cope with high track densities and large radiation damages while the outer layers use silicon strip detectors which have less radiation length by a comparable point resolution.
Due to the untriggered readout of the $\overline{\text{P}}$ANDA detector and the huge data rate produced in the MVD new readout ASICs for the MVD have to be developed. For the pixel part this is done in the electronics department of INFN Torino which successfully submitted the second prototype (ToPix2) of this chip this year. The work to test the prototypes is shared between the INFN Torino and the FZ Jülich to have complementary measurements and a cross check of the results. Here in Jülich we are able to use a versatile readout system which was developed together with the ZEL for these kind of measurements. It allows a fast readout of the chip combined with the ability to easily adopt the system for new types of measurements and prototypes.

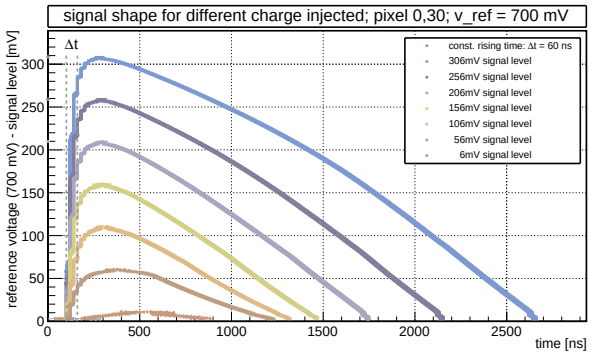

Fig. 47: Measured signal shape of a single pixel of the ToPix2 prototype for different injected charges.

Two results of theses measurements are shown as an example. Figure 47 shows the signal shape of the pream-

plifier for different signal levels of a single pixel. One can see the fast risi of the signal within 180 ns and the slow discharge. The slope of the falling edge of the signal should be independent of the amplitude of the signal, which is the case for not too low or too high signals. Especially the signals for low injected charges have a shape which strongly differs from signals with higher charges. Here a further optimization of the readout chip is necessary.

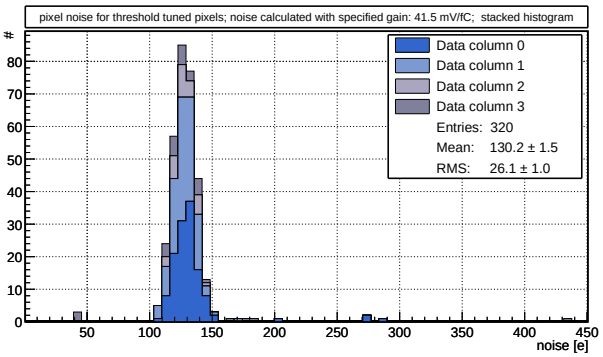

Fig. 48: Noise distribution of all 320 pixel cells of the ToPix2 prototype chip.

In Fig. 48 the noise distribution of all 320 pixel cells of the ToPix2 chip can be seen. The mean value of the distribution is at 130 e which is well below the required 200 e. To summarize all measurements done at the front end chip one can say, that the core elements of the chip are fully functional and meet the requirements. A few points could be identified which have to be improved, e. g. the signal shape for low injected charges. A new version of the readout chip is under development in Torino and will be submitted in spring 2011.

6.4 Straw-Tube-Tracker

The design of the $\overline{\text{P}}$ANDA central Straw Tube Tracker (STT) has been further optimized. Now, about 85 % of the cylindrical volume with an inner and outer diameter of 160 mm and 410 mm, and a length of 1500 mm, is filled with straws and there are up to 27 layers in radial direction for the reconstruction of the particle trajectories. In total the STT consists of 4580 straw tubes with a length of 1500mm, diameter of 10mm and wall thickness of 27 μm Mylar. The design meets a high spatial resolution and high sampling density at a very low material budget of about 1.2 % radiation length by using the technique of pressurized, close-packed and self-supporting straw layer stacks which has been first developed for the TOF-STT. 19 straw layers are oriented in beam axial direction and 4 double-layers in the middle section of the STT are alternately skewed by $\pm 2.89^\circ$ to resolve the track space points in all 3 dimensions. The projected spatial single hit resolutions are 150 μm ($\sigma_{r\phi}$) and 3 mm (σ_z). Together with the space points from the Micro-Vertex-Detector (MVD) a momentum resolution on the low percent level (σ_p/p=1-2 %) was obtained by a simulation and reconstruction of single tracks in the solenoidal magnetic field of 2 Tesla. Investigations to measure with the PANDA-STT in addition to the spatial track hits the particle energy loss for a particle identification have started and a first test measurement with a straw prototype detector and minimum ionizing beam protons at COSY was very encouraging, resulting in an energy loss resolution of about 10 %.
Since the assembly technique, the straw materials, calibration and track reconstruction algorithms are similar, the TOF-STT with its 2704 straw tubes is considered as an ideal test system for the PANDA-STT. The TOF-STT was successfully installed and a first experimental beam time was carried out in summer 2010. A high spatial single hit resolution of 140 μm (σ) was obtained. In particular, the reliable operation of the TOF-STT in the surrounding vacuum of the COSY-TOF barrel since now more than 2 years gives a strong confidence in the used materials and assembly techniques also for the PANDA-STT with a required lifetime of more than 10 years.

6.5 Luminosity Monitor

$\overline{\text{P}}$ANDA will achieve more than an order of magnitude higher mass resolution than available at the B-factories by performing resonance and threshold scans with the phase space cooled antiproton beams. The cross section will be analyzed as a function of the nominal beam momentum, therefore the integrated luminosity must be determined with high precision. In order to determine the integrated luminosity with even higher precision than available from Schottky measurements of the HESR beam, a concept for a luminosity monitor based on measuring elastic scattering in the Coulomb-strong interference region has been developed.The detector will be located at about 10 m downstream of the target and will measure forward outgoing antiprotons which are emitted at an angle of 3-8 mrad with respect to the beam axis. The angle of the scattered antiproton will be reconstructed by measuring the track with 4 planes of silicon strip detectors.

6.5.1 Beam test for tracking station

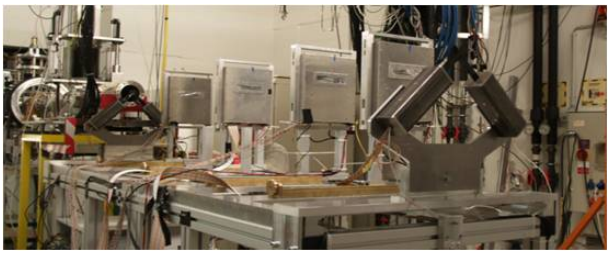

Fig. 49: Silicon strip tracking station for beam test at COSY.

To study the detector performance a full simulation chain within PANDARoot framework has been established. The specific simulations with proposed geometry have

been performed accordingly. The reconstructed angular resolution of the scattered antiproton is determined to be 0.1mrad and 0.15mrad for 150μm and 300μm thick double-sided silicon strip sensors with antiproton beam at momentum of 6.2 GeV/c, respectively. In order to verify the simulation, a dedicated beam test for a silicon strip tracking station with 4 detector planes has been performed at COSY as shown in Fig. 49. The response of silicon strip sensor to proton beam particles has been studied by tilting the silicon strip sensor with different angles. The comparison of strip multiplicity between simulation and beam test has been plotted in Fig. 50.

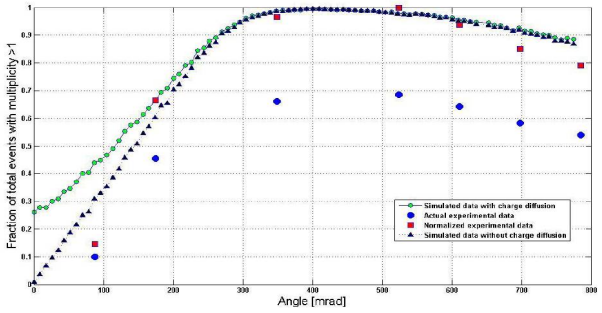

Fig. 50: Comparison of the strip multiplicity for simulation and test beam data as a function of the rotation of sensors about the normal to the beam axis.

In order to reconstruct the tracks of beam particles passing through the tracking station sensors, an alignment algorithm has been developed. Figure 51 shows simulation results in which the alignment with the developed algorithm has been achieved with no more than 3 iterations.

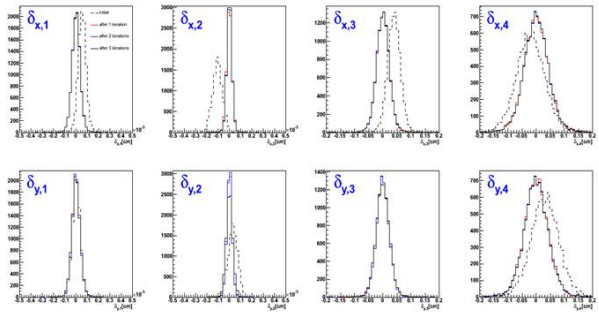

Fig. 51: Distribution of the spatial deviations for all 4 detector planes, show us that the alignment has been achieved with no more than 3 iterations.

6.5.2 Proposal for day-one experiment

In parallel, the simulation study focusing on the precision of the absolute integrated luminosity determination indicated that the absolute integrated luminosity can not be determined with sufficient precision due to a strong correlation of the parameters in the small range 4-momentum transfer t covered by the luminosity monitor detector. In order to alleviate the lack of existing data on this system in the relevant momentum region, a "day-one" experiment at HESR dedicated to antiproton-proton elastic scattering has been proposed. Figure 52 shows a sketch of the general design of the "day-one" experiment. The goal of this experiment is to measure a wide range of t(0.0008-0.1GeV^2) so that the contribution of the physical differential distributions to the absolute luminosity uncertainty will be less than 1%. The polar angle of the scattered antiprotons and the energy of the recoil protons will be measured at forward angles by tracking detectors and by thick energy detectors near 90°, respectively. The complete "day-one" experiment will be performed at HESR in its early running phase. The commissioning of the experiment equipment will take place with proton beams at COSY in the next couple of years.

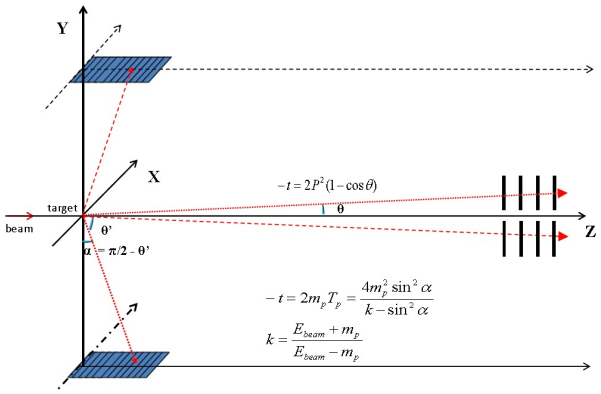

Fig. 52: A sketch of the day-one experiment with two arms.

A Councils

A.1 Hadron and Accelerator Physics Program Advisory Council

Prof. Mei Bai	Brookhaven National Laboratory, U.S.A.	
Prof. K.-T. Brinkmann	University Bonn	
Prof. M. Garçon	CEA-Saclay, FR	
Prof. A. Jankowiak	Helmholtz Zentrum Berlin	
Prof. K. Jungmann	KVI Groningen, NL	
Prof. K.-H. Kampert	University Wuppertal	
Prof. S. Paul	TU München	Chairperson
Prof. K. Peters	GSI Darmstadt	
Prof. D.-O. Riska	University Helsinki, FI	
Prof. C. Roberts	Argonne National Laboratory, U.S.A.	
Prof. S. Vigdor	Brookhaven National Laboratory, U.S.A.	

A.2 COSY Program Advisory Committee

Prof. M. Anselmino	L'Universita di Torino, IT	
Prof. D. Barber	DESY Hamburg	
Prof. J. Bijnens	Lund University, SE	
Prof. M. Garçon	CEA-Saclay, FR	
Prof. N. Herrmann	Universität Heidelberg	
Prof. N. Kaiser	TU München	
Prof. B. Kämpfer	FZ Dresden-Rossendorf	
Prof. H. Löhner	KVI Groningen, NL	
Prof. A. Magiera	Jagellonian University Cracow, PL	
Prof. W.T.H. van Oers	University of Manitoba, CA	Chairperson
Prof. A.K. Opper	George Washington University, USA	
Prof. U. Thoma	Universität Bonn	

B Publications

1. Experiment

1. **Determination of the total width of the η' meson**
   E. Czerwinski *et al.* [COSY Collaboration]
   Phys. Rev. Lett. **105**, 122001 (2010) [arXiv:1008.5294 [nucl-ex]]

2. **Centrifugal Separation of Antiprotons and Electrons**
   G. Gabrielse *et al.*,
   Phys. Rev. Lett. **105**, 213002 (2010)

3. **Production of a beam of tensor-polarized deuterons using a carbon target**
   H. Seyfarth *et al.*
   Phys. Rev. Lett. **104**, 222501 (2010)

4. **Precision determination of the $d\pi \to NN$ transition strength at threshold**
   T. Strauch *et al.*
   Phys. Rev. Lett. **104**, 142503 (2010) [arXiv:1003.4153 [nucl-ex]]

5. **Influence of N^*-resonances on hyperon production in the channel $pp \to K^+\Lambda p$ at 2.95, 3.20 and 3.30 GeV/c beam momentum**
   S. Abd El-Samad *et al.* [TOF Collaboration]
   Phys. Lett. B **688**, 142 (2010) [arXiv:1003.0603 [nucl-ex]]

6. **Cross section of the $pp \to K^+\Sigma^+ n$ reaction close to threshold**
   A. Budzanowski *et al.* [HiRes Collaboration]
   Phys. Lett. B **692**, 10 (2010) [arXiv:1007.1542 [hep-ex]]

7. **High resolution study of the Λp final state interaction in the reaction $p+p \to K^+ + (\Lambda p)$**
   A. Budzanowski *et al.*
   Phys. Lett. B **687**, 31 (2010) [arXiv:1003.0290 [nucl-ex]]

8. **Measurement of the invariant mass distributions for the $pp \to pp\eta'$ reaction at excess energy of $Q = 16.4$ MeV**
   P. Klaja *et al.*
   Phys. Lett. B **684**, 11 (2010) [arXiv:1001.5174 [nucl-ex]]

9. **Systematic study of the $pp \to pp\omega$ reaction**
   M. Abdel-Bary *et al.* [TOF Collaboration]
   Eur. Phys. J. A **44**, 7 (2010) [arXiv:1001.3043 [nucl-ex]]

10. **Production of Λ and Σ^0 hyperons in proton-proton collisions**
    M. Abdel-Bary *et al.* [COSY-TOF Collaboration]
    Eur. Phys. J. A **46**, 27 (2010) [Erratum-ibid. A **46**, 435 (2010)] [arXiv:1008.4287 [nucl-ex]]

11. **Invariant mass distributions for the $pp \to pp\eta$ reaction at $Q = 10$ MeV**
    P. Moskal *et al.*
    Eur. Phys. J. A **43**, 131 (2010) [arXiv:0912.1592 [nucl-ex]]

12. **Production of η and 3π mesons in the $pd \to {}^3\mathrm{He}X$ reaction at 1360 and 1450 MeV**
    K. Schonning *et al.*
    Eur. Phys. J. A **45**, 11 (2010) [arXiv:1001.4604 [nucl-ex]]

13. **Hydrogen spectroscopy with a Lamb-shift polarimeter — An alternative approach towards anti-hydrogen spectroscopy experiments**
    M.P. Westig *et al.*
    Eur. Phys. J. D **57**, 27 (2010)

14. **Comparison of nonequilibrium processes in p+Ni and p+Au collisions at GeV energies**
    A. Budzanowski *et al.*
    Phys. Rev. C **82**, 034605 (2010) [arXiv:0908.4487 [nucl-ex]]

15. **Deuteron breakup $pd \to (pp)_s n$ with forward emission of a fast S_{10} diproton**
S. Dymov *et al.*
Phys. Rev. C **81**, 044001 (2010)

16. **Upper limit of the total cross section for the $pn \to pn\eta'$ reaction**
J. Klaja *et al.*
Phys. Rev. C **81**, 035209 (2010) [arXiv:1003.4378 [nucl-ex]]

17. **The energy dependence of the $pp \to K^+ n\Sigma^+$ reaction close to threshold**
Yu. Valdau *et al.*
Phys. Rev. C **81**, 045208 (2010) [arXiv:1002.3459 [hep-ex]]

18. **High precision beam momentum determination in a synchrotron using a spin resonance method**
P. Goslawski *et al.*
Phys. Rev. ST Accel. Beams **13**, 022803 (2010) [arXiv:0908.3103 [physics.acc-ph]]

19. **Two-proton correlation function for the $pp \to pp + \eta$ and $pp \to pp + \pi$ reactions**
P. Klaja *et al.*
J. Phys. G **37**, 055003 (2010) [arXiv:1003.4377 [nucl-ex]]

20. **Energy dependence of hard bremsstrahlung production in proton-proton collisions in the $\Delta(1232)$ region**
D. Tsirkov *et al.*
J. Phys. G **37**, 105005 (2010) [arXiv:1005.2014 [nucl-ex]]

21. **Study of the η' meson structure, width and interactions with nucleons at COSY-11**
E. Czerwinski, J. Klaja, P. Klaja and P. Moskal
Acta Phys. Polon. Supp. **3**, 955 (2010) [arXiv:1007.2277 [nucl-ex]]

22. **Search for the η-mesic nuclei by means of COSY-11, WASA-at-COSY and COSY-TOF detector systems**
P. Moskal and J. Smyrski
Acta Phys. Polon. B **41**, 2281 (2010) [arXiv:1009.5011 [hep-ex]]

23. **Study of the near threshold $pp \to ppK^+K^-$ reaction in view of the K^+K^- final state interaction**
M. Silarski, P. Moskal and f. 1. collaboration
Acta Phys. Polon. Supp. **3**, 937 (2010) [arXiv:1003.4504 [hep-ph]]

24. **Polarized Antiprotons — How and why?**
H. Ströher
Acta Physica Polonica B **41**, 305 (2010)

25. **Use of a cryogenic corpuscular target for experiments on laser acceleration of the charged particles**
A.V. Boukharov, M. Büscher, A.S. Gerasimov, A.F. Ginevskii
Problems of Atomic Sc. and Technology, Series Plasma Physics, **53**, 60 (2010)

2. Theory

26. **Lattice effective field theory calculations for $A = 3,4,6,12$ nuclei**
E. Epelbaum, H. Krebs, D. Lee and U.-G. Meißner
Phys. Rev. Lett. **104**, 142501 (2010) [arXiv:0912.4195 [nucl-th]]

27. **Comment on "Possibility of Deeply Bound Hadronic Molecules from Single Pion Exchange"**
A. A. Filin *et al.*
Phys. Rev. Lett. **105**, 019101 (2010) [arXiv:1004.4789 [hep-ph]]

28. **Extracting the light quark mass ratio m_u/m_d from bottomonia transitions**
F. K. Guo, C. Hanhart and U.-G. Meißner
Phys. Rev. Lett. **105**, 162001 (2010) [arXiv:1007.4682 [hep-ph]]

29. **On the cross section ratio $\sigma(n)/\sigma(p)$ in η photoproduction**
M. Döring and K. Nakayama
Phys. Lett. B **683**, 145 (2010) [arXiv:0909.3538 [nucl-th]]

30. **Predictions for the strangeness $S = -3$ and -4 baryon-baryon interactions in chiral effective field theory**
J. Haidenbauer and U.-G. Meißner
Phys. Lett. B **684**, 275 (2010) [arXiv:0907.1395 [nucl-th]]

31. **The Reaction $\bar{p}p \to \bar{\Lambda}_c^- \Lambda_c^+$ close to threshold**
J. Haidenbauer and G. Krein
Phys. Lett. B **687**, 314 (2010) [arXiv:0912.2663 [hep-ph]]

32. **Redundancy of the off-shell parameters in chiral effective field theory with explicit spin-3/2 degrees of freedom**
H. Krebs, E. Epelbaum and U.-G. Meißner
Phys. Lett. B **683**, 222 (2010) [arXiv:0905.2744 [hep-th]]

33. **New insights into the neutron electric dipole moment**
K. Ottnad, B. Kubis, U.-G. Meißner and F. K. Guo
Phys. Lett. B **687**, 42 (2010) [arXiv:0911.3981 [hep-ph]]

34. **Interplay of quark and meson degrees of freedom in a near-threshold resonance**
V. Baru, C. Hanhart, Yu. S. Kalashnikova, A. E. Kudryavtsev and A. V. Nefediev
Eur. Phys. J. A **44**, 93 (2010) [arXiv:1001.0369 [hep-ph]]

35. **Helicity Amplitudes of the $\Lambda(1670)$ and two $\Lambda(1405)$ as dynamically generated resonances**
M. Döring, D. Jido and E. Oset
Eur. Phys. J. A **45**, 319 (2010) [arXiv:1002.3688 [nucl-th]]

36. **The Phase and pole structure of the $N^*(1535)$ in $\pi N \to \pi N$ and $\gamma N \to \pi N$**
M. Döring and K. Nakayama
Eur. Phys. J. A **43**, 83 (2010) [arXiv:0906.2949 [nucl-th]]

37. **Evaluation of the polarization observables I^S and I^C in the reaction $\gamma p \to \pi^0 \eta p$**
M. Döring, E. Oset and U.-G. Meißner
Eur. Phys. J. A **46**, 315 (2010) [arXiv:1003.0097 [nucl-th]]

38. **Lattice calculations for $A=3,4,6,12$ nuclei using chiral effective field theory**
E. Epelbaum, H. Krebs, D. Lee and U.-G. Meißner
Eur. Phys. J. A **45**, 335 (2010) [arXiv:1003.5697 [nucl-th]]

39. **Study of the $f_2(1270)$, $f_2'(1525)$, $f_0(1370)$ and $f_0(1710)$ in the J/ψ radiative decays**
L. S. Geng, F. K. Guo, C. Hanhart, R. Molina, E. Oset and B. S. Zou
Eur. Phys. J. A **44**, 305 (2010) [arXiv:0910.5192 [hep-ph]]

40. **Backward pion-nucleon scattering**
F. Huang, A. Sibirtsev, J. Haidenbauer, S. Krewald and U.-G. Meißner
Eur. Phys. J. A **44**, 81 (2010) [arXiv:0910.4275 [nucl-th]]

41. **Analysis of recent η photoproduction data**
A. Sibirtsev, J. Haidenbauer, S. Krewald and U.-G. Meißner
Eur. Phys. J. A **46**, 359 (2010) [arXiv:1007.3140 [nucl-th]]

42. **Proton-proton scattering above 3 GeV/c**
A. Sibirtsev, J. Haidenbauer, H. W. Hammer, S. Krewald and U.-G. Meißner
Eur. Phys. J. A **45**, 357 (2010) [arXiv:0911.4637 [hep-ph]]

43. **Primakoff effect in η-photoproduction off protons**
A. Sibirtsev, J. Haidenbauer, S. Krewald and U.-G. Meißner
Eur. Phys. J. A **44**, 169 (2010) [arXiv:1001.0646 [hep-ph]]

44. **Baryon-baryon interactions in effective field theory**
J. Haidenbauer
Nucl. Phys. A **835**, 168 (2010)

45. **Isospin violation in low-energy pion-nucleon scattering revisited**
M. Hoferichter, B. Kubis and U.-G. Meißner
Nucl. Phys. A **833**, 18 (2010) [arXiv:0909.4390 [hep-ph]]

46. **The Two-Nucleon System in Three Dimensions**
J. Golak *et al.*
Phys. Rev. C **81**, 034006 (2010) [arXiv:1001.1264 [nucl-th]]

47. **Vector and tensor analyzing powers in deuteron-proton breakup at 130 MeV**
E. Stephan *et al.*
Phys. Rev. C **82**, 014003 (2010)

48. **Novel analysis of the decays $\psi' \to h_c\pi^0$ and $\eta_c' \to \chi_{c0}\pi^0$**
F. K. Guo, C. Hanhart, G. Li, U.-G. Meißner and Q. Zhao
Phys. Rev. D **82**, 034025 (2010) [arXiv:1002.2712 [hep-ph]]

49. **Reconciling the *X(4630)* with the *Y(4660)***
F. K. Guo, J. Haidenbauer, C. Hanhart and U.-G. Meißner
Phys. Rev. D **82**, 094008 (2010) [arXiv:1005.2055 [hep-ph]]

50. **Lineshapes for composite particles with unstable constituents**
C. Hanhart, Yu. S. Kalashnikova and A. V. Nefediev
Phys. Rev. D **81**, 094028 (2010) [arXiv:1002.4097 [hep-ph]]

51. **The Chiral quark condensate and pion decay constant in nuclear matter at next-to-leading order**
A. Lacour, J. A. Oller and U.-G. Meißner
J. Phys. G **37**, 125002 (2010) [arXiv:1007.2574 [nucl-th]]

52. **Chiral Effective Field Theory for Nuclear Matter with long- and short-range Multi-Nucleon Interactions**
J. A. Oller, A. Lacour and U.-G. Meißner
J. Phys. G **37**, 015106 (2010) [arXiv:0902.1986 [nucl-th]]

53. **Beauty, charm and F(L) at HERA: New data vs. early predictions**
N. N. Nikolaev and V. R. Zoller
Phys. Atom. Nucl. **73**, 672 (2010) [arXiv:0903.2729 [hep-ph]]

54. **Resonances in an external field: The 1+1 dimensional case**
D. Hoja, U.-G. Meißner and A. Rusetsky
JHEP **1004**, 050 (2010) [arXiv:1001.1641 [hep-lat]]

3. Accelerator (including conference proceedings)

55. **Calculation of the magnetic interaction of neighboring magnets for the future High-Energy Storage Ring at the FAIR facility**
U. Bechstedt, H. Soltner
IEEE Transactions on Applied Superconductivity **20**, 234 (2010)

56. **Advanced gas-cooled accelerator-driven transmutation experiment AGATE**
K. Biß, K. Bongardt, R. Maier
Proc. of the 11th Information Exchange Meeting on Actinides and Fission Product Partioning; San Francisco, U.S.A., October 2010

57. **Gas scintillation beam profile monitor at COSY Jülich**
C. Boehme, J.L. Conradie, J. Dietrich, V. Kamerdzhiev, T. Weis
Proc. of the 2010 Beam Instrumentation Workshop; Santa Fe, U.S.A., 02. – 06.05.2010

58. **Results of electron cooling beam studies at COSY**
C. Böhme *et al.*
Proc. of the XXIIth Russian Conf. on Charged Particle Accelerators; Protvino, Russia, 27.09. – 01.10.2010

59. **Nondestructive beam instumentation and electron cooling beam studies at COSY**
C. Böhme *et al.*
Proc. of the 1st IPAC; Kyoto, Japan, 23. – 28.05.2010, p. 921

60. **Development of electron cooler components for COSY**
M.I. Bryzgunov
Proc. of the XXIIth Russian Conf. on Charged Particle Accelerators; Protvino, Russia, 27.09. – 01.10.2010, p. 151

61. **Current status and future projects of the iThemba LABS cyclotron facilities**
J.L. Conradie
Proc. of the 19th Int. Conf. on Cyclotrons and their Applications; Lanzhou, China, 6. – 10.09.2010

62. **Progress with the 2 MeV electron cooler for COSY-Jülich/HESR**
J. Dietrich
Proc. of the XXIIth Russian Conf. on Charged Particle Accelerators; Protvino, Russia, 27.09. – 01.10.2010, p. 147

63. **Status of the 2 MeV electron cooler for COSY Jülich**
J. Dietrich
Proc. of the 1st IPAC; Kyoto, Japan, 23. – 28.05.2010, p. 843

64. **Numerical study on simultaneous use of stochastic cooling and electron cooling with internal target at COSY**
Kikuchi, T. Proc. of the 1st IPAC, Kyoto, Japan, 23. – 28.05.2010, p. 852

65. **Interaction region design for the electron-nucleon Collider ENC at FAIR**
Ch. Montag, A. Lehrach, A. Jankowiak
Proc. of the 1st IPAC, Kyoto, Japan, 23. – 28.05.2010, p. 1635

66. **Transverse non-linear beam dynamics in the High-Energy Storage Ring HESR**
D. Welsch *et al.*
Proc. of the 1st IPAC, Kyoto, Japan, 23. – 28.05.2010, p. 4659

67. **Operations of the Tevatron electron lenses**
X.L. Zhang *et al.*
Proc. of the 46th ICFA Advanced Beam Dynamics Workshop on High-Intensity and High-Brightness Hadron Beams; Morschach, Switzerland, 27.09. – 01.10 2010

C Talks and Colloquia

1. V. Baru
   Pion production in nucleon-nucleon collisions at low energies: status and perspectives
   INT Program 10-1 Simulations and Symmetries: Cold Atoms, QCD, and Few-hadron Systems
   Seattle, U.S.A., 15. – 21.05.2010

2. V. Baru
   πNN system at low energy
   MESON 2010
   Krakow, Poland, 10. – 15.06.2010

3. V. Baru
   The role of spin in $NN \to NN\pi$
   19th International Spin Physics Symposium (SPIN2010)
   Jülich, 27.09. – 02.10.2010

4. Büscher, M.
   High intensity lasers and particle physics
   Lecture at the 4$^{\text{th}}$ Georgian-German School and Workshop in Basic Science (CGSWHP2010)
   Tbilisi, Georgia, 04.05.2010

5. Büscher, M.
   Particle acceleration in laser-induced relativistic plasmas — a novel approach for polarized sources?
   Leading talk at the 19th International Spin Physics Symposium (SPIN2010)
   Jülich, 28.09.2010

6. Büscher, M.
   Particle acceleration in laser-induced relativistic plasmas — a novel approach for polarized sources?
   470. Wilhelm und Else Heraeus Seminar on Particle Accelerator and High Intensity Lasers
   Bad Honnef, 13.10.2010

7. Dietrich, J.
   2 MeV Elektronenkühler für COSY/HESR
   COSY/ELSA Beschleuniger-Seminar
   Jülich, 19.01.2010

8. Dietrich, J.
   Status 2 MeV Cooler for COSY
   Winterseminar des Institutes für Angewandte Physik der J.W.Goethe-Universität Frankfurt/Main
   Riezlern, 08.03.2010

9. Dietrich, J.
   2 MeV Electron Cooler Status at COSY Jülich
   BINP Novosibirsk
   Novosibirsk, Russia, 29.03.2010

10. Dietrich, J.
    Status of the 2 MeV Electron Cooler for COSY Jülich
    Fermilab, Accel Physics & Tech Seminar
    Batavia, U.S.A., 13.05.2010

11. Dietrich, J.
    Status of the preperation of installing the 2 MeV cooler in COSY
    JINR Dubna
    Dubna, Russia, 10.06.2010

12. Dietrich, J.
    Progress with the 2 MeV electron cooler for COSY-Jülich/HESR
    RuPAC
    Protvino, Russia, 29.09.2010

13. Dietrich, J.
    Progress with the 2 MeV electron cooler for COSY-Jülich/HESR
    iThemba Labs
    Faure, South Africa, 08.12.2010

14. Gotta, D.
    Exotic Atoms
    Lecture at the 4th Georgian-German School and Workshop in Basic Science (CGSWHP2010)
    Tbilisi, Georgia, 03.05.2010

15. Gotta, D.
    Light antiprotonic atoms
    XLI. Expertentreffen der Kernphysik
    Schleching, 18. – 23.02.2010

16. Gotta, D.
    From Polarization towards an EDM storage ring at COSY
    Physics of fundamental Symmetries and Interactions (PSI2010)
    Villigen, Switzerland, 11. – 14.10.2010

17. Gotta, D.
    Pionic hydrogen
    Physics of fundamental Symmetries and Interactions (PSI 2010)
    Villigen, Switzerland, 11. – 14.10.2010

18. Grzonka, D.
    Ways to make polarised antiproton beams
    19th International Spin Physics Symposium (SPIN2010)
    Jülich, 27.09. – 02.10.2010

19. Guo, F.K.
    Heavy quark spin symmetry and heavy meson hadronic molecules
    12th International Conference on Meson-Nucleon Physics and the Structure of the Nucleon
    Williamsburg, U.S.A., 31.05. – 04.06.2010

20. Guo, F.K.
    Non-relativistic effective theory for heavy quarkonium transitions
    Institut für theoretische Physik II, Ruhr-Universität Bochum
    Bochum, 17.06.2010

21. Guo, F.K.
    Quark mass dependence of light and heavy systems
    Quark Connement and the Hadron Spectrum IX
    Madrid, Spain, 30.08. – 03.09.2010

22. Guo, F.K.
    Heavy quark spin symmetry and hadronic molecules
    19th International Spin Physics Symposium (SPIN2010)
    Jülich, 27.09. – 02.10.2010

23. Haidenbauer, J.
    Strangeness $S = -3$ and -4 baryon-baryon interactions in chiral effective field theory
    12th International Conference on Meson-Nucleon Physics and the Structure of the Nucleon (MENU 2010)
    Virginia, U.S.A., 31.05. – 04.06.2010

24. Haidenbauer, J.
    Charm production in antiproton-proton annihilation
    The 21st European Conference on Few-Body Problems in Physics (EFB21)
    Salamanca, Spain, 29.08. – 03.09.2010

25. Haidenbauer, J.
    Spin dependence of the antinucleon-nucleon interaction
    19th International Spin Physics Symposium (SPIN2010)
    Jülich, 27.09. – 02.10.2010

26. Haidenbauer, J.
Hyperon-nucleon and hyperon-hyperon interactions based on EFT
International conference on the structure of baryons (BARYONS10)
Osaka, Japan, 07. – 11.12.2010

27. Hanhart, C.
Charm quarks and the mysteries of the strong interaction
School of Physical, Environmental and Mathematical Sciences
Canberra, Australia, 05.02.2010

28. Hanhart, C.
Charm quarks and the mysteries of the strong interaction
School of Physics, University of New South Wales
Sydney, Australia, 09.02.2010

29. Hanhart, C.
Charm quarks and the mysteries of the strong interaction
School of Physics, University of Sydney
Sydney, Australia, 11.02.2010

30. Hanhart, C.
Highlights and challanges of hadron physics
Lecture at the 4^{th} Georgian-German School and Workshop in Basic Science (CGSWHP2010)
Tbilisi, Georgia, 05. – 07.05.2010

31. Hanhart, C.
Hadronic molecules
Quarkonium Working Group Workshop
Fermilab, U.S.A., 18. – 21.05.2010

32. Hanhart, C.
Recent progress in charmonium physics: role of heavy meson loops
11th International Workshop on Meson Production, Properties and Interaction (MESON2010)
Krakow, Poland, 10. – 15.06.2010

33. Hanhart, C.
QCD tests from low energy hadron physics
Chiral10 Workshop
Valencia, Spain, 21. – 24.06.2010

34. Hartmann, M.
ϕ-meson production and the in-medium ϕ-width in proton-nucleus collisions
Chiral10 Workshop
Valencia, Spain, 21. – 24.06.2010

35. Kamerdzhiev, V.
Results of electron cooling beam studies at COSY
RuPAC
Protvino, Russia, 29.09.2010

36. Krewald, S.
Meson-baryon dynamics as a tool for baryon resonance analysis
Workshop on "Achievements and New Directions in Subatomic Physics" in Honour of Tony Thomas' 60th Birthday
University of Adelaide, Australia, 15. – 19.02.2010

37. Krewald, S.
Jülich meson-baryon model
12th International Conference on Meson-Nucleon Physics and the Structure of the Nucleon (MENU 2010)
Williamsburg, U.S.A., 31.05. – 04.06.2010

38. Krewald, S.
Low density nuclear and neutron matter from effective field theory
LX International Conference on Nuclear Physics (NUCLEUS 2010)
St. Petersburg, Russia, 06. – 09.07.2010

39. Lehrach, A.
Beam dynamics for the HESR
Klausurtagung: Beam Physics for FAIR
Dannenfels, 05. – 06.07.2010

40. Lehrach, A.
Spin in der Beschleunigerphysik
Physikalisches Kolloquium RWTH Aachen
Physikzentrum Seffent-Melaten, 31.05.2010

41. Lehrach, A.
Spin in der Beschleunigerphysik
Universität Mainz, 19.11.2010

42. Lehrach, A.
The ENC@FAIR Project
19th International Spin Physics Symposium (SPIN2010)
Jülich, 27.09. – 02.10.2010

43. Meißner, U.-G.
Chiral extrapolation for baryons
ETM collaboration meeting
Universität Bonn, 09.03.2010

44. Meißner, U.-G.
Theory of nuclear forces
BCGS intensive week "hands-on shell-model"
Universität zu Köln, 22. – 26.03.2010

45. Meißner, U.-G.
Charmonium transitions
Chiral10 workshop, IFIC
Valencia, Spain, 21. – 24.06.2010

46. Meißner, U.-G.
Nuclear physics from simulations
21st European Few-Body Conference (EFB21)
Salamanca, Spain, 29.08. – 03.09.2010

47. Meißner, U.-G.
Continuous and discrete effective nuclear field theory
IXth Interational Conference on Quark Confinement and the Hadron Spectrum
Madrid, Spain, 30.08. – 03.09.2010

48. Meißner, U.-G.
Hadrons at varying quark masses — new results
Workshop on "Hadrons, Lattice QCD and Chiral Perturbation Theory"
Graz, Austria, 10.09.2010

49. Meißner, U.-G.
The beauty of spin
19th International Spin Physics Symposium (SPIN2010)
Jülich, 27.09. – 02.10.2010

50. Meißner, U.-G.
Open charm and charmonium states from effective field theory
Plenary talk, 4th International Workshop on Charm Physics (CHARM2010)
Beijing, China, 21. – 24.10.2010

51. Meißner, U.-G.
Nuclear lattice simulations
EMMI workshop on strongly coupled systems
GSI Darmstadt, 15.11. – 17.11.2010

52. Mertens, M.
Der PANDA Mikro Vertex Detektor zur Untersuchung von D-Mesonen: Entwicklung eines Labormesssystems für die Auslese von Frontendelektronik
Seminar zu experimentellen Methoden in der Kern- und Teilchenphysik
Ruhr-Universität Bochum, 25.06.2010

53. Mertens, M.
Investigation of the precision with which PANDA can measure the width of the $D^{\star}_{s0}(2317)$
PANDA Collaboration Meeting
Univ. Groningen, The Netherlands, 30.08. – 03.09.2010

54. Mertens, M.
Threshold scan of $\bar{D}D^{\star}(2317)$ production and the $D^{\star}$ width determination
PANDA Collaboration Meeting
GSI Darmstadt, 08. – 12.03.2010

55. A. Nogga
Few-nucleon contributions to π-nucleus scattering
Simulations and Symmetries: Cold Atoms, QCD, and Few-hadron Systems
Seattle, U.S.A., 15. – 21.05.2010

56. Oelert, W.
Physics with low and very low energy antiprotons
XLI. Arbeitstreffens Kernphysik
Schleching, 20.02.2010

57. Oelert, W.
Antimaterie — die geheimnisvolle Materie aus Antiteilchen — I
Theresien-Gymnasium Ansbach
Ansbach, 24.03.2010

58. Oelert, W.
Antimaterie — die geheimnisvolle Materie aus Antiteilchen — II
Theresien-Gymnasium Ansbach
Ansbach, 25.03.2010

59. Oelert, W.
On our way to antihydrogen at rest
Seminar
Geneva, Switzerland, 28.04.2010

60. Oelert, W.
Development towards ELENA
Seminar
Warsaw University, Poland, 14.05.2010

61. Oelert, W.
ELENA: An Upgrade to the antiproton decelerator at CERN
11th International Workshop on Meson Production, Properties and Interaction (MESON2010)
Krakow, Poland, 10. – 15.06.2010

62. Oelert, W.
ELENA as an upgrade to the AD
Talk at the SPC
Geneva, Switzerland, 14.12.2010

63. T. Petri
Study of anomalous η decays
PrimeNet Workshop in Lisbon
Lisbon, Portugal, 16. – 18.09.2010

64. Ritman, J.
Commissioning of PANDA
XXXIII PANDA Collaboration Meeting
Stockholm, Sweden, 14. – 18.06.2010

65. Ritman, J.
Hadronenphysik an COSY
KHuK Jahrestagung
Bad Honnef, 03.12.2010

66. Ritman, J.
Hadronic interactions and decays with WASA at COSY
Kolloquium at the EAEA Cairo Cyclotron Project
Cairo, Egypt, 14.04.2010

67. Ritman, J.
Preassembly of PANDA at Jülich
XXXIV PANDA Collaboration Meeting
Groningen, The Netherlands, 30.08. – 03.09.2010

68. D. Rönchen
The reaction $\pi^+ p \to K^+ \Sigma^+$ in a unitary coupled-channels model
19th International Spin Physics Symposium (SPIN2010)
Jülich, 27.09. – 02.10.2010

69. Schadmand, S.
Mesons in Nuclei: η and ω mesons
Workshop New Frontiers in QCD 2010, Yukawa Institute for Theoretical Physics
Kyoto, Japan, 18. – 19.03.2010

70. Schadmand, S.
Hadron-hadron interactions and hadron spectroscopy with WASA at COSY
Joint Symposium of "Exotic Hadron" and "Hadrons in Nculei", Yukawa Institute for Theoretical Physics
Kyoto, Japan, 18. – 19.03.2010

71. Schadmand, S.
Physics with WASA-at-COSY
Chiral10 Workshop
Valencia, Spain, 21. – 24.06.2010

72. Schadmand, S.
Experiments on hadrons in nuclei
INPC 2010
Vancouver, Canada, 04. – 09.07.2010

73. Schadmand, S.
Meson production and decays with WASA at COSY
Baryons 2010
Osaka, Japan, 07. – 11.12.2010

74. Speth, J.
Coherent patterns in nuclear physics and in financial markets
Achivements and New Directions in Subatomic Physics: Workshop in Honour of Tony Thomas' 60th Birthday
Adelaide, Australia, 15. – 19.02.2010

75. Speth, J.
Coherent structures in nuclear physics and in financial markets
Nucleus 2010
St. Petersburg, Russia, 06. – 09.07.2010

76. Tolba, T.
Investigations of double pion production in proton-proton collisions at T_p=1400 MeV
PrimeNet Workshop
Lisbon, Portugal, 15. – 18.09.2010

D Diploma and Ph.D. Theses

1. Bachelor, Master, Diploma

1. L. Atar,
   Simulationsstudien der Reaktion $\bar{p}p \to \Lambda\bar{\Lambda}$ zur Optimierung des PANDA Microvertex-Detektors,
   Diplomarbeit, Universität Bonn

2. C. Barschel,
   Calibration of the Breit-Rabi Polarimeter for the PAX Spin-Filtering Experiment at COSY/Jülich and AD/CERN,
   Diplomarbeit, RWTH Aachen

3. F. Dahmen,
   Stabilitätsverbesserung einer Hochstromversorgung für Magnetvermessungen am COSY-Beschleuniger,
   Diplomarbeit, Fachhochschule Aachen

4. J. Hampe,
   Measurement of the Response Characteristics of CsI(Na) Crystals,
   Diplomarbeit, RWTH Aachen

5. E. Jung,
   Vorbereitende Messungen für ein Pellet-Tracking-System,
   Masterarbeit, Fachhochschule Koblenz, Rhein-Ahr-Campus Remagen

6. J. Kuhs,
   Bestimmung der mittleren Betafunktion an den Quadrupolfamilien des Kühlersynchrotron COSY,
   Bachelorarbeit, RWTH Aachen

7. T. Mennicken,
   Simulation von Teilchentrajektorien in starken Magnetfeldern laser-induzierter Plasmen,
   Diplomarbeit, Fachhochschule Aachen

8. T. Petri,
   Anomalous decays of pseudoscalar mesons,
   Diplomarbeit, Universität Bonn

9. M.S. Rosenthal,
   Analyse und Vergleich von Orbitresponsematrizen am Kühlersynchrotron COSY,
   Bachelorarbeit, RWTH Aachen

10. M. Skurzok,
    Feasibility study of eta-mesic nuclei production by means of the WASA-at-COSY and COSY-TOFfacilities,
    Diploma Thesis, Jagiellonian University Cracow, Poland

11. T. Weber,
    Untersuchung von Orbitresponsematrizen am Kühlersynchrotron COSY,
    Bachelorarbeit, RWTH Aachen

12. S. Xiao,
    Monte Carlo Simulation of the $p+d \to {}^3He+\omega$ reaction with the WASA-at-COSY Detector,
    Bachelorarbeit, Fachhochschule Aachen

13. Q. Zhang,
    Entwicklung eines ortsempfindlichen Detektors samt Ausleseelektronik zur Untersuchung laserinduzierter Beschleunigung,
    Diplomarbeit, RWTH Aachen

2. Ph.D.

14. I. Ciepal,
Investigation of the Deuteron Breakup on Protons in the Forward Angular Region,
Jagiellonian University Cracow, Poland

15. M. Janusz,
Study of the η meson decay into $\pi^+\pi^-e^+e^-$ using WASA-at-COSY detector system,
Jagiellonian University Cracow

16. M. Mertens,
Der PANDA Mikro-Vertex-Detektor: Entwicklung eines Labormesssystems, Simulation der MVD- Betriebsparameter sowie Untersuchungen zur Auflösung der Breite des $D^{\star}_{s0}(2317)$,
Ruhr-Universit ät Bochum

17. T. Rausmann,
Untersuchung der Reaktion $dp \rightarrow {}^3He\eta$ im Bereich zwischen 20 und 60 MeV Überschussenergie am Experiment ANKE,
Universität Münster

18. C.F. Redmer,
In search of the Box-Anomaly with the WASA facility at COSY,
Bergische Universität Wuppertal

19. N. Shah,
Experimental study of pp eta dynamics with WASA-at-COSY,
IIT Bombay, India

20. T. Tolba,
Experimental Investigation of Double-Pion Production in Proton-Proton Interactions,
Ruhr-Universität Bochum

21. D.M. Welsch,
Auslegung eines Orbitkorrektursystems für den Hochenergie-Speicherring HESR im Projekt FAIR,
Universität Bonn

E Awards & Offers for Professorships

E. Epelbaum: Accepted call as Full Professor from the University of Bochum.

F Funded Projects

Project	Responsible	Partner Institute	Funded by
Virtual Institute Spin and Strong QCD	U.-G. Meißner	GSI, Univ.'s Bern, Bonn, Ferrara, Cracow, Torino	HGF
Few Nucleon Systems in χEFT	E. Epelbaum	Univ. Bonn	HGF
QCDnet	U.-G. Meißner	Network	EU/FP7
High energy electron cooler	J. Dietrich		HGF
DIRAC Secondary Beams	R. Tölle		EU/FP6
DIRAC Phase 1	R. Tölle		EU/FP6
Project FAIR	R. Toelle	GSI	EU/FP7
HadronPhysics 2	D. Grzonka		EU/FP7
POLPBAR 2	H. Ströher		EU/FP7
Meson-Baryon Scattering	M. Döring		DFG
Scalar Mesons	M. Büscher	ITEP, INR Moscow (Russia)	DFG
Pellet Target	M. Büscher	ITEP, MPEI Moscow (Russia)	DFG
Laser applications of a pellet target	M. Büscher	ITEP, MPEI Moscow (Russia), Univ. Düsseldorf	DFG
Signals of hadronic molecules	C. Hanhart	ITEP Moscow (Russia)	DFG
Polarized Nuclear Fusion	R. Engels	PNPI Gatchina (Russia)	DFG
Molecular polarized target	R. Engels	PNPI Gatchina (Russia)	DFG
Studies of pion production	A. Kacharava	JINR Dubna (Russia)	DFG
PAX/COSY	F. Rathmann		DFG
Response function of short-lived nuclear isotopes	S. Krewald		DFG
Experimental study of charge symmetry breaking and few-body interactions in dd collisions	V. Hejny	Univ. Cracow (Poland)	DAAD
Broken Symmetries	H. Machner	Univ. Helsinki (Finland)	DAAD
PPP Kanada	D. Grzonka	York Univ., Toronto (Canada)	DAAD
PANDA luminosity monitor	J. Ritman	Madagascar	HGF-DAAD
Rare Decays of η and η' Mesons	S. Schadmand	Indian Inst. of Technology Bombay	DAAD/DST India
Target Development for nuclear physics experiments at COSY and AEA cyclotron	J. Ritman	AEA Cairo (Egypt)	Int. Büro BMBF
Polarized Target	F. Rathmann	PNPI Gatchina (Russia)	ISTC
Baryon Resonance Analysis	U.-G. Meißner	JLAB (U.S.A.)	JLAB
Development of a high energy electron cooler	J. Dietrich	TU Dortmund; BINP Novosibirsk, JINR Dubna (Russia)	HGF
HGF/CSC Ph.D. fellowship	M. Büscher	IMP Lanzhou (China)	HGF/CSC
HGF/CSC Postdoc fellowship	M. Büscher	Xian Jiaotong Univ. (China)	HGF/CSC
Calculations of the Radiation Load to the PANDA MVD	J. Ritman	Israel	NRW-Israel

G COSY-FFE Projects

Project	Responsible	Institute
Entwicklung eines innovativen, kompakten Monitorsystems für einen elektromagnetischen Kristallkalorimeter und Entwicklung von Software-Werkzeugen zur Teilchenidentifikation	Prof. U. Wiedner	Univ. Bochum
Study of the rare decay $\eta \to e^+e^-\pi^+\pi^-$ in pp and pd reactions	Prof. U. Wiedner	Univ. Bochum
Entwicklung und Bau von Detektor-Komponenten für das WASA-at-COSY Experiment	Prof. K.-T. Brinkmann	Univ. Bonn
Prototyping for PANDA at COSY	Prof. K.-T. Brinkmann	Univ. Bonn
Investigation of ABC effect and Spin transfer coefficients at COSY	Prof. H.-W. Hammer	Univ. Bonn
Partialwellenanalyse von Daten aus Proton-induzierten Reaktionen	Prof. B. Metsch	Univ. Bonn
Inelastic baryon resonances from lattice QCD	Prof. A. Rusetsky	Univ. Bonn
Development of a Fast Orbit Feedback System for the HESR and Beam Tests at COSY	Prof. T. Weis	Univ. Dortmund
H-Strahl Laserdiagnose	Prof. T. Weis	Univ. Dortmund
COSY-TOF detector	Prof. H. Freiesleben	TU Dresden
Silicon Tracking Telescopes for ANKE and PAX	Prof. B. Kämpfer	FZ Dresden
Measurement of the degree of polarisation of laser accelerated protons	Prof. O. Willi	Univ. Düsseldorf
Vorbereitung und Durchführung von Experimenten an COSY-TOF und WASA	Prof. W. Eyrich	Univ. Erlangen-Nürnberg
Spin Experiments with ANKE and PAX	Prof. E. Steffens	Univ. Erlangen-Nürnberg
FPGA-based trigger system for WASA	Prof. W. Kühn	Univ. Gießen
Development of a DIRC Cherenkov detector for WASA	Prof. M. DÃ¼ren	Univ. Gießen
Mesonenproduktion in Nukleon-Nukleon- und Nukleon-Kern-Stößen an COSY	Prof. A. Khoukaz	Univ. Münster
Baryon resonance, g_A und die effektive Restrukturierung der chiralen Symmetrie	Prof. A. Schäfer	Univ. Regensburg
Installation und Inbetriebnahme des WASA-Detektors am COSY-Ring und Durchführung von Experimenten an WASA at COSY	Prof. H. Clement	Univ. Tübingen
Experimente an COSY-TOF	Prof. H. Clement	Univ. Tübingen

Project	Responsible	Institute
Lattice calculations of axial charges for baryons	Prof. C. Gattringer	Univ. Graz (Austria)
Design and realization of an interlock system for the PAX experiment	Dr. P. Lenisa	Univ. Ferrara (Italy)
np system study with polarized beams and polarized Targets at ANKE	Prof. M. Nioradze	Tbilisi State Univ. (Georgia)
Spin dependence in pd interactions	Prof. P. Dalpiaz	Univ. Ferrara (Italy)
Investigations of the CP symmetry with WASA	Prof. P. Moskal	Jagellionian Univ. Cracow (Poland)
Dalitz decays of Mesons with WASA-at-COSY	Prof. P. Moskal	Jagellionian Univ. Cracow (Poland)
Strangeness production with WASA-at-COSY	Prof. B. Kamys	Jagellionian Univ. Cracow (Poland)
Study of the decay $\eta' \to \eta\pi\pi$ with WASA	Prof. Z. Rudy	Jagellionian Univ. Cracow (Poland)
Development of the PID method based on the dE/dx measurement for the Straw Tube Tracker	Prof. M. Jezabek	INP Crakow (Poland)
Study of the nature of the $\Lambda(1405)$ with WASA	Prof. W. Zipper	Univ. Silesia (Poland)
Silicon Tracking Telescope for ANKE	Dr. V. Koptev	PNPI Gatchina (Russia)
Experiments with ANKE, WASA and PAX and FAIR	Prof. V. Kulikov	JINR Dubna (Russia)
Particle identification with straw detectors	Prof. V. Kulikov	JINR Dubna (Russia)
Study of ω-meson production with WASA-at-COSY	Prof. E. Strokovsky	JINR Dubna (Russia)
Development of a frozen-pellet target	Dr. A. Gerasimov	ITEP Moscow (Russia)
ϕ-meson production in pn and pA reactions	Prof. V. Kiselev	ITEP Moscow (Russia)
Development of online software tools for COSY-TOF	Dr. V. Afanasyev	MSU Moscow (Russia)
Development, commissioning and operation of components for the COSY experiments WASA and ANKE and spin-filtering studies at COSY as preparation of the PAX experiment in the framework of the FAIR project at GSI	Dr. A. Vasilyev	PNPI Gatchina (Russia)
A pellet tracking system for PANDA and for WASA	Dr. H. Calen	Uppsala Univ. (Sweden)
Cooperation COSY-WASA for $pp \to pp\eta$ and $pp \to pp\eta\pi^0$	Prof. T. Johansson	Uppsala Univ. (Sweden)
Unified analysis of meson production in hadron- and photon-induced reactions	Prof. K. Nakayama	Univ. of Georgia (U.S.A.)

H Conferences (co-)organized by the IKP

H.1 19th International Spin Physics Symposium (SPIN2010)

The 19th International Spin Physics Symposium (SPIN2010) took place between September 26 and October 2, 2010, at Forschungszentrum Jülich. It was organized by IKP with Hans Ströher and Frank Rathmann as co-chairman.

The meeting was attended by about 300 participants from all over the world. During the meeting, 38 plenary and about 165 parallel talks were presented. In addition a public lecture on "Drall in der Quantenwelt" was given by H.O. Meyer (IUCF) at RWTH Aachen.

SPIN2010 participants saw the most recent results in the field from COMPASS, COSY, ELSA, Fermilab, HERMES, JLAB, MAMI, PHENIX, SPring8, STAR and other places; they also heard about new ideas to exploit and to apply spin, *e.g.* in medicine and for the investigation of fundamental symmetries. New projects (eRHIC, JLab12, NICA, srEDM ...) were presented. The meeting also covered the latest theoretical developments from Effective Field Theory to Lattice QCD.

Talks of the meeting are available on-line, contributions will be published at IOPscience.

H.2 Hadron Physics Summer School (HPSS2010)

More than 50 graduate and advanced undergraduate students from 12 countries and 4 continents participated in the Hadron Physics Summer School HPSS 2010 held at Physikzentrum Bad Honnef, Germany, August 9–13, 2010. Similar to the preceding COSY Summer School (CSS) 2002, 2004, and 2006, and the HPSS 2008, this school consisted of lectures and working groups on theoretical, experimental, and accelerator aspects. The focus was on current issues in hadron physics with emphasis on the latest programs at the accelerators COSY and ELSA (Bonn), also featuring future FAIR projects like HESR/PANDA and PAX. During the very successful school, the students were given a guided tour to COSY. The HPSS 2010 was jointly organized by scientists working at the IKP and by the DFG Transregio TR 16 (Subnuclear Structure of Matter) of the Universities Bonn, Bochum, and Giessen. In addition, the HPSS 2010 was sponsored by DAAD (German Academic Exchange Service) and DPG (Deutsche Physikalische Gesellschaft), making the participation of young motivated students also from developing countries into this challenging enterprise possible. The HPSS is held every second year. This series is supplemented by lecture weeks in the alternate years, which consist of invited lectures and student contributions. The lecture weeks are self-contained and are an excellent opportunity for graduate students and early post-graduates to deepen the knowledge gained at HPSS. For more detailed information, see www.fz-juelich.de/ikp/hpss2010/.

Fig. 54: Participants and organizers of the HPSS2010 at the Physikzentrum Bad Honnef.

Fig. 53: Participants of the SPIN2010 symposium in front of the central lecture hall of the FZJ..

H.3 3rd Workshop High Energy Electron Cooling

The 3rd Workshop High Energy Electron Cooling within the framework of the Helmholtz Russia Joint Research Group "Development of a high energy electron cooler for hadron physics experiments at COSY and HESR, HRJRG-106" was organized from June 9–11, 2010, in the Joint Institute of Nuclear Research Dubna, Russia. It is a series of meetings, the first workshop took part in March 2009 at the Budker Institute Novosibirsk, the second in April 2010 at the Forschungszentrum Jülich. 20 Participants from Universities Dortmund and Mainz, Budker Institute Novosibirsk, JINR Dubna and Forschungszentrum Jülich discussed about: status of high energy electron cooler projects, high voltage generators and related problems and electron cooling technique and related problems.

Fig. 55: Participants of the e-cooling workshop in front of JINR's Laboratory of Nuclear Problems.

I Teaching Positions

Institute	Name	University
IKP-1	PD Dr. A. Gillitzer	Bonn
	PD Dr. F. Goldenbaum	Wuppertal
	Prof. Dr. J. Ritman	Bochum
	PD Dr. S. Schadmand	Köln
	Dr. T. Stockmanns	Bochum
IKP-2	PD Dr. M. Büscher	Köln
	Prof. Dr. D. Gotta	Köln
	PD Dr. F. Rathmann	Erlangen-Nürnberg
	Prof. Dr. H. Ströher	Köln
IKP-3/IAS-4	Prof. Dr. E. Epelbaum	Bonn (until ...
	Univ. Doz. Dr. J. Haidenbauer	Graz
	PD Dr. C. Hanhart	Bonn
	Prof. Dr. S. Krewald	Bonn
	Prof. Dr. U.-G. Meißner	Bonn
	Prof. Dr. N.N. Nikolaev	Moscow
	Dr. A. Nogga	Bonn
	PD Dr. A. Wirzba	Bonn
IKP-4	Prof. Dr. Dr. h.c. J. Dietrich	Dortmund
	PD Dr. A. Lehrach	Aachen, Bonn
	Prof. Dr. R. Maier	Bonn

J Personnel

J.1 Scientific Staff

M. Azis Hessan (IKP-2) (since 01 November, 2010)
Dr. V. Baru (IKP-3)
Dr. U. Bechstedt (IKP-4)
Dr. K. Bongardt (IKP-4)
DI N. Bongers (IKP-4)
DI R. Brings (IKP-4)
Y. Bsaisou (IKP-3)
PD Dr. M. Büscher (IKP-2)
M. Cleven (IKP-3) (since 01 March, 2010)
D. Coderre (IKP-3)
F.U. Dahmen (IKP-4) (since 12 May, 2010)
Prof. Dr.Dr.h.c. J. Dietrich (IKP-4)
DI N. Dolfus (IKP-TA)
Dr. M. Döring (IKP-3) (until 30 September, 2010)
R. Dzhygadlo (IKP-1) (sine 01 October, 2010)
Dr. R. Engels (IKP-2)
I. Engin (IKP-2) (since 15 July, 2010)
Prof. Dr. E. Epelbaum (IKP-3) (until 30 April, 2010)
S. Esch (IKP-1) (sine 01 August, 2010)
DI F.-J. Etzkorn (IKP-4)
Dr. P. Fedorets (IKP-2)
Dr. O. Felden (IKP-TA)
M. Gaißer (IKP-2) (sine 01 December, 2010)
Dr. W. Gast (IKP-1)
Dr. R. Gebel (IKP-4)
PD Dr. A. Gillitzer (IKP-1)
PD Dr. F. Goldenbaum (IKP-1)
PD Dr. D. Gotta (IKP-2)
Dr. F. Grümmer (IAS-4)
Dr. D. Grzonka (IKP-1)
B. Guerra (IKP-2) (since 08 September, 2010)
DI W. Günther (IKP-4)
Dr. F.-K. Guo (IKP-3) (until 30 September, 2010)
Univ. Doz. Dr. J. Haidenbauer (IAS-4)
PD Dr. C. Hanhart (IAS-4)
Dr. M. Hartmann (IKP-2)
Dr. V. Hejny (IKP-2)
DI K. Henn (IKP-4)
DP M. Hodana (IKP-1)
Dr. V. Jha (IKP-1) (until 31 August, 2010)
E. Jung (IKP-2) (until 15 May, 2010)
Dr. V. Kamerdjiev (IKP-4)
Dr. A. Kacharava (IKP-2)
L. Kröll (IKP-3)
DP St. Kölling (IKP-3)
Prof. Dr. S. Krewald (IAS-4)
L. Krol (IKP-2) (since 31 August, 2010)
DI K. Kruck (IKP-4) (until 28 February, 2010)
PD Dr. A. Lehrach (IKP-4)
DP S. Liebig (IKP-3)
Dr. B. Lorentz (IKP-4)
Prof. Dr. H. Machner (IKP-1) (until 30 January, 2010)
Prof. Dr. R. Maier (IKP-4)
Prof. Dr. U.-G. Meißner (IKP-3)
Th. Mennicken (IKP-2) (until 30 August, 2010)
DP M. Mertens (IKP-1)
Dr. S. Merzliakov (IKP-2) (since 01 August, 2010)
DP S. Mikirtychiants (IKP-2)
DP D. Minossi (IKP-3)
R. Mitter (IKP-2) (since 15 August, 2010)
Dr. M. Nekipelov (IKP-2) (until 30 April, 2010)
Prof. Dr. N.N. Nikolaev (IKP-3)
Dr. A. Nogga (IAS-4)
Prof. Dr. W. Oelert (IKP-1)
DP D. Oellers (IKP-2)
Dr. H. Ohm (IKP-2)
DI N. Paul (IKP-1)
Dr. C. Pauly (IKP-1)
Dr. M. Pavon-Valderrama (IKP-3) (until 31 May, 2010)
D.-L. Pohl (IKP-1)
Dr. D. Prasuhn (IKP-4)
DP N. Raab (IKP-4)
PD Dr. F. Rathmann (IKP-2)
Dr. Ch.F. Redmer (IKP-1)

DP M. Retzlaff (IKP-4)
DI A. Richert (IKP-4)
Prof. Dr. J. Ritman (IKP-1)
Dr. E. Roderburg (IKP-1)
DP M. Röder (IKP-1)
DI J. Sarkadi (IKP-TA)
PD Dr. S. Schadmand (IKP-1)
Dr. R. Schleichert (IKP-2)
DI G. Schug (IKP-4)
Dr. Th. Sefzick (IKP-TA)
Prof. Dr. Y. Senichev (IKP-4)
DI M. Simon (IKP-4)
N. Sharmazanashvili (IKP-4)
Dr. R. Stassen (IKP-4)
Dr. H. Stockhorst (IKP-4)
Dr. T. Stockmanns (IKP-1)
Prof. Dr. H. Ströher (IKP-2)
DP T. Tolba (IKP-1)
Dr. R. Tölle (IKP-4)
DI T. Vashegyi (IKP-4)
DP Chr. Weidemann (IKP-2)
DP D. Welsch (IKP-4) (until 31 August, 2010)
Dr. P. Wintz (IKP-1)
PD Dr. A. Wirzba (IAS-4)
DI J.-D. Witt (IKP-4)
DP P. Wurm (IKP-2)
Dr. H. Xu (IKP-1)
Dr. E. Zaplatin (IKP-4)

J.2 Technical and Administrative Staff

J. Artz (IKP-TA)

C. Berchem (IKP-TA)

M. Böhnke (IKP-4)

J. Borsch (IKP-TA)

P. Brittner (IKP-4)

J. But (IKP-TA)

W. Classen (IKP-4)

M. Comuth-Werner (IKP-TA)

B. Dahmen (IKP-4)

C. Deliege (IKP-4)

W. Derissen (IKP-TA)

G. D'Orsaneo (IKP-2)

R. Dosdall (IKP-1)

R. Enge (IKP-4)

P. Erben (IKP-2)

B. Erkes (IKP-4)

K. Esser (IKP-TA)

H.-W. Firmenich (IKP-TA)

J. Göbbels (IKP-TA)

H. Hadamek (IKP-TA)

R. Hecker (IKP-4)

E. Heßler (IKP-TA)

M. Holona (IKP-TA)

A. Kieven (IKP-4)

M. Kremer (IKP-TA)

G. Krol (IKP-4)

V. Kau (IKP-TA) (since 16 June, 2010)

M. Küven (IKP-4)

K.-G. Langenberg (IKP-4)

H. Metz-Nellen (IKP-TA)

S. Müller (IKP-TA)

R. Nellen (IKP-TA)

H. Pütz (IKP-4)

K. Reimers (IKP-4) (since 01 January, 2010)

G. Roes (IKP-TA)

N. Rotert (IKP-4)

D. Ruhrig (IKP-4)

F. Scheiba (IKP-4)

H. Schiffer (IKP-TA)

J. Schmitz (IKP-4)

F. Schultheiß (IKP-TA)

H. Singer (IKP-4)

D. Spölgen (IKP-2)

G. Sterzenbach (IKP-1)

J. Strehl (IKP-TA)

J. Uehlemann (IKP-1)

P. Wieder (IKP-2)

H. Zens (IKP-4)

IKP-1 = Experimental Hadron Structure
IKP-2 = Experimental Hadron Dynamics
IKP-3 = Theoretical Nuclear Physics
IKP-4 = Large-Scale Nuclear Physics Equipment
IKP-TA = Technical Services and Administration
IAS-4 = Theory of the Strong Interactions

K Substantiating Contributions

(articles available on-line: http://www.fz-juelich.de/ikp/publications/AR2010/en/contents.shtml)

1. Experimental Hadron Physics

   1.1 Recent results from the charge-exchange breakup reaction $dp \to pp_s n$ study at ANKE

   1.2 Vector analyzing power of the $pp \to pp_s\pi^0$ reaction at intermediate energies at ANKE/COSY

   1.3 Investigation of the ^{3}Heη-final state in dp-collisions

   1.4 Neural network application for proton kinetic energy reconstruction in ANKE STT

   1.5 Analysis of the $pd \to pp_{(\mathrm{STT})} + X$ reaction at 353 MeV using ANKE STTs

   1.6 The η meson mass determination with ANKE at COSY

   1.7 Double-polarized fusion

   1.8 Identification of the $pn \to d\omega$ reaction at ANKE

   1.9 Study of the $pn \to pp_s\pi$ reaction near the threshold at ANKE

   1.10 Coherent production of pion pairs in the reaction $pd \to pd\pi\pi$

   1.11 Analyzing power of $\vec{p}d \to {}^3\mathrm{H}\pi^+$ and $\vec{p}d \to {}^3\mathrm{He}\pi^0$ $T_p = 353$ MeV measured at ANKE-COSY

   1.12 Formation of the ^{1}S$_0$ diproton in the reaction $pp \to pp_s\pi^0$ in the Δ isobar region

   1.13 Multifragmentation of Aluminium Nuclei by GeV Protons